Fractional Order PID Controller Tuning by

Frequency Loop-Shaping:

Analysis and Applications

by

Khalid Saleh

A Dissertation Presented in Partial Fulfillment
of the Requirements for the Degree
Doctor of Philosophy

Approved October 2017 by the
Graduate Supervisory Committee:

Konstantinos Tsakalis, Chair
Armando Rodriguez
Jennie Si
Panagiotis Artemiadis

ARIZONA STATE UNIVERSITY

December 2017

ABSTRACT

The purpose of this dissertation is to develop a design technique for fractional PID controllers to achieve a closed loop sensitivity bandwidth approximately equal to a desired bandwidth using frequency loop shaping techniques. This dissertation analyzes the effect of the order of a fractional integrator which is used as a target on loop shaping, on stability and performance robustness. A comparison between classical PID controllers and fractional PID controllers is presented. Case studies where fractional PID controllers have an advantage over classical PID controllers are discussed. A frequency-domain loop shaping algorithm is developed, extending past results from classical PID's that have been successful in tuning controllers for a variety of practical systems.

ACKNOWLEDGMENTS

TABLE OF CONTENTS

LIST OF TABLES

viii

Figure Page

xii

CHAPTER 1

INTRODUCTION

It is known that the use of PID controllers began in the thirties of the last century. The designs of these controllers were based on mathematical and physical backgrounds. Scientific development in science and engineering has helped to develop the designs of these controllers. PID controllers are commonly used in process control industries because of their performance and simplicity that made their wide scale deployment, tuning and maintenance practically feasible. The first mathematical version of the fractional PID controller was introduced by the professor Igor Podlubny, twenty-three years ago, specifically in 1994.

The idea of developing classic PID controllers of three parameters into fractional PID controllers of five parameters began in the nineties of the last century. It is known that the parameters of a classic PID controller are proportional, integral, and derivative gains. The additional parameters in the fractional PID controller represent the fractional integral order and the fractional differential order.

Many techniques have been proposed to tune PID controllers, ranging from ad-hoc application of traditional tuning metrics, rules of thumb, and optimization of a variety of time and frequency domain criteria to find the best parameters in the design. Similarly, for fractional PID controllers, several studies addressed the development of their parameter tuning. Frequency Loop Shaping was a PID tuning technique that was developed in the 90's to design optimal or nearly optimal PID's in an efficient and reliable manner. It was motivated by the controller design problem from system

identification data. In this formulation, the identification step provides data on the nominal plant and its uncertainty description, translating into frequency domain bounds for the loop transfer function. In its simplest form, the frequency domain objective would be for the PID controller to achieve a closed loop bandwidth approximately equal to a desired, or target value. This basic idea was made particularly appealing by the applicability of convex optimization techniques that allowed for a quick and reliable numerical solution, including parameter constraints. Perhaps an equally important advantage of this approach was the availability of insight on how to choose meaningful loop shapes and interpreting the results of the frequency domain analysis and was naturally followed by many successful implementations in industrial systems.

The idea of this technique is to find the parameters of the controller by assuming that the PID controller and the plant in a feedback system behave as a certain target in the frequency domain. In other words, obtaining the shape of the open loop in the frequency domain similar to that of the target is an objective. Therefore, the magnitude of the target in the frequency domain can be considered as the shape of the open loop which consists of the controller and plant together. Finding the controller parameters to shape the loop and meet performance specifications and achieve desirable robustness properties are the objectives of designing the controller. The possibility of using only frequency response data from the system, made this approach particularly well-suited for tuning the parameters of fractional PIDs. Such a tuning can be obtained using the Frequency Loop Shaping methodology by minimizing the fitting error function for different values of the fractional integral order and the fractional differential order.

2

There are some many physical phenomena that can be represented by fractional differential equations. For example, the relationship between the current and voltage of a semi-infinite lossy RC transmission line is given by a fractional differential equation. Another example, the relationship between the temperature and heat flux in a semi-infinite composite body can be described by a fractional differential equation. The fractional calculus theory has been applied to control theories to improve control systems performance. The fractional calculus appeared in the year 1659, as a result of a question raised by Libnitz in a letter to L'Hospital, generalizing dervitives with non-integer orders cannot give the meaning of derivatives with integer order. A question raised and replied by L'Hospital: ''if the order was half what will be?''. Leibnitzs answered in a historic way, a paradox will happen which will leads to good results. In the dissertation, the frequency loop shaping technique is applied to three different fractional systems. The first system is the heating furnace system whose transfer function can be obtained as a fractional transfer function after using the Grunwald-Letnikov definition. The second system describes the motion of a rigid thin plate immersed in a Newtonian viscous fluid. The fractional transfer function of the system is given by the Bagely-Torvik equation. The last system is Buck converter which is a DC to DC power converter. The relationship between the input voltage and output voltage can be given by a fractional transfer function. Fractional PID controller will be applied to the three models in order to obtain good results and compare them classical controller.

Figure 1.1: Professor Igor Podlubny

1.1 Outline of the Dissertation

In chapter 2, a brief overview of some important function used in fractional calculus is explained. Chapter 3 includes some definitions in fractional calculus with their properties. Chapter 3 covers some equations used in the time and frequency domains of some fractional transfer functions with some examples. Also, it includes the stability conditions in a fractional LTI system and the Oustaolup recursive filter for approximation. Chapter 5 introduces the fractional PID controllers with their properties. An overview of robust control system is discussed in this chapter. Chapter 6 shows the obtained results of the fractional PID controller tuning by frequency loop shaping (FLS). Chapter 7 contains conclusions and future work.

CHAPTER 2

PRELIMINARY

This chapter includes some important functions used in the fractional calculus with their properties.

2.1 The Error Function

The error function of the variable (x) which is also called Gauss error function, written as $erf(x)$, is defined by the following relationship

$$erf(x) = \frac{2}{\sqrt{\pi}} \int_0^x e^{-u^2} du \qquad (2.1)$$

The complementary error function of the variable (x), denoted $erfc(x)$, is given by

$$erfc(x) = \frac{2}{\sqrt{\pi}} \int_x^\infty e^{-u^2} du \qquad (2.2)$$

The relationship between the error function and the complementary error function can be expressed as

$$erfc(x) = 1 - erf(x) \qquad (2.3)$$

Figure 2.1 shows the plot of the error function and the complementary error function.
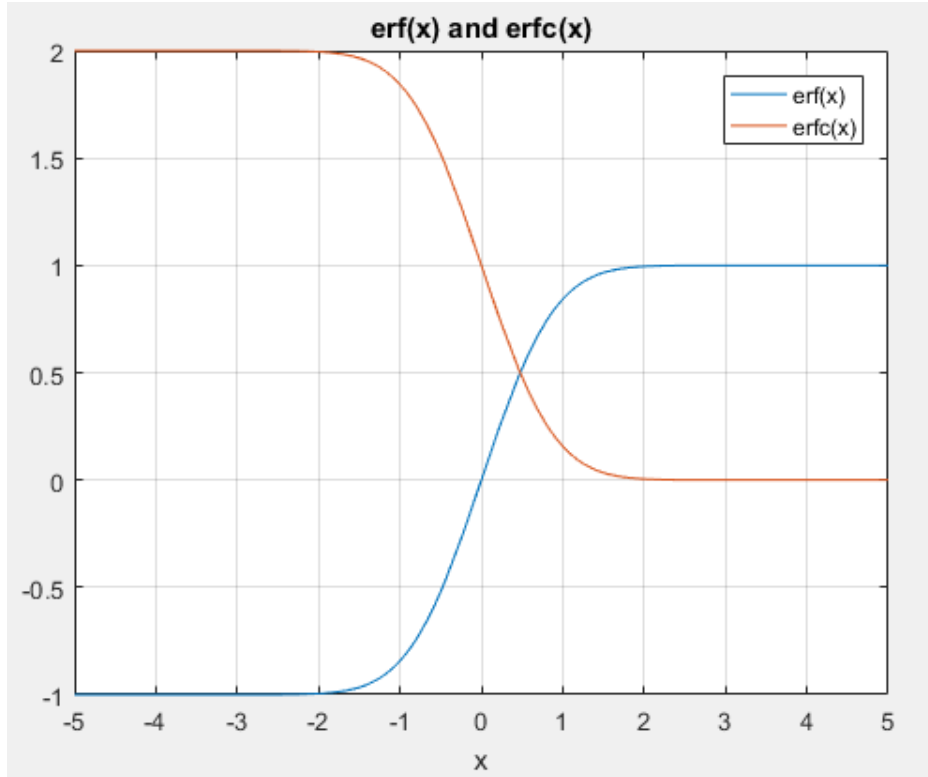
Figure 2.1: The error function and the complementary error function

The integral in (2.1) cannot be evaluated in closed form. It can be solved numerically by expanding the term e^{-u^2} into an infinite series and integrating term by term. The following table shows some values of the error function for $(0 \leq x \leq 2)$.

Table 2.1: Values of error function

x	$erf(x)$	x	$erf(x)$
0.00	0.0000000	1.00	0.8427008
0.05	0.0563720	1.05	0.8624361
0.10	0.1124629	1.10	0.8802051
0.15	0.1679960	1.15	0.8961238
0.20	0.2227026	1.20	0.9103140
0.25	0.2763264	1.25	0.9229001
0.30	0.3286268	1.30	0.9340079

0.35	0.3793821	1.35	0.9437622
0.40	0.4283924	1.40	0.9522851
0.45	0.4754817	1.45	0.9596950
0.50	0.5204999	1.50	0.9661051
0.55	0.5633234	1.55	0.9716227
0.60	0.6038561	1.60	0.9763484
0.65	0.6420293	1.65	0.9803756
0.70	0.6778012	1.70	0.9837904
0.75	0.7111556	1.75	0.9866717
0.80	0.7421010	1.80	0.9890905
0.85	0.7706681	1.85	0.9911110
0.90	0.7969082	1.90	0.9927904
0.95	0.8208908	1.95	0.9941793
1.00	0.8427008	2.00	0.9953223

The complementary error function satisfies the following inequalities for upper and lower bounds

- $$erfc(x) > \left(1 - \frac{1}{2x^2}\right)\frac{e^{-x^2}}{\sqrt{\pi}x} \qquad (2.4)$$

The plot of this inequality is shown in figure 2.2.
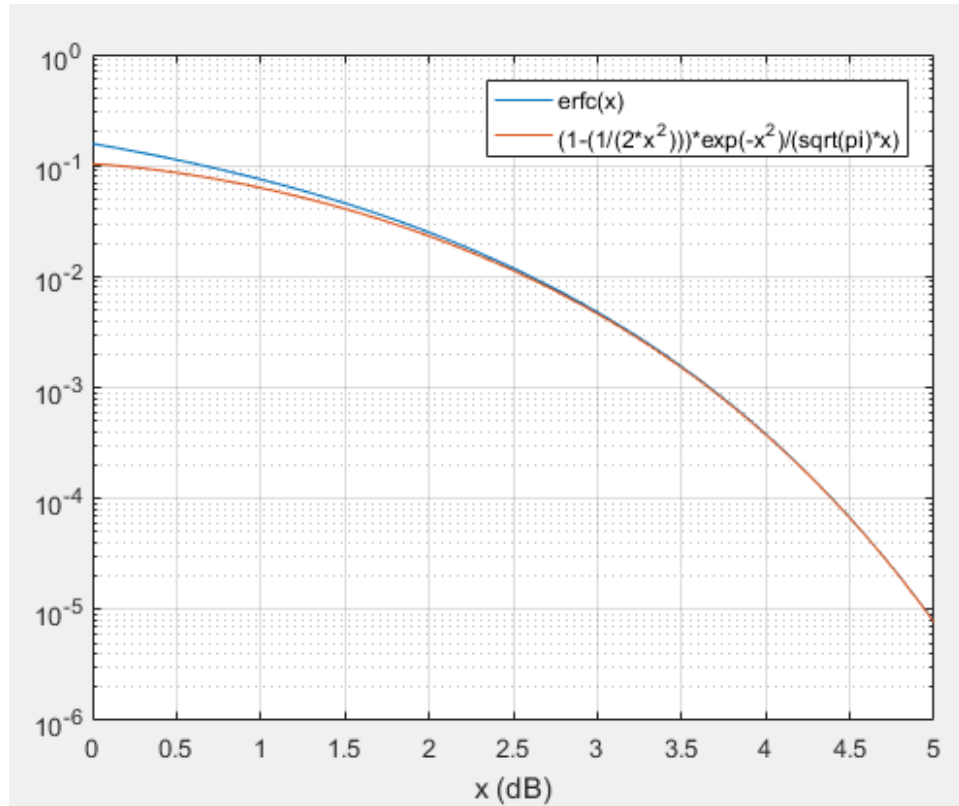
Figure 2.2: $erfc(x)$ and $\left(1-\dfrac{1}{2x^2}\right)\dfrac{e^{-x^2}}{\sqrt{\pi}x}$

- $erfc(x) < \dfrac{e^{-x^2}}{\sqrt{\pi}x}$ (2.5)

Figure 2.3 shows the plot of the inequality in (2.6).
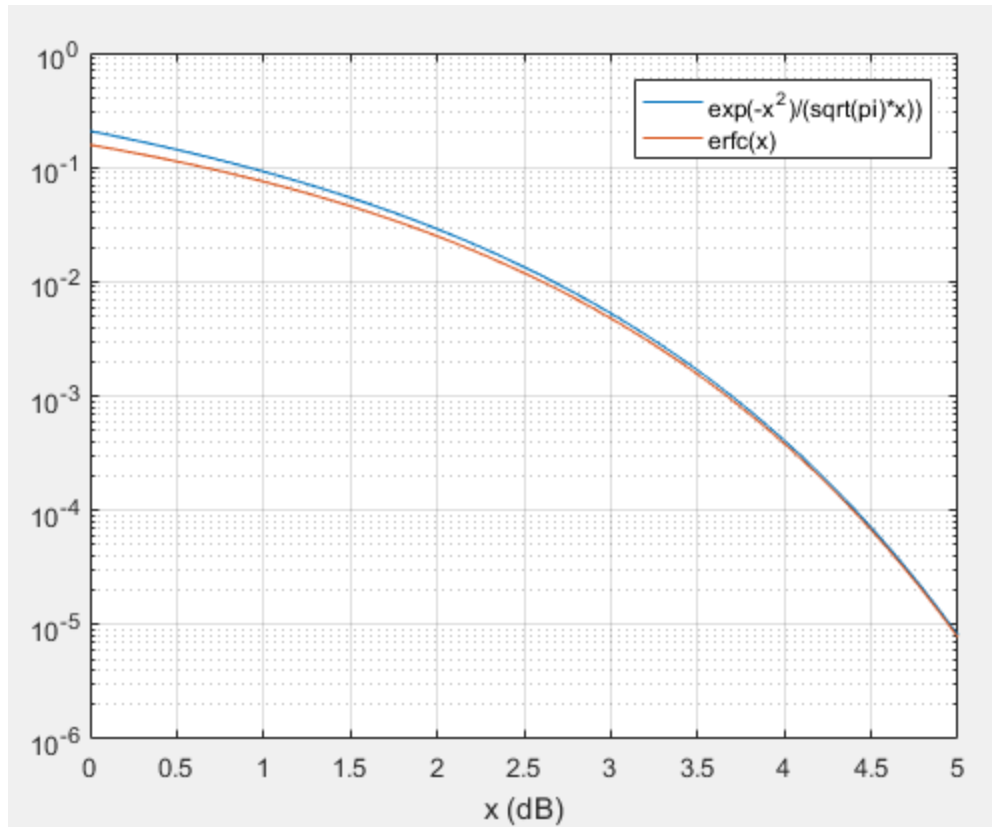
Figure 2.3: $erfc(x)$ and $\dfrac{e^{-x^2}}{\sqrt{\pi}\,x}$

The plots of (2.5) and (2.6) show that the complementary error function $erfc(x)$ is close to (x) for values $(x \geq 2)$.

Some properties of the error function are:

- $erf(0) = 0$ (2.6)

- $erf(\infty) = 1$ (2.7)

- $erfc(\infty) = 0$ (2.8)

- $erfc(-\infty) = 2$ (2.9)

- $erfc(0) = 1$ (2.10)

- $erf(-x) = -erf(x)$ (2.11)

- $erfc(-x) = 1 + erf(x) = 2 - erfc(x)$ (2.12)

- $erfc(x) = 1 + erf(-x) = 1 - erf(x)$ (2.13)

- $\dfrac{d}{dx} erf(x) = \dfrac{2}{\sqrt{\pi}} e^{-x^2}$ (2.14)

- $\displaystyle\int erf(x)dx = x\,erf(x) - \dfrac{e^{-x^2}}{\sqrt{\pi}} + c$ (2.15)

- $\displaystyle\int_0^x erf(y)dy = x\,erf(x) - \dfrac{1}{\sqrt{\pi}}\left(1 - e^{-x^2}\right)$ (2.16)

- $\displaystyle\int_0^\infty erfc(x)dx = \dfrac{1}{\sqrt{\pi}}$ (2.17)

- $\displaystyle\int_0^\infty erfc^2(x)dx = \dfrac{2 - \sqrt{2}}{\sqrt{\pi}}$ (2.18)

- $erf(x) = \dfrac{2}{\sqrt{\pi}} e^{-x^2} \displaystyle\sum_{n=0}^{\infty} \dfrac{2^{2n+1} x^{2n+1}(n+1)!}{(2n+2)!}$ (2.19)

- $erf(x) = \dfrac{2}{\sqrt{\pi}} \displaystyle\sum_{n=0}^{\infty} \dfrac{(-1)^n x^{2n+!}}{n!(2n+1)}$ (2.20)

2.2   The Imaginary Error Function

The imaginary error function, written as $erfi(x)$, is defined by

10

$$erfi(x) = \frac{2}{\sqrt{\pi}} \int_0^x e^{u^2} \, du \qquad (2.21)$$

The following figure shows the plot of the imaginary error function.
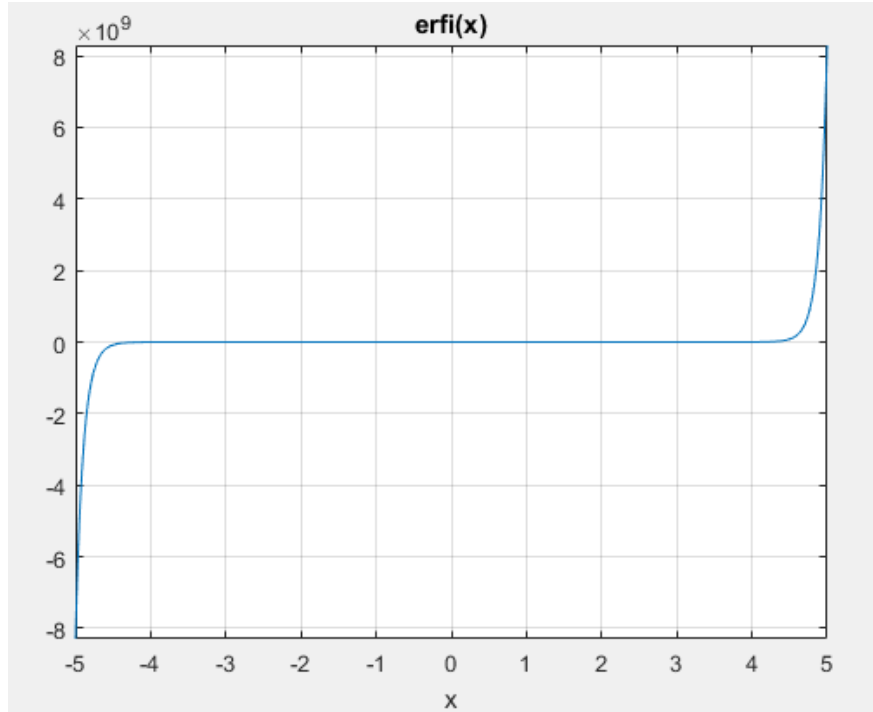
Figure 2.4: The imaginary error function

Some of the most important properties of the imaginary error function are:

- $erfi(\pm\infty) = \pm\infty$ \hfill (2.22)

- $erfi(\pm j\infty) = \pm j$ \hfill (2.23)

- $erfi(0) = 0$ \hfill (2.24)

- $erfi(x) = -j\,erf(j\,x)$ \hfill (2.25)

- $erfi(x) = \dfrac{1}{\pi}\left(2x + \dfrac{2}{3}x^3 + \dfrac{1}{5}x^5 + \dfrac{1}{21}x^7 + \ldots\right)$ (2.26)

where $j = \sqrt{-1}$

2.3   The Gamma Function

The Gamma function of the variable (x), written as $\Gamma(x)$, is defined by

$$\Gamma(x) = \int_0^{\infty} t^{x-1} e^{-t} dt \qquad x > 0$$ (2.27)

Figure 2.5 shows the plot of the Gamma function.
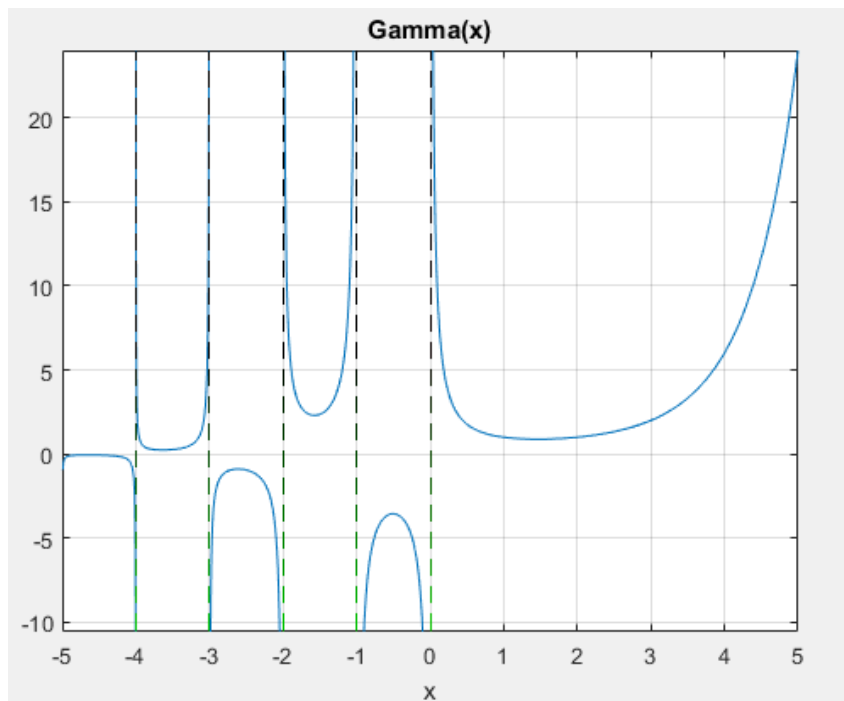
Figure 2.5: The Gamma function

Figure 2.5 shows that if (x) is negative integer, $\Gamma(-x)$ is infinite and $\Gamma(0)$ is also infinite. Some vales of the Gamma function are:

- $\Gamma\left(\dfrac{1}{2}\right)=\sqrt{\pi}$ (2.28)

- $\Gamma(1)=1$ (2.29)

- $\Gamma\left(\dfrac{3}{2}\right)=\dfrac{\sqrt{\pi}}{2}$ (2.30)

- $\Gamma\left(\dfrac{5}{2}\right)=\dfrac{3}{4}\sqrt{\pi}$ (2.31)

- $\Gamma\left(\dfrac{7}{2}\right)=\dfrac{15}{8}\sqrt{\pi}$ (2.32)

- $\Gamma\left(\dfrac{9}{2}\right)=\dfrac{105}{16}\sqrt{\pi}$ (2.33)

- $\Gamma\left(-\dfrac{1}{2}\right)=-2\sqrt{\pi}$ (2.34)

- $\Gamma\left(-\dfrac{3}{2}\right)=\dfrac{4}{3}\sqrt{\pi}$ (2.35)

Some properties of the Gamma function are:

- $\Gamma(x)=(x-1)!$ (2.36)

- $\Gamma(x+1)=x\,\Gamma(x)$ (2.37)

- $\Gamma\left(\dfrac{1}{2}+m\right)=\dfrac{1\times3\times5\times\cdots\times(2m-1)}{2^{m}}\sqrt{\pi}\quad m:1,2,3,.....$ (2.38)

- $\Gamma\left(\dfrac{1}{2}-m\right)=\dfrac{(-2)^{m}}{1\times3\times5\times\cdots\times(2m-1)}\sqrt{\pi}\quad m:1,2,3,.....$ (2.39)

13

- $\Gamma(x)\Gamma(1-x) = \dfrac{\pi}{\sin(\pi x)} = \pi\,\mathrm{cosec}(\pi x)$ $\hspace{3cm}$ (2.40)

- $\dfrac{\Gamma(2x)}{2^{2x-1}} = \dfrac{\Gamma(x)\Gamma\left(x+\dfrac{1}{2}\right)}{\sqrt{\pi}}$ $\hspace{3cm}$ (2.41)

- $\dfrac{\Gamma(v+m)}{\Gamma(v+1)} = v(v+1)(v+2)(v+3)\ldots(v+m)$ $\hspace{2cm}$ (2.42)

CHAPTER 3

FRACTIONAL CALCULUS DEFINITIONS

This chapter presents some definitions of fractional derivatives and integrals. It includes some important relationships between different definitions and their main properties.

3.1   Left and Right Fractional Derivatives

The left and right fractional derivatives of a function $f(t)$ can be illustrated by as assuming that the function $f(t)$ which is defined in the interval $[a,b]$. The intervals $[a,t]$ and $[t,b]$ represent the past and the future of function $f(t)$, respectively as shown in Figure 3.1. The fractional derivative at the left end of $[a,b]$ is the left fractional derivative. The fractional derivative at the right end of $[a,b]$ is the right fractional derivative. The left derivative describes the behavior of the function $f(t)$ in the past while the right derivative describes the behavior of the function $f(t)$ in the future.

Left derivative $_aD_t^p f(t)$ Present   Right derivative $_tD_b^p f(t)$

a The past of $f(t)$ t The future of $f(t)$ b
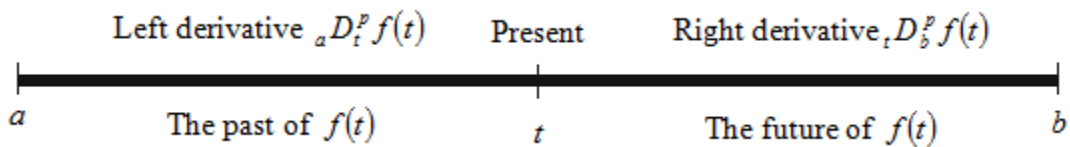
Figure 3.1: The left and right derivatives of $f(t)$

Definition 3.1.1 The left and right Riemann- Liouville fractional integrals of a given function $f(t)$ are given by

$$^{RL}_{a}D_{t}^{-\alpha}f(t)=\frac{1}{\Gamma(\alpha)}\int_{a}^{t}\frac{f(\tau)}{(t-\tau)^{1-\alpha}}d\tau, \qquad t>a, \quad \alpha>0 \tag{3.1}$$

and

$$^{RL}_{b}D_{t}^{-\alpha}f(t)=\frac{1}{\Gamma(\alpha)}\int_{t}^{b}\frac{f(\tau)}{(t-\tau)^{1-\alpha}}d\tau, \qquad t<b, \quad \alpha>0 \tag{3.2}$$

respectively, where $t\in(a,b)$, $(-\infty<a<b<\infty)$ and the order $\alpha\in R^{+}$.

When $\alpha=n\in R^{+}$, the previous integrals provide the (n-th) integrals as

$$_{a}D_{t}^{-n}f(t)=\frac{1}{(n-1)!}\int_{a}^{t}\frac{f(\tau)}{(t-\tau)^{1-n}}d\tau \tag{3.3}$$

and

$$_{t}D_{b}^{-\alpha}f(t)=\frac{1}{(n-1)!}\int_{t}^{b}\frac{f(\tau)}{(\tau-t)^{1-n}}d\tau \tag{3.4}$$

Definition 3.1.2 The left and right Grunwald –Letnikov fractional derivatives of a given function $f(t)$ are defined as

$$^{GL}_{a}D_{t}^{\alpha}f(t)=\lim_{h\to 0}h^{-\alpha}\sum_{j=0}^{N}(-1)^{j}\binom{\alpha}{j}f(t-jh) \tag{3.5}$$

and

16

$$ {}^{GL}_{t}D^{\alpha}_{b}f(t) = \lim_{h \to 0} h^{-\alpha} \sum_{j=0}^{N} (-1)^{j} \binom{\alpha}{j} f(t+jh) \tag{3.6} $$

respectively, where

$$ \binom{\alpha}{j} = \frac{\alpha!}{j!(\alpha-j)!} = \frac{\Gamma(\alpha+1)}{\Gamma(j+1)\Gamma(\alpha-j+1)} \tag{3.7} $$

denotes the binomial coefficients.

Definition 3.1.3 The left and right Riemann–Liouville fractional derivatives of a given function $f(t)$ are given respectively by

$$ {}^{RL}_{a}D^{\alpha}_{t}f(t) = \frac{d^{m}}{dt^{m}}\left[{}_{a}D^{-(m-\alpha)}_{t}f(t)\right] $$

$$ = \frac{1}{\Gamma(m-\alpha)}\frac{d^{m}}{dt^{m}}\int_{a}^{t}\frac{f(\tau)}{(t-\tau)^{1+\alpha-m}}\,d\tau, \qquad t > a \tag{3.8} $$

and

$$ {}^{RL}_{t}D^{\alpha}_{b}f(t) = \frac{d^{m}}{dt^{m}}\left[{}_{a}D^{-(m-\alpha)}_{t}f(t)\right] $$

$$ = \frac{(-1)^{m}}{\Gamma(m-\alpha)}\frac{d^{m}}{dt^{m}}\int_{t}^{b}\frac{f(\tau)}{(t-\tau)^{1+\alpha-m}}\,d\tau, \qquad t < b \tag{3.9} $$

Respectively, where m is a positive integer which satisfies the following relationship $m-1 \leq \alpha < m$ and the function $f(t)$ has absolutely derivatives up to order $m-1$. In general, the Riemann–Liouville fractional derivative is given by

$$_{0}^{RL}D_{t}^{\alpha} f(t) = \frac{1}{\Gamma(m-\alpha)} \frac{d^{m}}{dt^{m}} \int_{0}^{t} \frac{f(\tau)}{(t-\tau)^{1+\alpha-m}} d\tau, \qquad m-1 \leq \alpha < m$$

$$= \sum_{k=0}^{m-1} \frac{t^{k-\alpha}}{\Gamma(k-\alpha+1)} f^{(k)}(0) + \frac{1}{\Gamma(m-\alpha)} \int_{0}^{t} \frac{f^{(m)}(\tau)}{(t-\tau)^{1+\alpha-m}} \qquad (3.10)$$

where $f^{(k)}(\cdot)$ is the (k-th) order derivative of the function $f(\cdot)$.

if $\alpha \in (0,1)$ the definitions in (3.8) and (3.9) can be expressed as

$$_{a}^{RL}D_{t}^{\alpha} f(t) = \frac{1}{\Gamma(1-\alpha)} \frac{d}{dt} \int_{a}^{t} \frac{f(\tau)}{(t-\tau)^{\alpha}} d\tau, \qquad t > a \qquad (3.11)$$

and

$$_{t}^{RL}D_{b}^{\alpha} f(t) = -\frac{1}{\Gamma(1-\alpha)} \frac{d}{dt} \int_{t}^{b} \frac{f(\tau)}{(\tau-t)^{\alpha}} d\tau, \qquad t < b \qquad (3.12)$$

The Grunwald –Letnikov and Riemann–Liouville fractional derivatives are equivalent if the function $f(t)$ is suitably smooth. Therefore

$$_{a}^{GL}D_{t}^{\alpha} f(t) = _{a}^{RL}D_{t}^{\alpha} f(t) \qquad (3.13)$$

and

$$_{t}^{GL}D_{b}^{\alpha} f(t) = _{t}^{RL}D_{b}^{\alpha} f(t) \qquad (3.14)$$

18

$$^C_a D^n_t f(t) = f^n(t) \tag{3.15}$$

and

$$^C_t D^n_b f(t) = (-1)^n f^n(t) \tag{3.16}$$

Definition 3.1.4 The left and right Caputo fractional derivatives of a given function $f(t)$ are given by

$$
\begin{aligned}
^C_a D^\alpha_t f(t) &= {_a}D_t^{-(m-\alpha)} f^{(m)}(t) \\
&= \frac{1}{\Gamma(m-\alpha)} \int_a^t \frac{f^{(m)}(\tau)}{(t-\tau)^{1+\alpha-m}} d\tau, \qquad t > a
\end{aligned} \tag{3.17}
$$

and

$$
\begin{aligned}
^C_t D^\alpha_b f(t) &= {_a}D_t^{-(m-\alpha)} f^{(m)}(t) \\
&= \frac{(-1)^m}{\Gamma(m-\alpha)} \int_t^b \frac{f^{(m)}(\tau)}{(\tau-t)^{1+\alpha-m}} d\tau, \qquad t < b
\end{aligned} \tag{3.18}
$$

respectively, where m is a positive integer which satisfies the following relationship $m-1 \le \alpha < m$.

For $\alpha \in (0,1)$ the left and right Caputo fractional derivatives have the following form

$$^C_a D^\alpha_t f(t) = \frac{1}{\Gamma(1-\alpha)} \int_a^t \frac{f^{(1)}(\tau)}{(t-\tau)^\alpha} d\tau \tag{3.19}$$

and

$$^C_tD^\alpha_b f(t) = \frac{-1}{\Gamma(1-\alpha)}\int_t^b \frac{f^{(1)}(\tau)}{(\tau-t)^\alpha}d\tau, \qquad (3.20)$$

The regularized Caputo derivative has the form

$$^C_0D^\alpha_t f(t) = \frac{1}{\Gamma(m-\alpha)}\int_0^t \frac{f^{(m)}(\tau)}{(t-\tau)^{1+\alpha-m}}d\tau, \qquad m-1<\alpha<m \qquad (3.21)$$

Also, equations (3.19) and (3.20) can be written as

$$^C_aD^\alpha_t f(t) = {}^{RL}_aD^\alpha_t\left[f(t) - \sum_{k=0}^{m-1}\frac{f^{(k)}(a)}{k!}(t-a)^k\right],$$

$$= {}^{RL}_aD^\alpha_t - \sum_{k=0}^{m-1}\frac{f^{(k)}(a)}{\Gamma(k-\alpha+1)}(t-a)^k, \qquad m-1<\alpha<m \qquad (3.22)$$

and

$$^C_tD^\alpha_b f(t) = {}^{RL}_tD^\alpha_b\left[f(t) - \sum_{k=0}^{n-1}\frac{f^{(k)}(b)}{k!}(t-b)^k\right],$$

$$= {}^{RL}_tD^\alpha_b - \sum_{k=0}^{n-1}\frac{f^{(k)}(b)}{\Gamma(k-\alpha+1)}(t-b)^k, \qquad m-1<\alpha<m \qquad (3.23)$$

which represent the relationship between Riemann–Liouville and Caputo fractional derivatives (right and left), respectively.

For $\alpha \in (0,1)$, we have

$$\prescript{C}{a}{D}_t^\alpha f(t) = \prescript{RL}{a}{D}_t^\alpha \left[f(t) - f(a) \right]$$

$$= \prescript{RL}{a}{D}_t^\alpha f(t) - \frac{f(a)}{\Gamma(1-\alpha)(t-a)^\alpha} \tag{3.24}$$

and

$$\prescript{C}{t}{D}_b^\alpha f(t) = \prescript{RL}{t}{D}_b^\alpha \left[f(t) - f(a) \right]$$

$$= \prescript{RL}{t}{D}_b^\alpha f(t) - \frac{f(b)}{\Gamma(1-\alpha)(b-t)^\alpha} \tag{3.25}$$

The general relationship between Riemann–Liouville and Caputo operators has the following form

$$\prescript{C}{0}{D}_t^\alpha f(t) = \prescript{RL}{0}{D}_t^\alpha \left[f(t) - \sum_{k=0}^{m-1} \frac{f^{(k)}(a)}{k!}(t)^k \right],$$

$$= \prescript{RL}{a}{D}_t^\alpha - \sum_{k=0}^{m-1} \frac{f^{(k)}(0)}{\Gamma(k-\alpha+1)} t^{k-\alpha}, \qquad m-1 < \alpha < m \tag{3.26}$$

Table 3.1 shows the fractional derivatives of some functions used in many applications using Riemann-Liouville definition.

Table 3.1: Riemann-Liouville Fractional Derivatives of Some Functions

$f(t)$	$\prescript{RL}{0}{D}_t^\alpha f(t) \quad (t > 0, \quad \alpha \in R)$
$\mu(t)$	$\dfrac{t^{-\alpha}}{\Gamma(1-\alpha)}$

$\mu(t-\beta)$	$\begin{cases} \dfrac{(t-\beta)^{-\alpha}}{\Gamma(1-\alpha)}, & (t > \beta) \\ 0 & (0 \leq t \leq \beta) \end{cases}$
$c, \quad c:\text{Constant}$	$\dfrac{c}{\Gamma(1-\alpha)}t^{-\alpha}$
$t^{\gamma}, \quad \gamma \geq -1$	$\dfrac{\Gamma(\gamma+1)}{\Gamma(\gamma+1-\alpha)}t^{\gamma-\alpha}$
$e^{\eta t}$	$t^{-\alpha}E_{1,1-\alpha}(\eta t)$
$\ln(t)$	$\dfrac{t^{-\alpha}}{\Gamma(1-\alpha)}\left(\ln(t)+\psi(1)-\psi(1-\alpha)\right)$
$t^{\gamma-1}\ln(t)$	$\dfrac{t^{\gamma-\alpha-1}}{\Gamma(\gamma-\alpha)}\left(\ln(t)+\psi(\gamma)-\psi(\gamma-\alpha)\right), \quad (\mathrm{Re}(\gamma) > 0)$

where

$\mu(t)$ The Heaviside unit step.

$\psi(\cdot)$ The Digamma function.

Example 3.1

This example shows the fractional derivative of the function $f(t) = t^3$ using Riemann-Liouville and Caputo definitions.

$$^{RL}_{0}D_t^{\frac{3}{4}} f(t) = {}^{RL}_{0}D_t^{\frac{1}{2}}(t^3) = \frac{1}{\Gamma\left(m-\dfrac{3}{4}\right)} \frac{d^m}{dt^m} \int_0^t \frac{\tau^3}{(t-\tau)^{1+\frac{3}{4}-m}} d\tau \tag{3.27}$$

Choosing $m = 1$, we get

$$\,^{RL}_0 D_t^{\frac{1}{2}}\!\left(t^3\right) = \frac{1}{\Gamma\!\left(1-\frac{3}{4}\right)} \frac{d}{dt}\int_0^t \frac{\tau^3}{(t-\tau)^{1+\frac{3}{4}-1}}\,d\tau$$

$$= \frac{1}{\Gamma\!\left(\frac{1}{4}\right)} \frac{d}{dt}\int_0^t \frac{\tau^3}{(t-\tau)^{\frac{3}{4}}}\,d\tau$$

$$= \frac{1}{\Gamma\!\left(\frac{1}{4}\right)} \frac{d}{dt}\int_0^t \tau^3 (t-\tau)^{-\frac{3}{4}}\,d\tau$$

$$= \frac{1}{\Gamma\!\left(\frac{1}{4}\right)} \frac{d}{dt}\left(\frac{512 t^{\frac{13}{4}}}{195}\right)$$

$$= \frac{1}{\Gamma\!\left(\frac{1}{4}\right)} \frac{128}{15} t^{\frac{9}{4}} \tag{3.28}$$

where $\Gamma\!\left(\frac{1}{4}\right)$ can be expressed as following infinite product

$$\Gamma\!\left(\frac{1}{4}\right) = (2\pi)^{\frac{3}{4}} \prod_{k=1}^{\infty} \tanh\!\left(\frac{\pi k}{2}\right) \tag{3.29}$$

Using Caputo definition

$$\,^C_0 D_t^{\frac{3}{4}} f(t) = \,^C_0 D_t^{\frac{3}{4}}\!\left(t^3\right) = \frac{1}{\Gamma\!\left(m-\frac{3}{4}\right)} \int_0^t \frac{\dfrac{d^m}{d\tau^m}\!\left(\tau^3\right)}{(t-\tau)^{1+\frac{3}{4}-m}}\,d\tau \tag{3.30}$$

Choosing $m=1$, we get

$$
{}_{0}^{C}D_{t}^{\frac{3}{4}}f(t) = {}_{0}^{C}D_{t}^{\frac{3}{4}}(t^{3}) = \frac{1}{\Gamma\left(1-\frac{3}{4}\right)} \int_{0}^{t} \frac{\frac{d}{d\tau}(\tau^{3})}{(t-\tau)^{1+\frac{3}{4}-1}} d\tau
$$

$$
= \frac{1}{\Gamma\left(\frac{1}{4}\right)} \int_{0}^{t} 3\tau^{2}(t-\tau)^{-\frac{3}{4}} d\tau
$$

$$
= \frac{1}{\Gamma\left(\frac{1}{4}\right)} \frac{128}{15} t^{\frac{9}{4}} \tag{3.31}
$$

It can be concluded that

$$
\sum_{k=0}^{m-1} \frac{f^{(k)}(0)}{\Gamma(k-\alpha+1)} t^{k-\alpha} = 0 \tag{3.32}
$$

since

$$
{}_{0}^{C}D_{t}^{\alpha}f(t) = {}_{a}^{RL}D_{t}^{\alpha}f(t) - \sum_{k=0}^{m-1} \frac{f^{(k)}(0)}{\Gamma(k-\alpha+1)} t^{k-\alpha}, \qquad m-1 < \alpha < m
$$

There are reasons made Caputo arrived at his definition. Such as making the fractional divertive of a constant is zero and finding the fractional derivative of some special functions such as the Dirac delta function. The Caputo definition may take the following form

$$
{}_{-\infty}^{C}D_{t}^{\alpha}f(t) = \frac{1}{\Gamma(m-\alpha)} \int_{-\infty}^{t} \frac{f^{(m)}(\tau)}{(t-\tau)^{1+\alpha-m}} d\tau, \qquad (m-1 < \alpha < m) \tag{3.33}
$$

Therefore

$$\,_{-\infty}^{C}D_t^{\alpha}\{C\} = 0 \tag{3.34}$$

where C is a constant.

Example 3.2

This example shows the fractional derivative of the Dirac delta function $\delta(t)$.

Solution

It is known that the Dirac delta function has the following property

$$\int_a^b \phi(t)\delta(t)dt = \begin{cases} \phi(0) & a < 0 < b \\ 0 & a < b < 0 \quad or \quad 0 < a < b \\ \text{Undefined} & a = 0 \quad or \quad b = 0 \end{cases} \tag{3.35}$$

Using Caputo definition is appropriate to find the fraction derivative of the given function. Therefore

$$D^{\alpha}\delta(t) = \frac{1}{\Gamma(-\alpha)}\int_{-\infty}^{t}\frac{\delta(\tau)}{(t-\tau)^{\alpha+1}}d\tau$$

$$= \frac{1}{\Gamma(-\alpha)}\int_{-\infty}^{t}\delta(\tau)(t-\tau)^{-\alpha-1}d\tau$$

$$= \frac{t^{-\alpha-1}}{\Gamma(-\alpha)} \quad 0 < \alpha < 1 \tag{3.36}$$

It is known that the first derivative of the function is when $\alpha = 1$. In this case, the first

derivative of the Dirac delta function $\delta(t)$ is called doublet function or the unit doublet

which can be evaluation as the following

$$\delta(t) = \lim_{\varepsilon \to 0} \frac{1}{\varepsilon} \Pi\left(\frac{t}{\varepsilon}\right) \tag{3.37}$$

The unit rectangular pulse function $\Pi\left(\dfrac{t}{\varepsilon}\right)$ is shown in Figure 3.2 and can be expressed

as

$$\Pi\left(\frac{t}{\varepsilon}\right) = \begin{cases} 1 & for \quad |t| \le \dfrac{\varepsilon}{2} \\ 0 & otherwise \end{cases} \tag{3.38}$$

or

$$\Pi\left(\frac{t}{\varepsilon}\right) = \mu\left(t + \frac{\varepsilon}{2}\right) - \mu\left(t - \frac{\varepsilon}{2}\right) \tag{3.39}$$
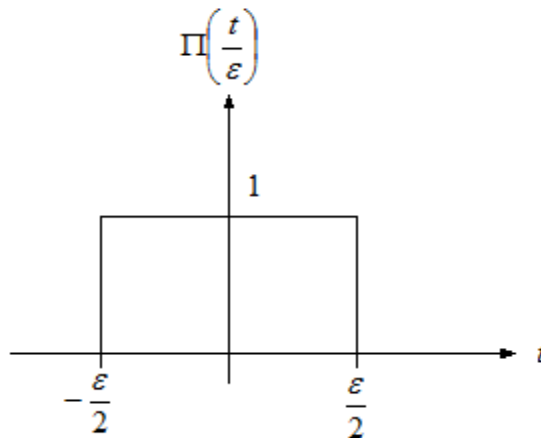
Figure 3.2: The representation of $\Pi\left(\dfrac{t}{\varepsilon}\right)$

26

Therefore

$$\overset{\bullet}{\delta}(t) = \lim_{\varepsilon \to 0} \frac{1}{\varepsilon} \frac{d}{dt}\left[\mu\left(t + \frac{\varepsilon}{2}\right) - \mu\left(t - \frac{\varepsilon}{2}\right)\right]$$

$$= \lim_{\varepsilon \to 0} \frac{1}{\varepsilon} \delta\left(t + \frac{\varepsilon}{2}\right) - \lim_{\varepsilon \to 0} \frac{1}{\varepsilon} \delta\left(t - \frac{\varepsilon}{2}\right) \tag{3.40}$$

which can be shown in Figure 3.3
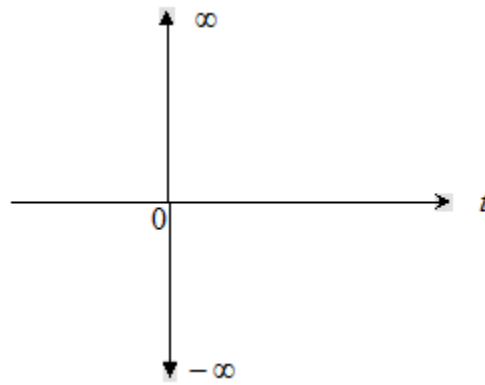
Figure 3.3: The doublet function $\overset{*}{\delta}(t)$

It can be noticed that the Dirac delta function $\delta(t)$ is an even function and its first derivative is odd. It is known that the unit doublet represents the inverse Laplace of $\{s\}$. Therefore

$$L^{-1}\{s\} = \overset{\bullet}{\delta}(t) \tag{3.41}$$

27

3.2 Properties of Fractional Derivatives

Some of the most properties in fractional calculus are:

3.2.1 Linearity

The fractional derivative is a linear operator

$$D^\alpha\left(\gamma\, f(t)+\eta\, g(t)\right)=\gamma\, D^\alpha f(t)+\eta\, D^\alpha g(t) \tag{3.42}$$

Proof

Using Grunwald –Letnikov fractional derivative definition

$$^{GL}_{a}D^\alpha_t\left(\gamma\, f(t)+\eta\, g(t)\right)=\lim_{h\to 0}h^{-\alpha}\sum_{j=0}^{N}(-1)^j\binom{\alpha}{j}\left(\gamma\, f(t-jh)+\eta\, g(t-jh)\right)$$

$$=\gamma\lim_{h\to 0}h^{-\alpha}\sum_{j=0}^{N}(-1)^j\binom{\alpha}{j}\left(f(t-jh)\right)+\eta\lim_{h\to 0}h^{-\alpha}\sum_{j=0}^{N}(-1)^j\binom{\alpha}{j}\left(g(t-jh)\right) \tag{3.43}$$

Therefore

$$^{GL}_{a}D^\alpha_t\left(\gamma\, f(t)+\eta\, g(t)\right)=\gamma\;^{GL}_{a}D^\alpha_t f(t)+\eta\;^{GL}_{a}D^\alpha_t g(t) \tag{3.44}$$

Similarly, using Riemann–Liouville fractional derivative definition

$$^{RL}_{a}D^\alpha_t\left(\gamma\, f(t)+\eta\, g(t)\right)=\frac{1}{\Gamma(m-\alpha)}\frac{d^m}{dt^m}\int_a^t\frac{\left(\gamma\, f(\tau)+\eta\, g(\tau)\right)}{(t-\tau)^{1+\alpha-m}}d\tau$$

$$=\frac{\gamma}{\Gamma(m-\alpha)}\frac{d^m}{dt^m}\int_a^t\frac{f(\tau)}{(t-\tau)^{1+\alpha-m}}d\tau+\frac{\eta}{\Gamma(m-\alpha)}\frac{d^m}{dt^m}\int_a^t\frac{g(\tau)}{(t-\tau)^{1+\alpha-m}}d\tau \tag{3.45}$$

Therefore

$$
{}^{RL}_{a}D^{\alpha}_{t}\left(\gamma\,f(t)+\eta\,g(t)\right)=\gamma\;{}^{RL}_{a}D^{\alpha}_{t}f(t)+\eta\;{}^{RL}_{a}D^{\alpha}_{t}g(t)
\tag{3.46}
$$

Also, this property can be proven using Caputo fractional derivative definition

$$
{}^{C}_{a}D^{\alpha}_{t}\left(\gamma\,f(t)+\eta\,g(t)\right)=\frac{1}{\Gamma(m-\alpha)}\int_{a}^{t}\frac{\left(\gamma\,f^{(m)}(\tau)+\eta\,g^{(m)}(\tau)\right)}{(t-\tau)^{1+\alpha-m}}d\tau
$$

$$
=\frac{\gamma}{\Gamma(m-\alpha)}\int_{a}^{t}\frac{f^{(m)}(\tau)}{(t-\tau)^{1+\alpha-m}}d\tau+\frac{\eta}{\Gamma(m-\alpha)}\int_{a}^{t}\frac{g^{m}(\tau)}{(t-\tau)^{1+\alpha-m}}d\tau
\tag{3.47}
$$

Therefore

$$
{}^{C}_{a}D^{\alpha}_{t}\left(\gamma\,f(t)+\eta\,g(t)\right)=\gamma\;{}^{C}_{a}D^{\alpha}_{t}f(t)+\eta\;{}^{C}_{a}D^{\alpha}_{t}g(t)
\tag{3.48}
$$

3.2.2   Non-Commutation

The law of exponents in the fractional calculus does not hold for the standard fractional derivative. In other words, it is non-commutative. Therefore

$$
D^{\alpha}D^{n}f(t)=D^{n}D^{\alpha}f(t)\neq D^{\alpha+n}f(t)\qquad \alpha\in R,\; n\in N
\tag{3.49}
$$

$$
D^{\alpha}D^{n}f(t)\neq D^{n}D^{\alpha}f(t)=D^{\alpha+n}f(t)\qquad \alpha\in R,\; n\in N
\tag{3.50}
$$

where $(n-1<\alpha<n)$

The following relationship holds for $\alpha, n < 0$

$$
{}_{a}D^{\alpha}_{t}\left({}_{a}D^{n}_{t}f(t)\right)={}_{a}D^{\alpha+n}_{t}f(t)
\tag{3.51}
$$

It can be said that the fractional integral is commutative. This property holds for fractional derivative under this condition $f^{(k)}(a)=0,\;(k=0,1,\ldots,n-1)$. Therefore

$$_aD_t^\alpha\left(_aD_t^n f(t)\right)=_aD_t^{\alpha+n}f(t), \qquad \alpha,n>0 \tag{3.52}$$

In other words, it is always true that

$$_aD_t^\alpha\left(_aD_t^n f(t)\right)=_aD_t^{\alpha+n}f(t), \qquad \alpha,n<0 \tag{3.53}$$

But not always true that

$$_aD_t^\alpha\left(_aD_t^n f(t)\right)=_aD_t^{\alpha+n}f(t), \qquad \alpha,n>0 \tag{3.54}$$

Where $_aD_t^\alpha$ is the fractional derivative operator of all different definitions such as Riemann-Liouville, Grunwald-Letnikov, Caputo and others.

CHAPTER 4

FRACTIONAL ORDER SYSTEMS

This chapter includes time and frequency domain analysis of some transfer functions using some special functions. It covers the stability conditions of fractional order systems with some examples.

4.1 Fractional Transfer Function

The fractional LTI system in Figure 4.1 can be represented by the following fractional differential equation

$$a_n D^{\alpha_n} y(t) + a_{n-1} D^{\alpha_{n-1}} y(t) + \cdots + a_0 D^{\alpha_0} y(t)$$
$$= b_m D^{\beta_m} u(t) + b_{m-1} D^{\beta_{m-1}} u(t) + \cdots + b_0 D^{\beta_0} u(t) \tag{4.1}$$

This also can be expressed as

$$\sum_{k=0}^{n} a_k D^{\alpha_k} y(t) = \sum_{k=0}^{m} b_k D^{\beta_k} u(t) \tag{4.2}$$

The fractional transfer function of the fractional LTI system can be given by taking the Laplace transform and assuming that initial conditions are zero. Therefore

$$G(s) = \frac{Y(s)}{U(s)} = \frac{b_m s^{\beta_m} + b_{m-1} s^{\beta_{m-1}} + \cdots + b_0 s^{\beta_0}}{a_n s^{\alpha_n} + a_{n-1} s^{\alpha_{n-1}} + \cdots + a_0 s^{\alpha_0}} \tag{4.3}$$

For commensurate transfer function

$$G(s) = \frac{\displaystyle\sum_{k=0}^{m} b_k \left(s^{\alpha}\right)^k}{\displaystyle\sum_{k=0}^{n} a_k \left(s^{\alpha}\right)^k} \tag{4.4}$$

where $\left(\alpha_k\right)$ and $\left(\beta_k\right)$ are integer multiple of a least common divisor $\alpha > 0$. Therefore, a pseudo-rational transfer function $H(\lambda)$ is given by

$$H(\lambda) = \frac{\displaystyle\sum_{k=0}^{m} b_k \lambda^k}{\displaystyle\sum_{k=0}^{n} a_k \lambda^k} = \frac{Q(\lambda)}{P(\lambda)} \tag{4.5}$$

where $\lambda = s^{\alpha}$.

$$u(t) \longrightarrow \boxed{\begin{array}{c} \text{Fractional} \\ \text{LTI} \end{array}} \longrightarrow y(t)$$
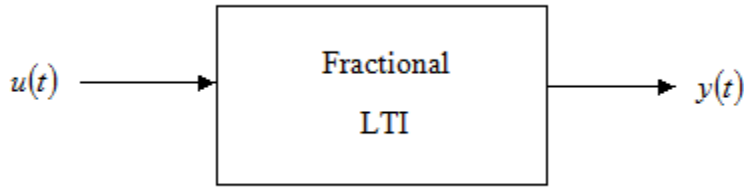
Figure 4.1: The fractional LTI

4.2   Time and Frequency Domains Analysis

The characteristic of fractional LTI systems can be obtained using some mathematical tools. These tools analyze the system for stability and frequency response using Laplace transform. The transient response of the fractional LTI can be obtained using the inverse Laplace transform.

4.2.1   Laplace Transform

The fractional LTI systems can be analyzed easily using Laplace transforms. Some special functions are important for obtaining the Laplace transform. These

functions are introduced in chapter 2 which includes some of their properties. Table 4.1 shows the Laplace transform pairs. The table contains some fractional and irrational operators.

Table 4.1: Laplace transform pairs

$f(t)$	$F(s)$
$\dfrac{t^{n-1}}{\Gamma(n)}, \quad (n:0,1,2,\ldots)$	$\dfrac{1}{s^n}$
$\dfrac{2^n t^{n-\frac{1}{2}}}{1\times3\times5\times\cdots(2n-1)\sqrt{\pi}}, \quad (n:0,1,2,\ldots)$	$\dfrac{1}{s^n\sqrt{s}}$
$\dfrac{t^{-1-\frac{n}{2}}}{\Gamma\left(-\dfrac{n}{2}\right)}, \quad (n:0,1,2,\ldots)$	$s^{\frac{n}{2}}$
$erf(at)$	$\dfrac{e^{\left(\frac{s}{2a}\right)^2}}{s}erfc\left(\dfrac{s}{2a}\right)$
$erfc\left(\dfrac{a}{2\sqrt{t}}\right)$	$\dfrac{e^{-a\sqrt{s}}}{s}$
$\dfrac{1}{a}e^{a^2t}erf\left(a\sqrt{t}\right)$	$\dfrac{1}{\sqrt{s}\left(s-a^2\right)}$
$\dfrac{\cos\left(2\sqrt{at}\right)}{\sqrt{t}}$	$\sqrt{\dfrac{\pi}{s}}e^{-\frac{a}{s}}$
$\dfrac{\cosh\left(2\sqrt{at}\right)}{\sqrt{t}}$	$\sqrt{\dfrac{\pi}{s}}e^{\frac{a}{s}}$
$\dfrac{\sin\left(2\sqrt{at}\right)}{\sqrt{t}}$	$\dfrac{1}{s}\sqrt{\dfrac{\pi}{s}}e^{-\frac{a}{s}}$
$\dfrac{\sinh\left(2\sqrt{at}\right)}{\sqrt{t}}$	$\dfrac{1}{s}\sqrt{\dfrac{\pi}{s}}e^{\frac{a}{s}}$

Example 4.1

This example shows the Laplace transform $F(s)$ of the following function

$$f(t) = \frac{1}{a} e^{a^2 t} erf(a\sqrt{t})$$

Solution

Using equation (2.19), we have

$$erf(x) = \frac{2}{\sqrt{\pi}} e^{-x^3} \sum_{n=0}^{\infty} \frac{2^{2n+1} x^{2n+1}}{(2n+2)!}(n+1)! \qquad (4.6)$$

Therefore

$$erf(a\sqrt{t}) = \frac{2}{\sqrt{\pi}} e^{-a^3 t} \sum_{n=0}^{\infty} \frac{2^{2n+1} (a\sqrt{t})^{2n+1}}{(2n+2)!}(n+1)! \qquad (4.7)$$

So

$$\frac{1}{a} e^{a^3 t} erf(a\sqrt{t}) = \frac{1}{a} e^{a^3 t} \frac{2}{\sqrt{\pi}} e^{-a^3 t} \sum_{n=0}^{\infty} \frac{2^{2n+1} (a\sqrt{t})^{2n+1}}{(2n+2)!}(n+1)!$$

$$= \frac{1}{a} \frac{2}{\sqrt{\pi}} \sum_{n=0}^{\infty} \frac{2^{2n+1} (a\sqrt{t})^{2n+1}}{(2n+2)!}(n+1)! \qquad (4.8)$$

Equation (4.8) can be expanded as

$$\frac{1}{a} \frac{2}{\sqrt{\pi}} \sum_{n=0}^{\infty} \frac{2^{2n+1} (a\sqrt{t})^{2n+1}}{(2n+2)!}(n+1)! =$$

$$\left\{ \frac{2\sqrt{t}}{\sqrt{\pi}} + \frac{4a^2}{3\sqrt{\pi}} t^{\frac{3}{2}} + \frac{8a^4}{15\sqrt{\pi}} t^{\frac{5}{2}} + \frac{16a^2}{105\sqrt{\pi}} t^{\frac{7}{2}} + \frac{32a^2}{945\sqrt{\pi}} t^{\frac{9}{2}} + \dots \right\} \qquad (4.9)$$

Taking the Laplace transform of equation (4.9), we have

$$L\left\{\frac{2\sqrt{t}}{\sqrt{\pi}} + \frac{4a^2}{3\sqrt{\pi}}t^{\frac{3}{2}} + \frac{8a^4}{15\sqrt{\pi}}t^{\frac{5}{2}} + \frac{16a^2}{105\sqrt{\pi}}t^{\frac{7}{2}} + \frac{32a^2}{945\sqrt{\pi}}t^{\frac{9}{2}} + \dots\right\}$$

$$= \left\{\frac{2}{\sqrt{\pi}}\frac{\Gamma\left(\frac{3}{2}\right)}{s^{\frac{3}{2}}} + \frac{4a^2}{3\sqrt{\pi}}\frac{\Gamma\left(\frac{5}{2}\right)}{s^{\frac{5}{2}}} + \frac{4a^4}{15\sqrt{\pi}}\frac{\Gamma\left(\frac{7}{2}\right)}{s^{\frac{7}{2}}} + \frac{16a^6}{105\sqrt{\pi}}\frac{\Gamma\left(\frac{9}{2}\right)}{s^{\frac{9}{2}}} + \frac{32a^8}{945\sqrt{\pi}}\frac{\Gamma\left(\frac{11}{2}\right)}{s^{\frac{11}{2}}} + \dots\right\} \quad (4.10)$$

where

$$\Gamma\left(\frac{1}{2}\right) = \sqrt{\pi} \quad , \quad \Gamma\left(\frac{3}{2}\right) = \frac{\sqrt{\pi}}{2} \quad , \quad \Gamma\left(\frac{5}{2}\right) = \frac{3}{4}\sqrt{\pi}, \quad \Gamma\left(\frac{7}{2}\right) = \frac{15}{2}\sqrt{\pi}, \quad \Gamma\left(\frac{9}{2}\right) = \frac{105}{16}\sqrt{\pi}$$

$$\Gamma\left(\frac{11}{2}\right) = \frac{945}{32}\sqrt{\pi}$$

So, equation (4.10) can be written as

$$= \left\{\frac{1}{s^{\frac{3}{2}}} + \frac{a^2}{s^{\frac{5}{2}}} + \frac{a^4}{s^{\frac{7}{2}}} + \frac{a^6}{s^{\frac{9}{2}}} + \frac{a^8}{s^{\frac{11}{2}}} + \dots\right\}$$

$$= \frac{1}{s^{\frac{3}{2}}}\left\{1 + \frac{a^2}{s} + \frac{a^4}{s^2} + \frac{a^6}{s^3} + \frac{a^8}{s^4} + \dots\right\}$$

$$= \frac{1}{s^{\frac{3}{2}}}\sum_{n=0}^{\infty}\left(\frac{a^2}{s}\right)^n \qquad (4.11)$$

Using the power series expansion, we get

$$\frac{1}{s^{\frac{3}{2}}}\sum_{n=0}^{\infty}\left(\frac{a^2}{s}\right)^n = \frac{1}{s^{\frac{3}{2}}}\frac{1}{1-\frac{a^2}{s}} \quad , \quad \left|\frac{a^2}{s}\right| < 1$$

$$= \frac{1}{s^{\frac{3}{2}}} \frac{s}{s-a^2} \tag{4.12}$$

Therefore

$$F(s) = \frac{1}{\sqrt{s}} \frac{1}{s-a^2} \tag{4.13}$$

4.2.2   Inverse Laplace Transform

The inverse Laplace transform of a non fractional transfer function is usually obtained by using partial fraction expansion which can be used only for proper rational functions. The inverse Laplace of a fractional transfer function can be found using some special functions such as the Mittag-Liffler, Wright, and Minardi functions to avoid using partial fraction method.

4.2.2.1   The Mittag-Liffler Function

The Mittag-Liffler function was introduced in 1903 by the Swedish mathematician Gosta Mittag Liffler. The Mittag-Liffler function in one parameter (α) is defined by the following expression

$$E_\alpha(z) = \sum_{k=0}^{\infty} \frac{z^k}{\Gamma(\alpha k + 1)} \qquad \alpha > 0, \ z \in C, \tag{4.14}$$

The generalization Mittag-Liffler function in two parameters (α, β) is given by

$$E_{\alpha,\beta}(z) = \sum_{k=0}^{\infty} \frac{z^k}{\Gamma(\alpha k + \beta)} \qquad \alpha, \beta > 0, \ z \in C, \tag{4.15}$$

36

The generalization Mittag-Liffler function in three parameters (α, β, γ) is defined by

$$E_{\alpha,\beta}^{\gamma}(z) = \sum_{k=0}^{\infty} \frac{(k+\gamma)! z^k}{(k!)\Gamma(\alpha k + \alpha\gamma + \beta)} \qquad \alpha, \beta, \gamma > 0, \ z \in C, \qquad (4.16)$$

Some properties of the Mittag-Liffler function are:

$$E_{\alpha,\beta}(z) = z E_{\alpha,\alpha+\beta}(z) + \frac{1}{\Gamma(\beta)} \qquad (4.17)$$

$$E_{\alpha,\beta}(z) = \beta E_{\alpha,\beta+1}(z) + \alpha z \frac{d}{dz} E_{\alpha,\beta+1}(z) \qquad (4.18)$$

$$\left(\frac{d}{dz}\right)\left[z^{\beta-1} E_{\alpha,\beta}(z^\alpha)\right] = z^{\beta-2} E_{\alpha,\beta-1}(z^\alpha) \qquad (4.19)$$

$$\left(\frac{d}{dz}\right)^m \left[z^{\beta-1} E_{\alpha,\beta}(z^\alpha)\right] = z^{\beta-m-1} E_{\alpha,\beta-m}(z^\alpha), \qquad \mathrm{Re}(\beta-m) > 0, \quad m = 0,1,\dots \qquad (4.20)$$

$$E_{\alpha,\beta}(z) + E_{\alpha,\beta}(-z) = 2 E_{2\alpha,\beta}(z^2) \qquad (4.21)$$

$$E_{\alpha,\beta}(z) - E_{\alpha,\beta}(-z) = 2z E_{2\alpha,\alpha+\beta}(z^2) \qquad (4.22)$$

Some values of the Mittag-Liffler function are:

$$E_0(-z) = \frac{1}{1+z} \qquad (4.23)$$

$$E_{\frac{1}{2}}(-z) = e^{z^2} erfc(z) \qquad (4.24)$$

$$E_1(-z) = e^{-x} \qquad (4.25)$$

$$E_2(-z) = \cos(\sqrt{z}) \qquad (4.26)$$

37

$$E_{0,2}(z) = \frac{1}{1-z} \tag{4.27}$$

$$E_{\frac{1}{2},\frac{1}{2}}(z) = \frac{1}{\sqrt{\pi}} + z e^{z^2} erfc(-z) \tag{4.28}$$

$$E_{\frac{1}{2},1}(z) = e^{z^2} erfc(-z) \tag{4.29}$$

$$E_{\frac{1}{2},\frac{3}{2}}(z) = \frac{1}{z}\left[e^{z^2} erfc(z) - 1\right] \tag{4.30}$$

$$E_{\frac{1}{2},2}(z) = \frac{1}{z^2}\left[e^{z^2} erfc(-z) - \frac{2z}{\sqrt{\pi}} - 1\right] \tag{4.31}$$

$$E_{1,1}(z) = E_1(z) = e^z \tag{4.32}$$

$$E_{1,2}(z) = \frac{e^{-z} - 1}{z} \tag{4.33}$$

$$E_{1,3}(z) = \frac{e^z - z - 1}{z^2} \tag{4.34}$$

$$E_{2,1}(z^2) = \cosh(z) \tag{4.35}$$

$$E_{2,2}(-z) = \frac{\sin(\sqrt{z})}{\sqrt{z}} \tag{4.36}$$

4.2.2.2 The Wright and Mainardi Functions

The two functions are defined by the series representation. The Wright function is given as

$$W_{\alpha,\beta}(z)=\sum_{k=0}^{\infty}\frac{z^k}{(k!)\Gamma(\alpha k+\beta)} \qquad \alpha>-1,\ \beta\in C, \tag{4.37}$$

The Mainardi function takes the following form

$$M_{\alpha}(z)=\sum_{k=0}^{\infty}\frac{(-1)^k z^k}{(k!)\Gamma(-\alpha k+(1-\alpha))} \qquad 0<\alpha<1,\ z\in C, \tag{4.38}$$

It can be noticed that the Minardi function is a special case of the Wright function. The relationship between the two functions is given by

$$M_{\alpha}(z)=W_{-\alpha,1-\alpha}(-z) \qquad 0<\alpha<1,\ z\in C, \tag{4.39}$$

and

$$M_{\alpha}(z)=\frac{1}{\alpha z}W_{-\alpha,0}(-z) \qquad 0<\alpha<1,\ z\in C, \tag{4.40}$$

Some values of the Wright and Mainardi functions are:

$$W_{-\frac{1}{2},1}(-z)=erfc\left(\frac{z}{2}\right) \tag{4.41}$$

$$M_{\frac{1}{2}}(z)=\frac{1}{\sqrt{\pi}}e^{-\frac{z^2}{4}} \tag{4.42}$$

$$M_{\frac{1}{3}}(z)=\sqrt[3]{9}\ Ai\left(\frac{z}{\sqrt[3]{3}}\right) \tag{4.43}$$

$$M_{\frac{2}{3}}(z)=e^{-\frac{2}{27}z^3}\left[\frac{z}{\sqrt[3]{3}}\ Ai\left(\frac{z^2}{\sqrt[3]{81}}\right)-\sqrt[3]{3}Ai^{'}\left(\frac{z^2}{\sqrt[3]{81}}\right)\right] \tag{4.44}$$

where $Ai(z)$ and $Ai^{'}(z)$ are the Airy function and its derivative, respectively.

39

The Mittag-Liffler, Wright, and Minardi functions are important in solving fractional differential equations and finding the inverse Laplace transform without using partial fraction method as shown in the following relations.

$$L^{-1}\left\{\frac{s^{\alpha-1}}{s^{\alpha}\pm\lambda}\right\}=E_{\alpha}\left(\mp\lambda t^{\alpha}\right) \tag{4.45}$$

$$L^{-1}\left\{\frac{1}{s^{\alpha}\pm\lambda}\right\}=t^{\alpha-1}E_{\alpha,\alpha}\left(\mp\lambda t^{\alpha}\right) \tag{4.46}$$

$$L^{-1}\left\{\frac{s^{\alpha-\beta}}{s^{\alpha}\pm\lambda}\right\}=t^{\beta-1}E_{\alpha,\beta}\left(\mp\lambda t^{\alpha}\right) \tag{4.47}$$

$$L^{-1}\left\{\frac{1}{s\left(s^{\alpha}\pm\lambda\right)}\right\}=t^{\alpha}E_{\alpha,\alpha+1}\left(\mp\lambda t^{\alpha}\right) \tag{4.48}$$

$$L^{-1}\left\{\frac{1}{\left(s^{\alpha}\pm\lambda\right)^{\gamma}}\right\}=t^{\alpha\gamma-1}E_{\alpha,\alpha\gamma}^{\gamma}\left(\mp\lambda t^{\alpha}\right) \tag{4.49}$$

$$L^{-1}\left\{\frac{1}{s\left(s^{\alpha}\pm\lambda\right)^{\gamma}}\right\}=t^{\alpha\gamma}E_{\alpha,\alpha\gamma+1}^{\gamma}\left(\mp\lambda t^{\alpha}\right) \tag{4.50}$$

$$L^{-1}\left\{\frac{(\gamma!)s^{\alpha-\beta}}{\left(s^{\alpha}\pm\lambda\right)^{\gamma}}\right\}=t^{\alpha\gamma+\beta-1}E_{\alpha,\beta}^{\gamma}\left(\mp\lambda t^{\alpha}\right) \tag{4.51}$$

$$L^{-1}\left\{e^{-\lambda s^{\alpha}}\right\}=\frac{\alpha\lambda}{t^{\alpha+1}}M_{\alpha}\left(\lambda t^{-\alpha}\right) \qquad 0<\alpha<1,\ \lambda>0 \tag{4.52}$$

$$L^{-1}\left\{s^{\alpha-1}e^{-\lambda s^{\alpha}}\right\}=\frac{1}{t^{\alpha}}M_{\alpha}\left(\lambda t^{-\alpha}\right) \qquad 0<\alpha<1,\ \lambda>0 \tag{4.53}$$

$$L^{-1}\left\{s^{-\beta}e^{-\lambda s^{\alpha}}\right\}=t^{\beta-1}W_{-\alpha,\beta}\left(-\lambda t^{-\alpha}\right) \qquad 0<\alpha<1, \ \lambda>0 \tag{4.54}$$

Example 4.2

This example shows the inverse Laplace $f(t)$ of the given function $F(s)=e^{-a\sqrt{s}}$.

Solution:

The inverse Laplace of the given function can be solved using different methods as the following

Method 1:

The function $F(s)=e^{-a\sqrt{s}}$ can expressed using the power series expansion as

$$e^{-a\sqrt{s}} = \sum_{n=0}^{\infty}\frac{\left(-a\sqrt{s}\right)^{n}}{n!} \tag{4.55}$$

Taking the inverse Laplace of both sides of the previous equation, yields

$$L^{-1}\left\{e^{-a\sqrt{s}}\right\}=L^{-1}\left\{\sum_{n=0}^{\infty}\frac{\left(-a\sqrt{s}\right)^{n}}{n!}\right\}$$

$$=\sum_{n=0}^{\infty}L^{-1}\left\{\frac{\left(-a\sqrt{s}\right)^{n}}{n!}\right\}$$

$$=\sum_{n=0}^{\infty}\frac{\left(-a\right)^{n}}{n!}L^{-1}\left\{s^{\frac{n}{2}}\right\} \tag{4.56}$$

Using Table 4.1, we have

$$L^{-1}\left\{s^{\frac{n}{2}}\right\} = \frac{t^{-1-\frac{n}{2}}}{\Gamma\left(-\frac{n}{2}\right)} \tag{4.57}$$

Therefore:

$$L^{-1}\left\{e^{-a\sqrt{s}}\right\} = \sum_{n=0}^{\infty} \frac{(-a)^n}{n!} \frac{t^{-1-\frac{n}{2}}}{\Gamma\left(-\frac{n}{2}\right)}$$

$$= \frac{t^{-1}}{\Gamma(0)} + \frac{-a}{1!} \frac{t^{-\frac{3}{2}}}{\Gamma\left(-\frac{1}{2}\right)} + \frac{(-a)^2}{2!} \frac{t^{-2}}{\Gamma(-1)} + \frac{(-a)^3}{3!} \frac{t^{-\frac{5}{2}}}{\Gamma\left(-\frac{3}{2}\right)} + \dots$$

$$= \frac{-a}{1!} \frac{t^{-\frac{3}{2}}}{\Gamma\left(-\frac{1}{2}\right)} + \frac{(-a)^3}{3!} \frac{t^{-\frac{5}{2}}}{\Gamma\left(-\frac{3}{2}\right)} + \frac{(-a)^5}{5!} \frac{t^{-\frac{7}{2}}}{\Gamma\left(-\frac{5}{2}\right)} + \dots \tag{4.58}$$

where $\Gamma\left(-\frac{1}{2}\right) = -2\Gamma\left(\frac{1}{2}\right)$, $\Gamma\left(-\frac{3}{2}\right) = \frac{4}{3}\Gamma\left(\frac{1}{2}\right)$, $\Gamma\left(-\frac{5}{2}\right) = -\frac{8}{15}\Gamma\left(\frac{1}{2}\right)$

So

$$L^{-1}\left\{e^{-a\sqrt{s}}\right\} = \frac{-a}{1!} \frac{t^{-\frac{3}{2}}}{-2\Gamma\left(\frac{1}{2}\right)} + \frac{(-a)^3}{3!} \frac{t^{-\frac{5}{2}}}{\frac{4}{3}\Gamma\left(\frac{1}{2}\right)} + \frac{(-a)^5}{5!} \frac{t^{-\frac{7}{2}}}{-\frac{8}{15}\Gamma\left(\frac{1}{2}\right)} + \dots$$

$$L^{-1}\left\{e^{-a\sqrt{s}}\right\} = \frac{a}{1!} \frac{t^{-\frac{3}{2}}}{2\Gamma\left(\frac{1}{2}\right)} - \frac{a^3}{3!} \frac{t^{-\frac{5}{2}}}{\frac{4}{3}\Gamma\left(\frac{1}{2}\right)} + \frac{a^5}{5!} \frac{t^{-\frac{7}{2}}}{\frac{8}{15}\Gamma\left(\frac{1}{2}\right)} - \dots$$

$$= \frac{at^{-\frac{3}{2}}}{2\Gamma\left(\frac{1}{2}\right)}\left[1 - \frac{a^2}{3!}\frac{t^{-1}}{\frac{2}{3}} + \frac{a^4}{5!}\frac{t^{-2}}{\frac{4}{15}} - \cdots\right]$$

$$= \frac{at^{-\frac{3}{2}}}{2\Gamma\left(\frac{1}{2}\right)}\left[1 - \frac{1}{1!}\left(\frac{a^2}{4t}\right) + \frac{1}{2!}\left(\frac{a^2}{4t}\right)^2 - \cdots\right] \tag{4.59}$$

Knowing that

$$\left[1 - \frac{1}{1!}\left(\frac{a^2}{4t}\right) + \frac{1}{2!}\left(\frac{a^2}{4t}\right)^2 - \cdots\right] = e^{-\left(\frac{a^2}{4t}\right)} \tag{4.60}$$

Therefore

$$f(t) = \frac{a}{2\Gamma\left(\frac{1}{2}\right)}e^{-\left(\frac{a^2}{4t}\right)}t^{-\frac{3}{2}}$$

$$= \frac{a}{2\sqrt{\pi}}e^{-\left(\frac{a^2}{4t}\right)}t^{-\frac{3}{2}} \tag{4.61}$$

Method 2:

Assuming that

$$Y(s) = e^{-a\sqrt{s}} \tag{4.62}$$

Therefore

$$\dot{Y}(s) = -\frac{a}{2\sqrt{s}}e^{-a\sqrt{s}}$$

43

$$= -\frac{a}{2\sqrt{s}} Y(s)$$

(4.63)

and

$$\ddot{Y}(s) = \frac{a^2}{4s} Y(s) - \frac{1}{2s} Y'(s)$$

$$= \frac{2a^2 s Y(s) - 4s Y'(s)}{8s^2}$$

(4.64)

So

$$8s^2 Y''(s) = 2a^2 s Y(s) - 4s Y'(s)$$

(4.65)

We get

$$4s Y''(s) + 2Y'(s) - a^2 Y(s) = 0$$

(4.66)

Using the properties of inverse Laplace transforms, we have

$$Y(s) \leftarrow L^{-1} \rightarrow y(t)$$
$$Y'(s) \leftarrow L^{-1} \rightarrow -ty(t)$$
$$Y''(s) \leftarrow L^{-1} \rightarrow t^2 y(t)$$
$$sY''(s) \leftarrow L^{-1} \rightarrow \frac{d}{dt}(t^2 y(t)) = t^2 y'(t) + 2ty(t)$$

Substituting the values above into equation (4.66), we get

$$4\{t^2 y'(t) + 2ty(t)\} - 2ty(t) - a^2 y(t) = 0$$

(4.67)

Therefore

$$4t^2 y'(t) + 8ty(t) - 2ty(t) - a^2 y(t) = 0 \tag{4.68}$$

$$4t^2 y'(t) + 6ty(t) - a^2 y(t) = 0 \tag{4.69}$$

So

$$4t^2 y'(t) = a^2 y(t) - 6ty(t) \tag{4.70}$$

$$4t^2 \frac{dy(t)}{dt} = \left(a^2 - 6t\right) y(t) \tag{4.71}$$

Alternatively, it can be written as

$$\frac{dy(t)}{y(t)} = \left(\frac{a^2 - 6t}{4t^2}\right) dt \tag{4.72}$$

It can be solved by integrating both sides, so

$$\ln(y(t)) = -\frac{a^2}{4t} + \ln\left(t^{-\frac{3}{2}}\right) + c \tag{4.73}$$

Therefore

$$y(t) = Ke^{-\frac{a^2}{4t}} t^{-\frac{3}{2}} \tag{4.74}$$

where $K = -\dfrac{a^2}{4t} + c$ \hfill (4.75)

The constant K can be evaluated using the initial and finial theorems as

$$\lim_{t \to 0} y(t) = \lim_{s \to \infty} sY(s) \tag{4.76}$$

45

$$\lim_{t \to \infty} y(t) = \lim_{s \to 0} sY(s) \tag{4.77}$$

$$\lim_{t \to \infty} ty(t) = \lim_{s \to 0} \left(-\frac{d}{ds} Y(s) \right) \tag{4.78}$$

For large value of t, we have

$$\lim_{t \to \infty} ty(t) = Kt^{-\frac{1}{2}} \tag{4.79}$$

Therefore

$$L[ty(t)] = L\left[Kt^{-\frac{1}{2}} \right] = \frac{K\sqrt{\pi}}{\sqrt{s}} \tag{4.80}$$

Similarly, for small value of s

$$\lim_{s \to 0} \left(-\frac{d}{ds} Y(s) \right) = \lim_{s \to 0} \left(\frac{ae^{-a\sqrt{s}}}{2\sqrt{s}} \right) = \frac{a}{2\sqrt{s}} \tag{4.81}$$

Using equations (4.78), (4.80), and (4.81), we have

$$\frac{K\sqrt{\pi}}{\sqrt{s}} = \frac{a}{2\sqrt{s}} \tag{4.82}$$

Therefore

$$K = \frac{a}{2\sqrt{\pi}} \tag{4.83}$$

So

$$y(t) = \frac{a}{2\sqrt{\pi}} e^{-\frac{a^2}{4t}} t^{-\frac{3}{2}} \tag{4.84}$$

46

Method 3

Using (4.52), we have

$$
L^{-1}\left\{e^{-a\sqrt{s}}\right\} = \frac{a}{2}\frac{1}{t^{\frac{3}{2}}}M_{\frac{1}{2}}\left(at^{-\frac{1}{2}}\right)
\tag{4.85}
$$

Using (4.42), it yields

$$
M_{\frac{1}{2}}\left(at^{-\frac{1}{2}}\right) = \frac{1}{\sqrt{\pi}}e^{-\frac{a^2}{4t}}
\tag{4.86}
$$

Therefore

$$
y(t) = \frac{a}{2\sqrt{\pi}}e^{-\frac{a^2}{4t}}t^{-\frac{3}{2}}
\tag{4.87}
$$

It can be seen that the three different methods lead to the same result.

Example 4.3

This example illustrates the inverse Laplace transform $f(t)$ using Mittage liffler function

of the function $F(s) = \dfrac{1}{\sqrt{s}+a}$

Solution

Using the property (4.46), we have

$$
L^{-1}\left\{\frac{1}{\sqrt{s}+a}\right\} = t^{-\frac{1}{2}}E_{\frac{1}{2},\frac{1}{2}}\left(-at^{\frac{1}{2}}\right)
\tag{4.88}
$$

Using the property (4.17), yields

$$E_{\frac{1}{2},\frac{1}{2}}\left(-at^{\frac{1}{2}}\right) = -at^{\frac{1}{2}}E_{\frac{1}{2},1}\left(-at^{\frac{1}{2}}\right) + \frac{1}{\Gamma\left(\frac{1}{2}\right)} \tag{4.89}$$

Therefore

$$t^{-\frac{1}{2}}E_{\frac{1}{2},\frac{1}{2}}\left(-at^{\frac{1}{2}}\right) = -aE_{\frac{1}{2},1}\left(-at^{\frac{1}{2}}\right) + \frac{t^{-\frac{1}{2}}}{\Gamma\left(\frac{1}{2}\right)} \tag{4.90}$$

It is known that

$$E_{\frac{1}{2},1}(z) = e^{z^2}erfc(-z)$$

So

$$E_{\frac{1}{2},\frac{1}{2}}\left(-at^{\frac{1}{2}}\right) = e^{\left(-at^{\frac{1}{2}}\right)^2}erfc\left(at^{\frac{1}{2}}\right)$$

$$= e^{a^2t}erfc\left(at^{\frac{1}{2}}\right) \tag{4.91}$$

Therefore

$$t^{-\frac{1}{2}}E_{\frac{1}{2},\frac{1}{2}}\left(-at^{\frac{1}{2}}\right) = -ae^{a^2t}erfc\left(at^{\frac{1}{2}}\right) + \frac{t^{-\frac{1}{2}}}{\sqrt{\pi}} \tag{4.92}$$

Thus

48

$$L^{-1}\left\{\frac{1}{\sqrt{s}+a}\right\} = \frac{1}{\sqrt{\pi t}} - ae^{a^2 t}erfc\left(a\sqrt{t}\right) \tag{4.93}$$

Example 4.4

This example illustrates the inverse Laplace transform $f(t)$ using Mittage liffler function of the function

$$F(s) = \frac{s^3}{\left(s^2 + a^2\right)^2}$$

Solution

Using the property (4.51), we have

$$L^{-1}\left\{\frac{s^3}{\left(s^2 + a^2\right)^2}\right\} = E_{2,-1}^1\left(-a^2 t^2\right) \tag{4.94}$$

Also, it is known that

$$E_{2,-1}^1(z) = \sum_{n=0}^{\infty} \frac{(n+1)! z^n}{n!\Gamma(2n+1)}$$

$$= \cosh\left(\sqrt{z}\right) + \frac{\sqrt{z}}{2}\sinh\left(\sqrt{z}\right) \tag{4.95}$$

Therefore

$$E_{2,-1}^1(z) = \cosh\left(\sqrt{z}\right) + \frac{\sqrt{z}}{2}\sinh\left(\sqrt{z}\right) \tag{4.96}$$

So

$$E_{2,-1}^1\left(-a^2t^2\right) = \cosh\left(\sqrt{-a^2t^2}\right) + \frac{\sqrt{-a^2t^2}}{2}\sinh\left(\sqrt{-a^2t^2}\right)$$

$$= \cos(at) - \frac{at}{2}\sin(at) \tag{4.97}$$

Thus

$$L^{-1}\left\{\frac{s^3}{\left(s^2+a^2\right)^2}\right\} = \cos(at) - \frac{at}{2}\sin(at) \tag{4.98}$$

This example shows that the inverse Laplace of the given function can be solved without using the partial fraction method.

4.2.3   Steady-State Error Response

Figure 4.2 shows a simple closed loop system using a unity negative feedback. The steady state error in time domain can be given as

$$e_{ss} = \lim_{t\to\infty} e(t) \tag{4.99}$$

It is also given in Laplace domain using final value theorem as

$$e_{ss} = \lim_{s\to0} sE(s) \tag{4.100}$$

where

$$E(s) = \frac{R(s)}{1+G(s)} \tag{4.101}$$

Therefore

$$e_{ss} = \lim_{s \to 0} s \frac{R(s)}{1 + L(s)}$$

(4.102)

It can be seen that the steady state error depends on the reference input $R(s)$ and the open loop transfer function $L(s)$.
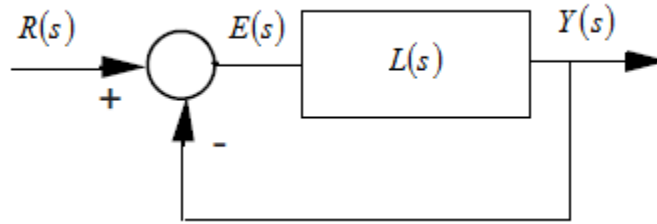

Figure 4.2: A unity negative feedback system

The open loop of a fractional transfer function can be expressed as

$$L(s) = \frac{\left(b_1 + \sum_{k=2}^{m} b_k s^{\beta_k} \right)}{s^{\gamma} \left(a_1 + \sum_{k=2}^{n} a_k s^{\alpha_k} \right)}$$

(4.103)

The error static constant of the system are Position, velocity, and acceleration coefficients. Position error coefficient of the system denoted as K_p is given by

$$K_p = \lim_{s \to 0} L(s)$$

(4.104)

Velocity error coefficient denoted as K_v is given by

$$K_v = \lim_{s \to 0} s L(s)$$

(4.105)

51

Acceleration coefficient denoted as K_a is given by

$$K_a = \lim_{s \to 0} s^2 L(s)$$ (4.106)

For the reference input $r(t) = t^v$ whose Laplace transform is given by $R(s) = \dfrac{\Gamma(1+v)}{s^{1+v}}$, the

steady error can be calculated as

$$e_{ss} = \lim_{s \to 0} s \frac{\Gamma(1+v)}{s^{1+v}} \frac{s^\gamma \left(a_1 + \sum_{k=2}^{n} a_k s^{\alpha_k} \right)}{s^\gamma \left(a_1 + \sum_{k=2}^{m} a_k s^{\alpha_k} \right) + \left(b_1 + \sum_{k=2}^{m} b_k s^{b_k} \right)}$$

$$= \lim_{s \to 0} \Gamma(1+v) \frac{s^{\gamma-v} \left(a_1 + \sum_{k=2}^{n} a_k s^{\alpha_k} \right)}{s^\gamma \left(a_1 + \sum_{k=2}^{m} a_k s^{\alpha_k} \right) + \left(b_1 + \sum_{k=2}^{m} b_k s^{b_k} \right)}$$ (4.107)

There are three cases for finding the steady state error of the expression above.

- Case : $\gamma - v < 0$

  $e_{ss} = \infty$

- Case : $\gamma - v = 0$, $(\gamma = v)$

  $e_{ss} = \dfrac{a_1}{b_1} \Gamma(1+v)$

- Case : $\gamma - v > 0$

  $e_{ss} = 0$

52

It can be seen that, the steady state error appears as a value when the fractional order system with type (γ) is equal to the negative exponent (v) of the reference input.

For the reference input $r(t) = t^{v-1}$ whose Laplace transform is given by $R(s) = \dfrac{\Gamma(v)}{s^v}$, the steady error can be calculated as

$$e_{ss} = \lim_{s \to 0} s \frac{\Gamma(v)}{s^v} \frac{s^\gamma \left(a_1 + \sum_{k=2}^{n} a_k s^{\alpha_k} \right)}{s^\gamma \left(a_1 + \sum_{k=2}^{m} a_k s^{\alpha_k} \right) + \left(b_1 + \sum_{k=2}^{m} b_k s^{b_k} \right)}$$

$$= \lim_{s \to 0} s \Gamma(v) \frac{s^{\gamma-v} \left(a_1 + \sum_{k=2}^{n} a_k s^{\alpha_k} \right)}{s^\gamma \left(a_1 + \sum_{k=2}^{m} a_k s^{\alpha_k} \right) + \left(b_1 + \sum_{k=2}^{m} b_k s^{b_k} \right)} \qquad (4.108)$$

The expression above is zero when the order of the fractional system is equal to the exponent (v) of the reference input in the frequency domain. In other words, for a fractional reference input whose form is $R(s) = \dfrac{\Gamma(v)}{s^v}$, the open loop of the system must contain a fractional integrator of order (v) to obtain a zero steady state error.

4.3 Stability

The Matignon's stability theorem states that a commeasure order system which is given by a rational transfer function is stable if only if

$$\left| \arg(\lambda_i) \right| > \frac{\alpha\pi}{2} \tag{4.109}$$

where λ_i is (i-th) root of the denominator $P(\lambda)$.

The location of roots of $P(\lambda)$ can be represented in the Riemann surface. The Riemann surface is an extension of the non-fractional (s-plane) to show the stable and unstable regions of commeasure transfer functions. The stability region of a commeasure transfer function is bounded by a cone whose vertex at the origin. The stable region covers the region determined by $\left| \arg(\lambda_i) \right| > \frac{\alpha\pi}{2}$ while unstable region covers the region $\left| \arg(\lambda_i) \right| < \frac{\alpha\pi}{2}$ as shown in Figure 4.3.
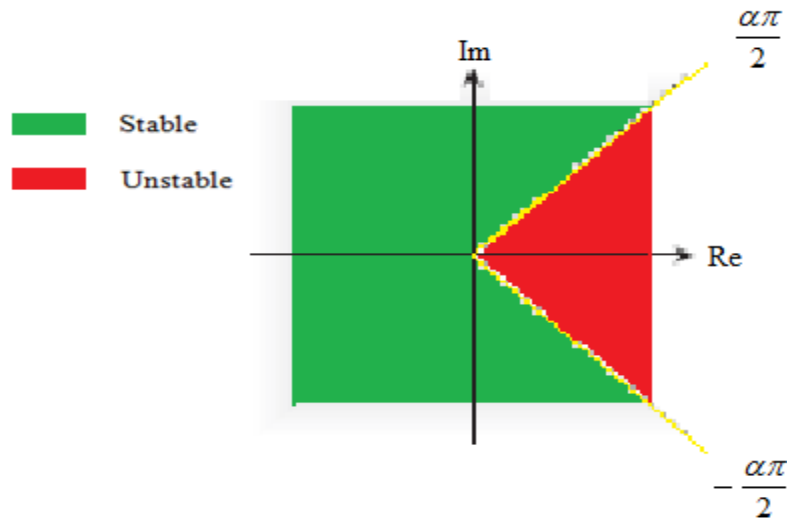

Figure 4.3: The stability regions in the Riemann surface

Example 4.5

This example illustrates the stability of the following fractional transfer function

$$G(s) = \frac{1}{s^{\frac{2}{5}} - 2s^{\frac{1}{5}} + 4}$$

Solution

By assuming that $\lambda = s^{\frac{1}{5}}$, we get $\alpha = \frac{1}{5}$. So

$$G(\lambda) = \frac{1}{\lambda^2 - 2\lambda + 4} \qquad (4.110)$$

The roots of the denominator are $\lambda_{1,2} = 1 \pm j\sqrt{3}$. Hence, $\left| \arg(\lambda_{1,2}) \right| = \frac{\pi}{3}$

Therefore, the system is stable. Since

$$\left| \arg(\lambda_{1,2}) \right| > \frac{\pi}{10} \qquad (4.111)$$

The roots and the stable region can be represented in the Riemann surface as shown in Figure 4.4.
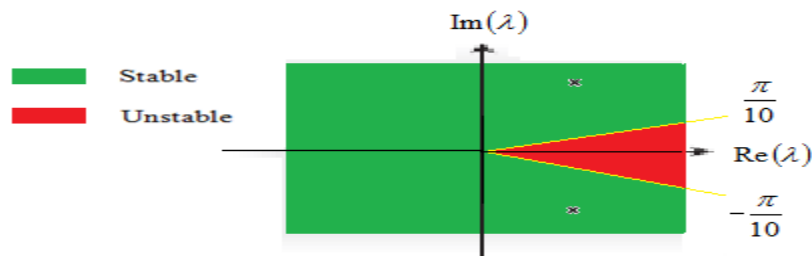

Figure 4.4: The location of the roots in the Riemann surface

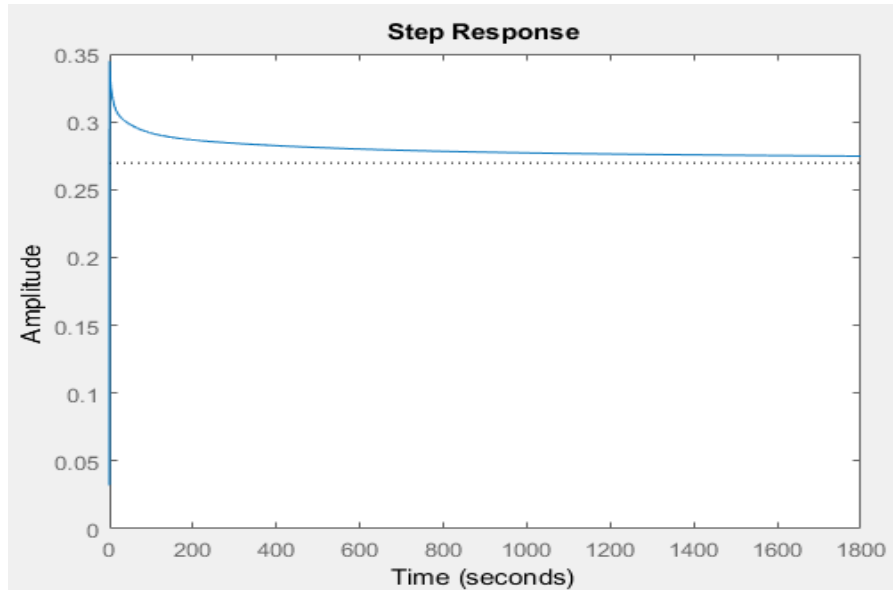The step response of the system can be shown in Figure 4.5.

Figure 4.5: The step response of $G(s) = \dfrac{1}{s^{\frac{2}{5}} - 2s^{\frac{1}{5}} + 4}$

The following table shows the effect of pole location on system behavior.

Table 4.2: Impact of pole location on system behavior

Pole λ_k	Corresponding natural response component	Stability condition	Location of the pole	Step response
Real pair, negative, equal	Pure exponential	Absolutely stable		

Complex conjugate pair with negative real parts	Pure exponential	Absolutely stable		
Complex conjugate pair with zero real parts	Pure exponential	Absolutely stable		
Complex conjugate pair with positive real parts with $\frac{\alpha\pi}{2} < \left|\arg(\lambda_k)\right|$	Exponentially decaying sinusoid	Under damped (Stable)		
Complex conjugate pair with positive real parts With $\left|\arg(\lambda_k)\right| = \frac{\alpha\pi}{2}$	Sinusoid	Un damped (marginally stable)		
Complex conjugate pair with positive real parts ok	Exponentially saturating sinusoid	Oscillatory instability		

4.4 Some Examples of Fractional Transfer Functions

This section reviews some fractional transfer functions. They can be used as targets for the tuning of the fractional PID using the frequency loop shaping technique (FLS) in chapter 6.

4.4.1 $L(s) = \dfrac{1}{s^\alpha}$

The logarithmic magnitude of the fractional integrator in dB is

$$20\log|L(j\omega)| = 20\log\left|\frac{1}{(j\omega)^\alpha}\right| = -20\alpha\log|\omega| \qquad (4.112)$$

The phase is given by

$$\angle L(j\omega) = \angle\frac{1}{(j\omega)^\alpha} = -\frac{\alpha\pi}{2} \qquad (4.113)$$

Figure 4.6 shows the frequency response of the fractional integrator for different values of the integral order.

It can be seen the magnitude plot is a straight line with a slop of (-20α) dB/decade, passing through the 0 dB line at $(\omega = 1)$ rad/sec. The phase angle is constant and equal to $\left(-\dfrac{\alpha\pi}{2}\right)$.
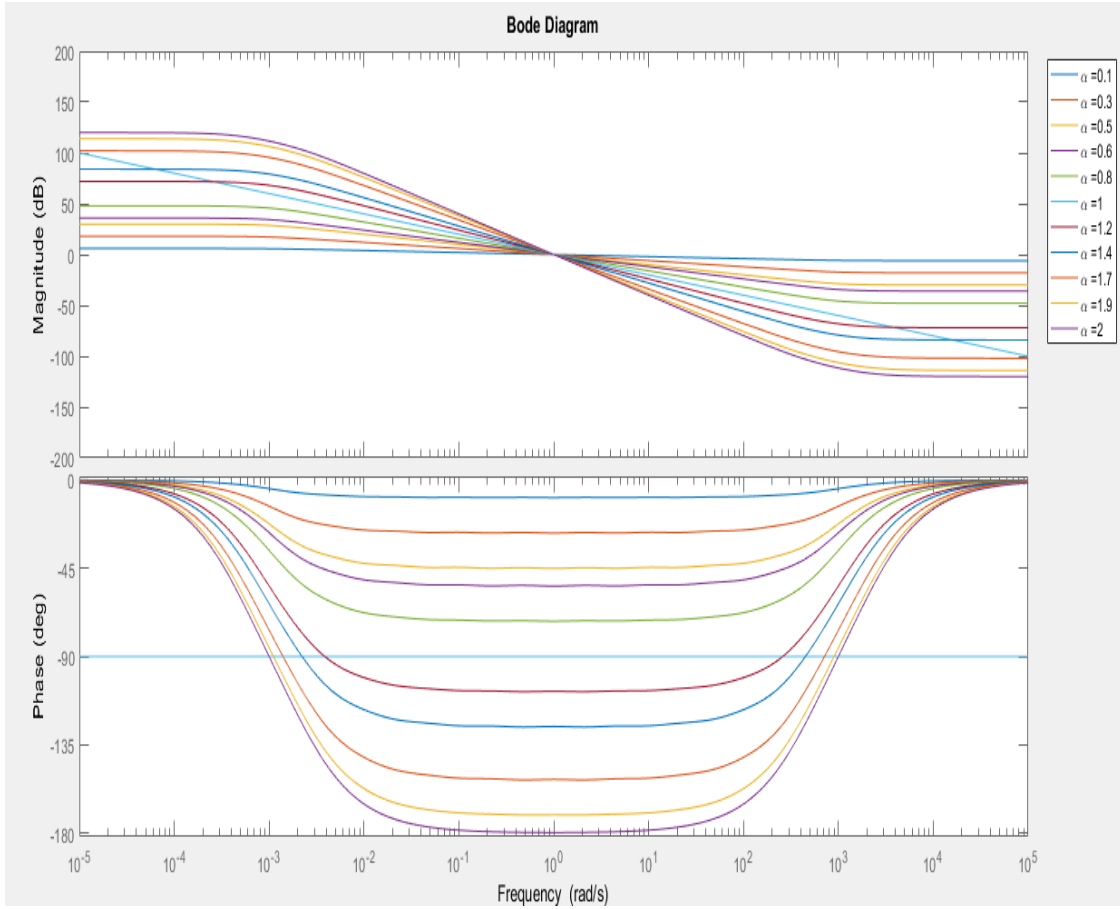
Figure 4.6: The frequency response for different values of the integral order

The step response of the unity feedback system in Figure 4.7 is given by

$$y(t) = L^{-1}\left\{ \frac{1}{s(s^{\alpha} + 1)} \right\}$$

(4.114)

Therefore

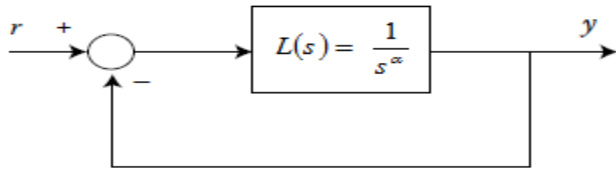$$y(t) = t^{\alpha} E_{\alpha,\alpha+1}\left(-t^{\alpha} \right)$$

(4.115)

Figure 4.7: Unity feedback system

Figure 4.8 shows the step response of the system in Figure 4.7 for different values of the integral order.
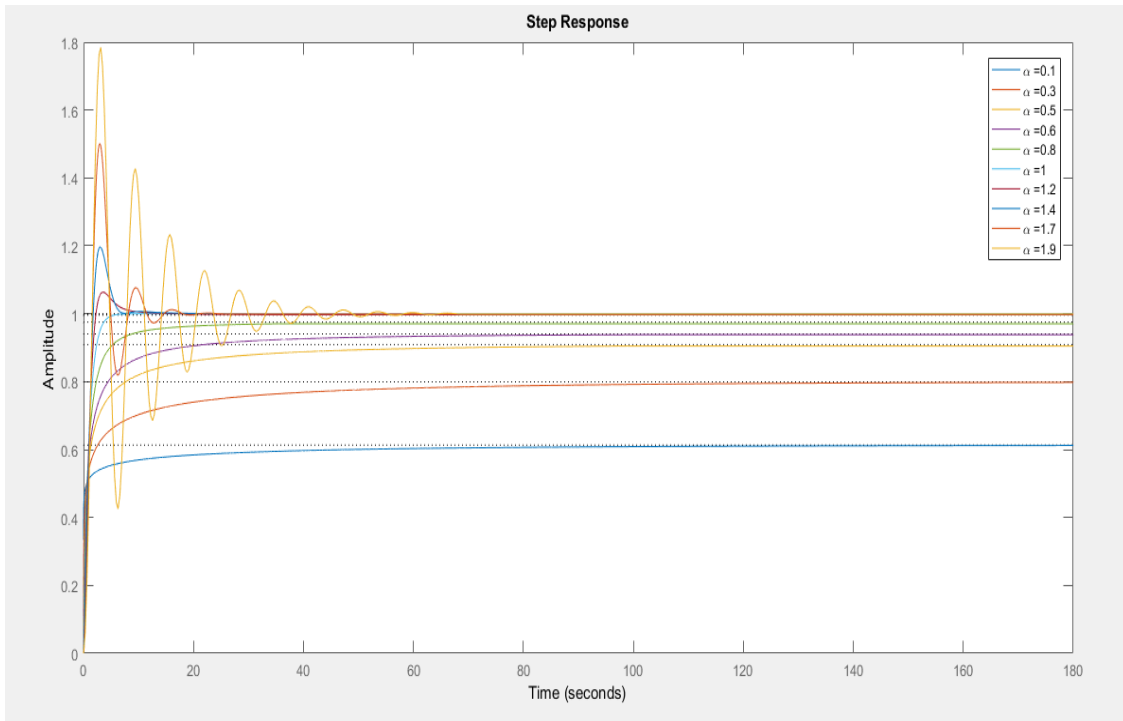

Figure 4.8: The step response for different values of the integral order

The stability region of a fractional integrator with $(0 < \alpha < 1)$ can be shown in Figure 4.9.
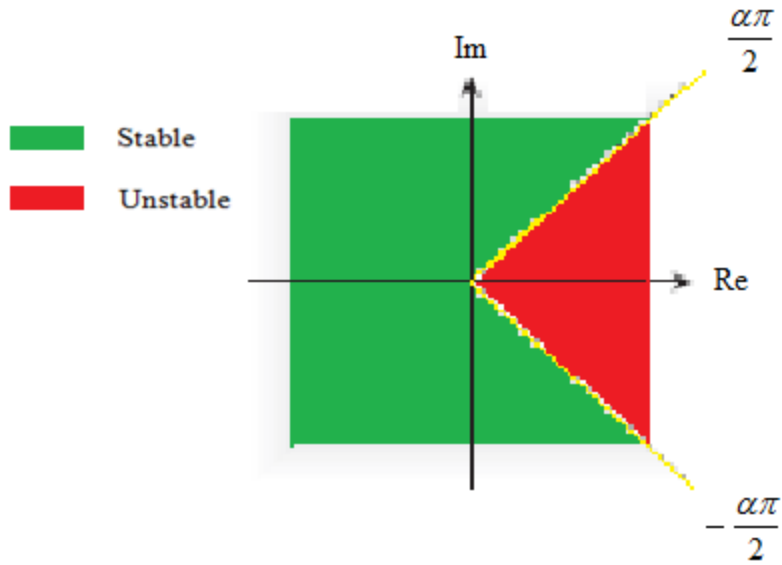
60

Figure 4.9: The stability region of the fractional integrator with $(0 < \alpha < 1)$
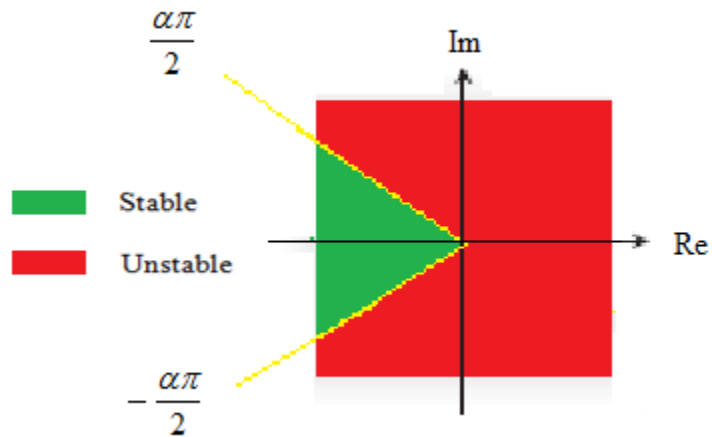

Figure 4.10: The stability region of the fractional integrator with $(1 < \alpha < 2)$

Figure 4.10 shows the effect of adding a pure integrator to the system in Figure 4.9 which decreases the region of stability.

4.4.2 $L(s) = s^{\alpha}$

The logarithmic magnitude of the fractional integrator in dB is

$$20\log|L(j\omega)| = 20\log|(j\omega)^{\alpha}| = 20\alpha\log|\omega| \quad (4.116)$$

The phase is given by

$$\angle L(j\omega) = \angle(j\omega)^{\alpha} = \frac{\alpha\pi}{2} \quad (4.117)$$

Figure 4.11 shows the frequency response of the fractional differentiator for different values of the differential order. It can be seen that the magnitude plot is a straight line with a slop of (20α) dB/decade, passing through the 0 dB line at $(\omega = 1)$ rad/sec. The phase angle is constant and equal to $\left(\dfrac{\alpha\pi}{2}\right)$.
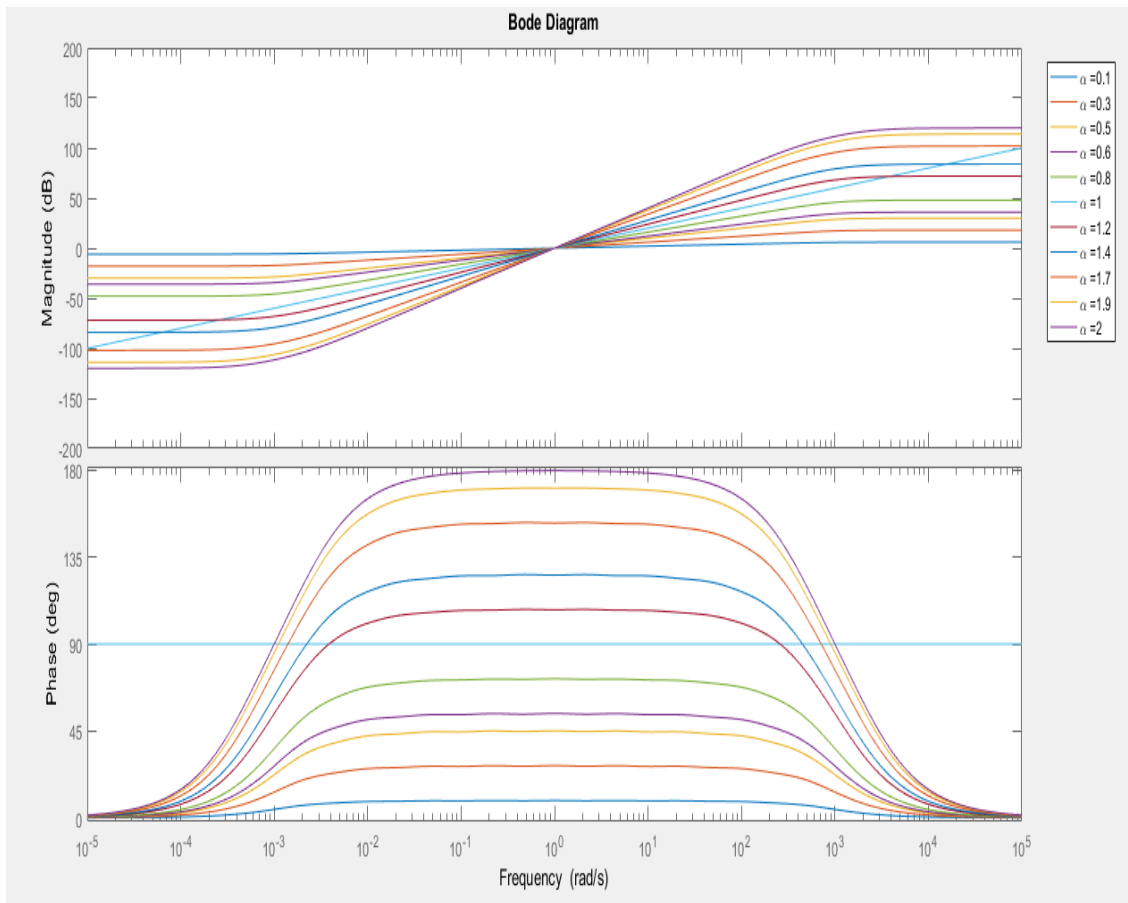

Figure 4.11: The frequency response for different values of the differential order

The step response of the unity feedback system in Figure 4.12 is given by

$$y(t) = L^{-1}\left\{\frac{s^{\alpha}}{s(s^{\alpha}+1)}\right\} \qquad (4.118)$$

Therefore

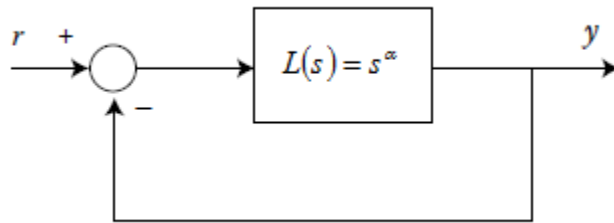$$y(t) = E_{\alpha}\left(-t^{\alpha}\right) \qquad (4.119)$$

Figure 4.12: Unity feedback system

Figure 4.13 shows the step response of the system in Figure 4.12 for different values of the differential order.
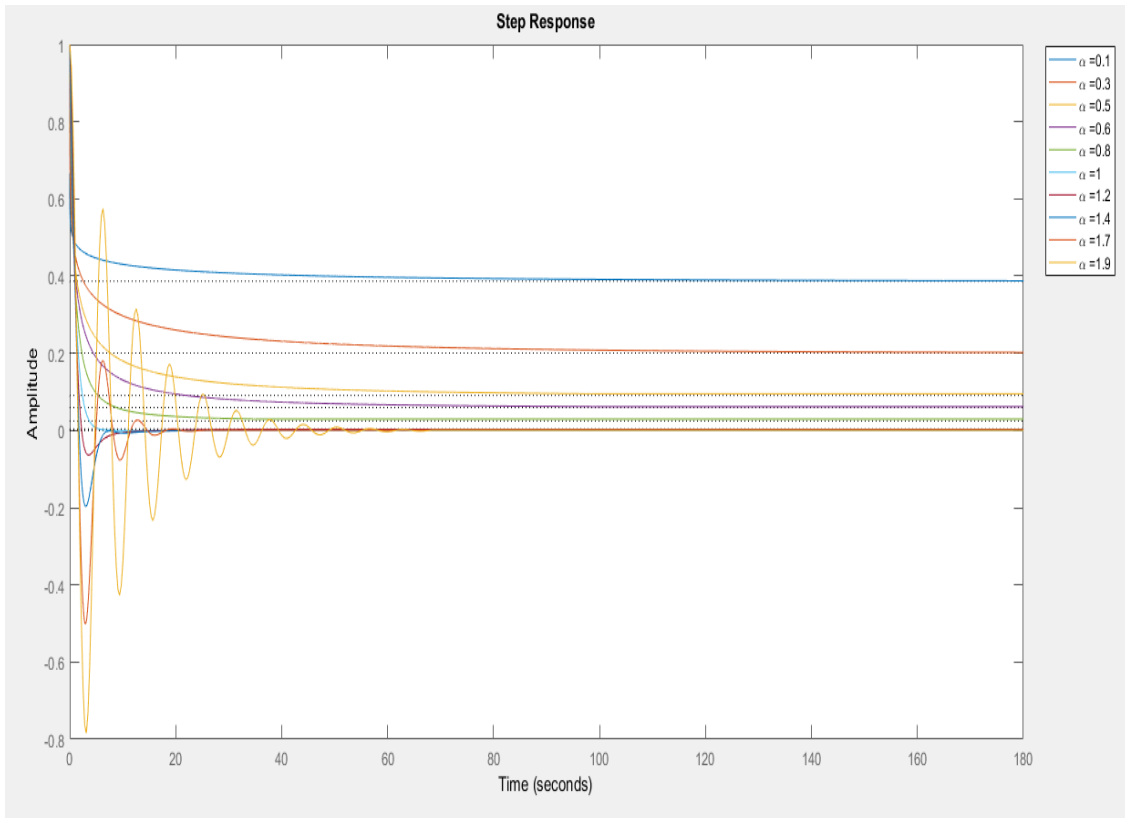
Figure 4.13: The step response for different values of the differential order

4.4.3 $L(s) = \dfrac{(s+a)^{\lambda}}{s^{2.2}}$

It is known that the term $\dfrac{1}{s^{2.2}}$ is not stable since the order of the fractional integrator is greater than two. The step response of this term is shown in Figure 4.14.
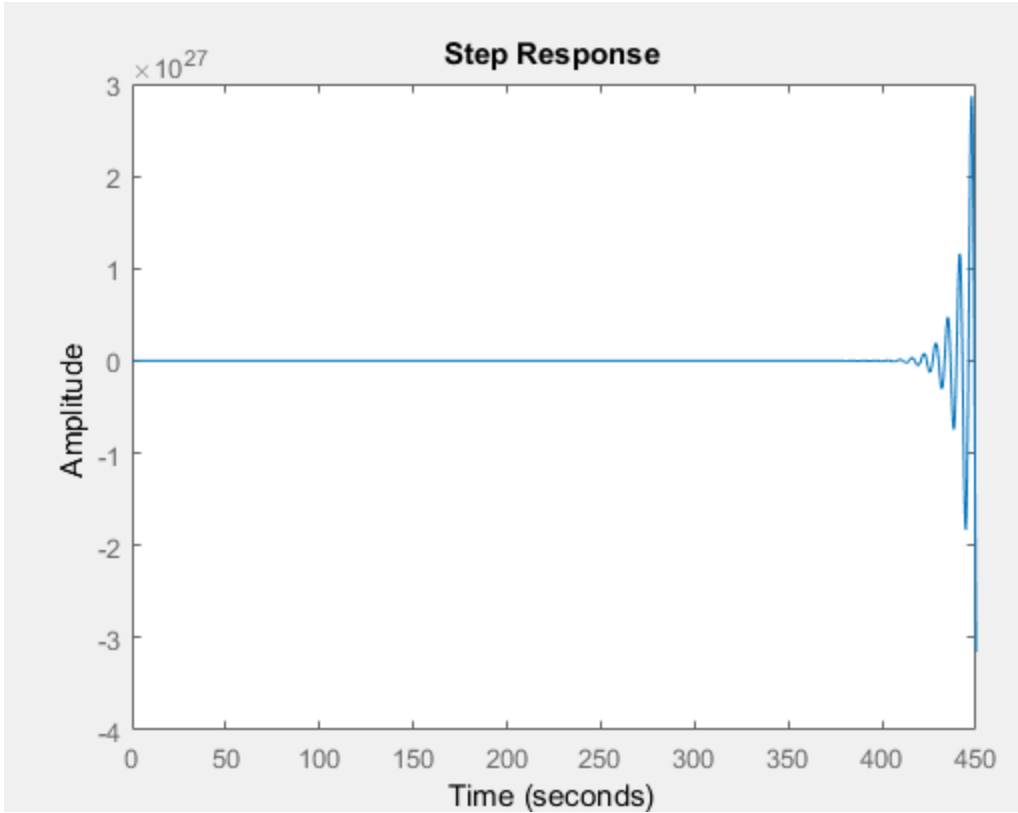
Figure 4.14: The step response of the term $\left(\dfrac{1}{s^{2.2}}\right)$

The fractional term $(s+a)^{\lambda}$ can be added to the previous term to make the system in Figure 4.15 stable.

Figure 4.15: Unity feedback system

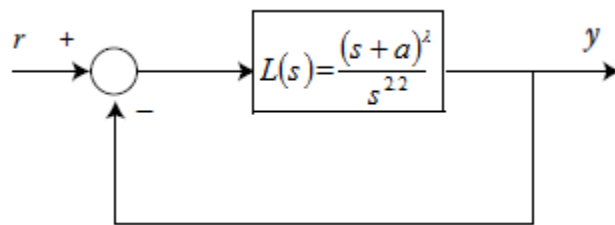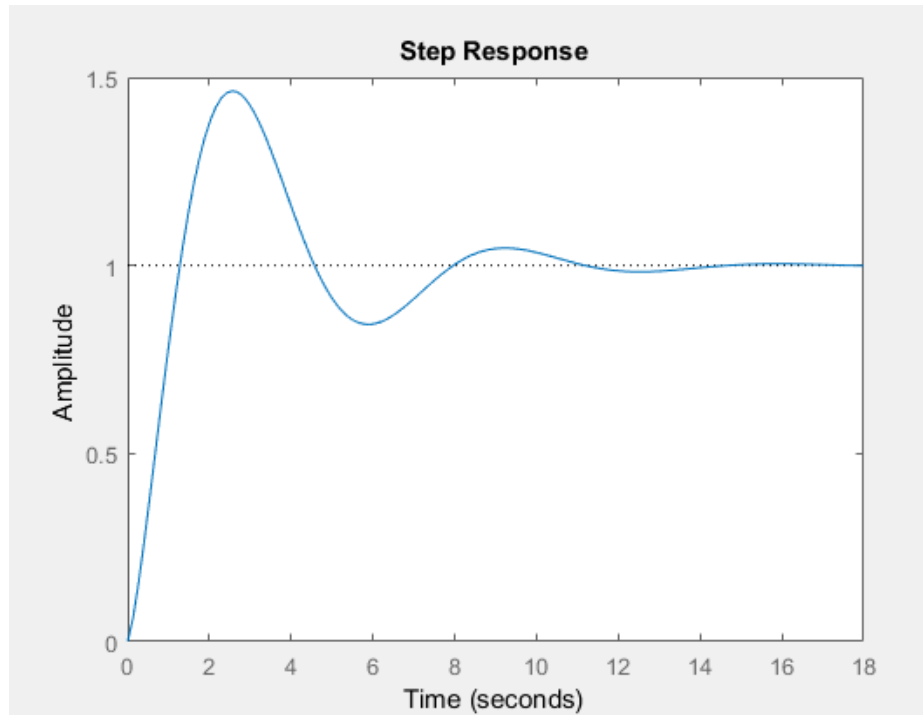The step response of the unity feedback system is shown in Figure 4.16.

Figure 4.16: The step response of the system for $\left(a = 0.7 \quad \lambda = 0.9\right)$

It can be seen that the system behaves as a fractional integrator of order $\left(2.2 - \lambda\right)$ when the value of $\left(a\right)$ approaches zero (the origin). The frequency response of the system is shown in Figure 4.17.
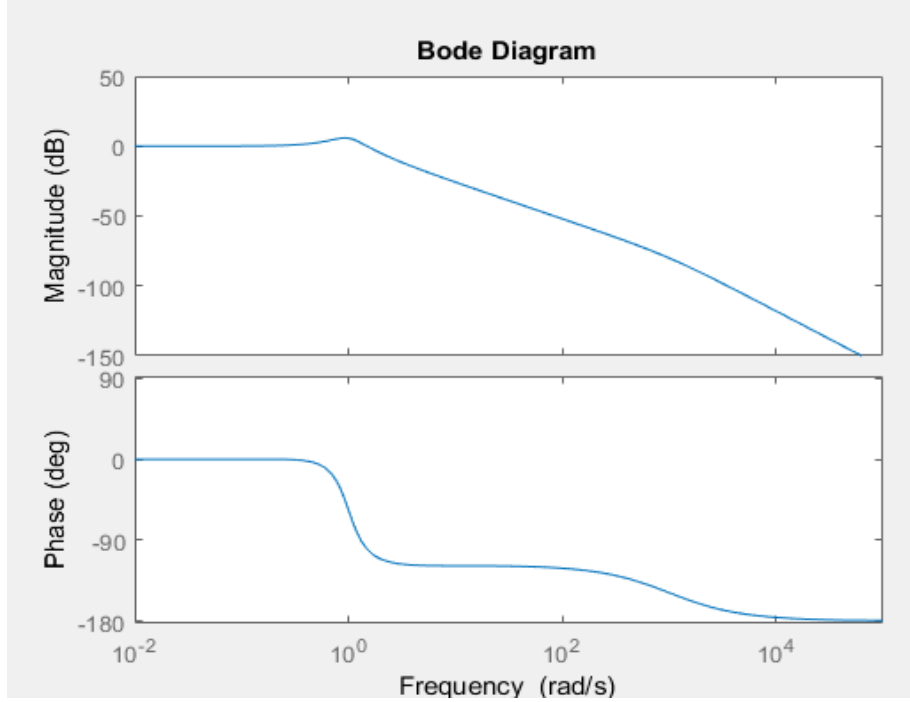
Figure 4.17: The frequency response of the unity feedback system

4.4.4 $L(s) = \dfrac{1}{\left(\dfrac{s}{\omega_n}\right)^{2\alpha} + 2\zeta\left(\dfrac{s}{\omega_n}\right)^{\alpha} + 1}$

The characteristic equation of the system is given by

$$\left(\frac{s}{\omega_n}\right)^{2\alpha} + 2\zeta\left(\frac{s}{\omega_n}\right)^{\alpha} + 1 = 0 \qquad\qquad (4.120)$$

The roots are $s_{1,2}^{\alpha} = \omega_n^{\alpha}\left(-\zeta \pm \sqrt{\zeta^2 - 1}\right)$ $\qquad\qquad$ (4.121)

The nature of these roots is dependent on damping ratio (ζ). Therefore, the stability of

the system has some cases based on the value of the damping ratio (ζ) as the following

67

- Case $\left(\zeta \geq 1\right)$

The roots of the characteristic equation are real and negative. According to the theorem of stability, the system is always stable since

$$\omega_n^\alpha\left(-\zeta \pm \sqrt{\zeta^2 - 1}\right) < 0$$

- Case $\left(\zeta \leq -1\right)$

The roots of the characteristic equation are real and positive. According to the theorem of stability, the system is unstable since

$$\omega_n^\alpha\left(-\zeta \pm \sqrt{\zeta^2 - 1}\right) > 0$$

- Case $\left(\zeta = 0\right)$

The roots of the characteristic equation are complex on the imaginary axis. According to the theorem of stability, the system is stable if $\left(\alpha < 1\right)$

- Case $\left(|\zeta| < 1\right)$

The roots of the characteristic equation are complex. The phase of the roots is given as

$$\angle\theta = \begin{cases} \tan^{-1}\left(\dfrac{\sqrt{1-\zeta^2}}{-\zeta}\right) & -1 < \zeta \leq 0 \\[4mm] \tan^{-1}\left(\dfrac{\sqrt{1-\zeta^2}}{-\zeta}\right) + \pi & 0 < \zeta \leq 1 \end{cases} \qquad (4.122)$$

When $\left(-1 < \zeta \leq 0\right)$ and $\left(0 < \alpha \leq 1\right)$, the system is stable if

68

$$\tan^{-1}\left(\frac{\sqrt{1-\zeta^2}}{-\zeta}\right) > \frac{\alpha\pi}{2} \tag{4.123}$$

since (ζ) is negative, Therefore

$$\frac{\sqrt{1-\zeta^2}}{-\zeta} > \tan\left(\frac{\alpha\pi}{2}\right) \tag{4.124}$$

since (α) is positive, so

$$\zeta^2 < \cos^2\left(\frac{\alpha\pi}{2}\right) \tag{4.125}$$

Therefore, the system is stable under this condition

$$\zeta > -\cos\left(\frac{\alpha\pi}{2}\right) \tag{4.126}$$

When $(-1 < \zeta \leq 0)$ and $(1 < \alpha \leq 2)$, the system is unstable because the roots of the characteristic equation are off the stable area.

When $(0 \leq \zeta < 1)$ and $(1 \leq \alpha < 2)$, the system is stable if

$$\tan^{-1}\left(\frac{\sqrt{1-\zeta^2}}{-\zeta}\right) + \pi > \frac{\alpha\pi}{2} \tag{4.127}$$

since (ζ) is positive, Therefore

$$\frac{\sqrt{1-\zeta^2}}{-\zeta} > \tan\left(-\frac{\alpha\pi}{2}\right) \tag{4.128}$$

or

$$\frac{1-\zeta^2}{\zeta^2} < \tan^2\left(\frac{\alpha\pi}{2}\right) \tag{4.129}$$

since (α) is positive, so

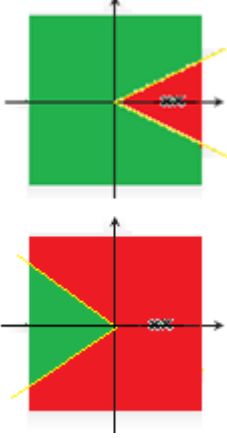$$\zeta^2 > \cos^2\left(\frac{\alpha\pi}{2}\right) \tag{4.130}$$
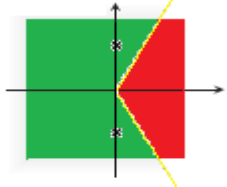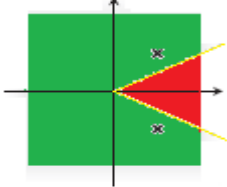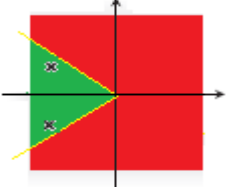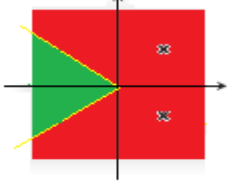
Therefore, the system is stable under this condition

$$\zeta > -\cos\left(\frac{\alpha\pi}{2}\right) \tag{4.131}$$

Table 4.3 shows the effect of (ζ) on the system stability.

Table 4.3: Effect of (ζ) on the system stability

Case	Stability	Condition	The roots location
$\zeta \geq 1$	Stable	None	

$\zeta \leq -1$	Unstable	None	
$\zeta = 0$ and $0 < \alpha < 1$	Stable	None	
$-1 < \zeta \leq 0$ and $0 < \alpha < 1$	Stable	$\zeta > -\cos\left(\dfrac{\alpha\pi}{2}\right)$	
$0 < \zeta \leq 1$ and $1 < \alpha < 2$	Stable	$\zeta > -\cos\left(\dfrac{\alpha\pi}{2}\right)$	
$-1 < \zeta \leq 0$ and $1 < \alpha < 2$	Unstable	None	

The number of resonance peaks of the system can be calculated from

$$\frac{d\left|L\left(j\frac{\omega}{\omega_n}\right)\right|_{dB}}{d\left(\frac{\omega}{\omega_n}\right)} = 0 \tag{4.132}$$

where

$$L\left(j\frac{\omega}{\omega_n}\right) = \frac{1}{\left(\frac{j\omega}{\omega_n}\right)^{2\alpha} + 2\zeta\left(\frac{j\omega}{\omega_n}\right)^{\alpha} + 1} \tag{4.133}$$

Therefore

$$\left|L\left(j\frac{\omega}{\omega_n}\right)\right| = \frac{1}{\left|j^{2\alpha}\left(\frac{\omega}{\omega_n}\right)^{2\alpha} + 2\zeta j^{\alpha}\left(\frac{\omega}{\omega_n}\right)^{\alpha} + 1\right|}$$

$$= \frac{1}{\left|[\cos(\alpha\pi) + j\sin(\alpha\pi)]\left(\frac{\omega}{\omega_n}\right)^{2\alpha} + 2\zeta\left[\cos\left(\frac{\alpha\pi}{2}\right) + j\sin\left(\frac{\alpha\pi}{2}\right)\right]\left(\frac{\omega}{\omega_n}\right)^{\alpha} + 1\right|}$$

$$= \frac{1}{\left|\left[\cos(\alpha\pi)\left(\frac{\omega}{\omega_n}\right)^{2\alpha} + 2\zeta\cos\left(\frac{\alpha\pi}{2}\right)\left(\frac{\omega}{\omega_n}\right)^{\alpha} + 1\right] + j\left[\sin(\alpha\pi)\left(\frac{\omega}{\omega_n}\right)^{2\alpha} + 2\zeta\sin\left(\frac{\alpha\pi}{2}\right)\left(\frac{\omega}{\omega_n}\right)^{\alpha}\right]\right|}$$

$$= \frac{1}{\sqrt{\left[\cos(\alpha\pi)\left(\frac{\omega}{\omega_n}\right)^{2\alpha} + 2\zeta\cos\left(\frac{\alpha\pi}{2}\right)\left(\frac{\omega}{\omega_n}\right)^{\alpha} + 1\right]^2 + \left[\sin(\alpha\pi)\left(\frac{\omega}{\omega_n}\right)^{2\alpha} + 2\zeta\sin\left(\frac{\alpha\pi}{2}\right)\left(\frac{\omega}{\omega_n}\right)^{\alpha}\right]^2}} \tag{4.134}$$

The gain in dB,

$$\left| L\left(j\frac{\omega}{\omega_n}\right)\right|_{dB} = -10\log\left\| \left[\cos(\alpha\pi)\left(\frac{\omega}{\omega_n}\right)^{2\alpha} + 2\zeta\cos\left(\frac{\alpha\pi}{2}\right)\left(\frac{\omega}{\omega_n}\right)^{\alpha} + 1\right]^2\right.$$

$$\left. + \left[\sin(\alpha\pi)\left(\frac{\omega}{\omega_n}\right)^{2\alpha} + 2\zeta\sin\left(\frac{\alpha\pi}{2}\right)\left(\frac{\omega}{\omega_n}\right)^{\alpha}\right]^2\right\|$$

$$= -10\log\left| \left(\frac{\omega}{\omega_n}\right)^{4\alpha} + 4\zeta\cos\left(\frac{\alpha\pi}{2}\right)\left(\frac{\omega}{\omega_n}\right)^{3\alpha} + 4\zeta^2\left(\frac{\omega}{\omega_n}\right)^{2\alpha}\right.$$

$$\left. + 2\left(\frac{\omega}{\omega_n}\right)^{2\alpha}\cos(\alpha\pi) + 4\zeta\cos\left(\frac{\alpha\pi}{2}\right)\left(\frac{\omega}{\omega_n}\right)^{\alpha} + 1\right| \qquad (4.135)$$

we have

$$\frac{d\left| L\left(j\frac{\omega}{\omega_n}\right)\right|_{dB}}{d\left(\frac{\omega}{\omega_n}\right)} = 0$$

So

$$4\alpha\left(\frac{\omega}{\omega_n}\right)^{4\alpha-1} + 4\zeta(3\alpha)\cos\left(\frac{\alpha\pi}{2}\right)\left(\frac{\omega}{\omega_n}\right)^{3\alpha-1} + 4\zeta^2(2\alpha)\left(\frac{\omega}{\omega_n}\right)^{2\alpha-1}$$

$$+ 2(2\alpha)\left(\frac{\omega}{\omega_n}\right)^{2\alpha-1}\cos(\alpha\pi) + 4\zeta(\alpha)\cos\left(\frac{\alpha\pi}{2}\right)\left(\frac{\omega}{\omega_n}\right)^{\alpha-1} + 1 = 0 \qquad (4.136)$$

Therefore

$$\left(\frac{\omega}{\omega_n}\right)^{4\alpha-1} + \zeta(3\alpha)\cos\left(\frac{\alpha\pi}{2}\right)\left(\frac{\omega}{\omega_n}\right)^{3\alpha-1} + \left(\zeta^2 + \cos(\alpha\pi)\right)\left(\frac{\omega}{\omega_n}\right)^{2\alpha-1} + \zeta\cos\left(\frac{\alpha\pi}{2}\right)\left(\frac{\omega}{\omega_n}\right)^{\alpha-1} = 0$$

$$\Rightarrow \left(\frac{\omega}{\omega_n}\right)^{\alpha-1}\left[\left(\frac{\omega}{\omega_n}\right)^{3\alpha} + 3\zeta\cos\left(\frac{\alpha\pi}{2}\right)\left(\frac{\omega}{\omega_n}\right)^{2\alpha} + \left(\zeta^2 + \cos(\alpha\pi)\right)\left(\frac{\omega}{\omega_n}\right)^{\alpha} + \zeta\cos\left(\frac{\alpha\pi}{2}\right)\right] = 0 \qquad (4.137)$$

The number of resonance peaks depends on the number of positive real valued of $\left(\frac{\omega}{\omega_n}\right)$

in the following equation

$$\left(\frac{\omega}{\omega_n}\right)^{3\alpha} + 3\zeta\cos\left(\frac{\alpha\pi}{2}\right)\left(\frac{\omega}{\omega_n}\right)^{2\alpha} + \left(\zeta^2 + \cos(\alpha\pi)\right)\left(\frac{\omega}{\omega_n}\right)^{\alpha} + \zeta\cos\left(\frac{\alpha\pi}{2}\right) = 0 \qquad (4.138)$$

The positive real valued of $\left(\frac{\omega}{\omega_n}\right)$ should be corresponded to maxima of $\left|L\left(j\frac{\omega}{\omega_n}\right)\right|_{dB}$ not

minima. The following figure shows the distribution of the stability and the number of

peak frequencies based on the values of (ζ) and (α).
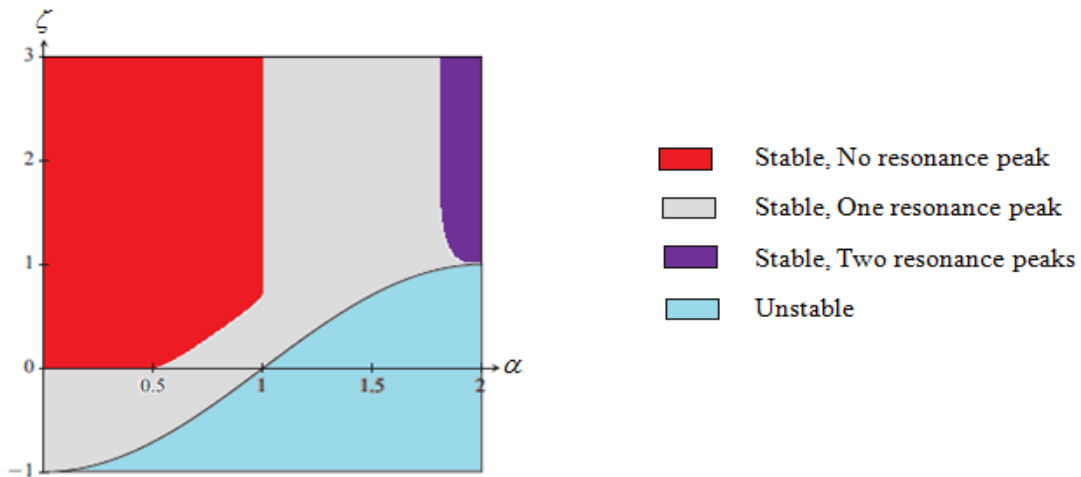

Figure 4.18: The stability and resonance peak frequencies of the system

The following fractional transfer function has two resonance peaks as shown in Figure 4.19.
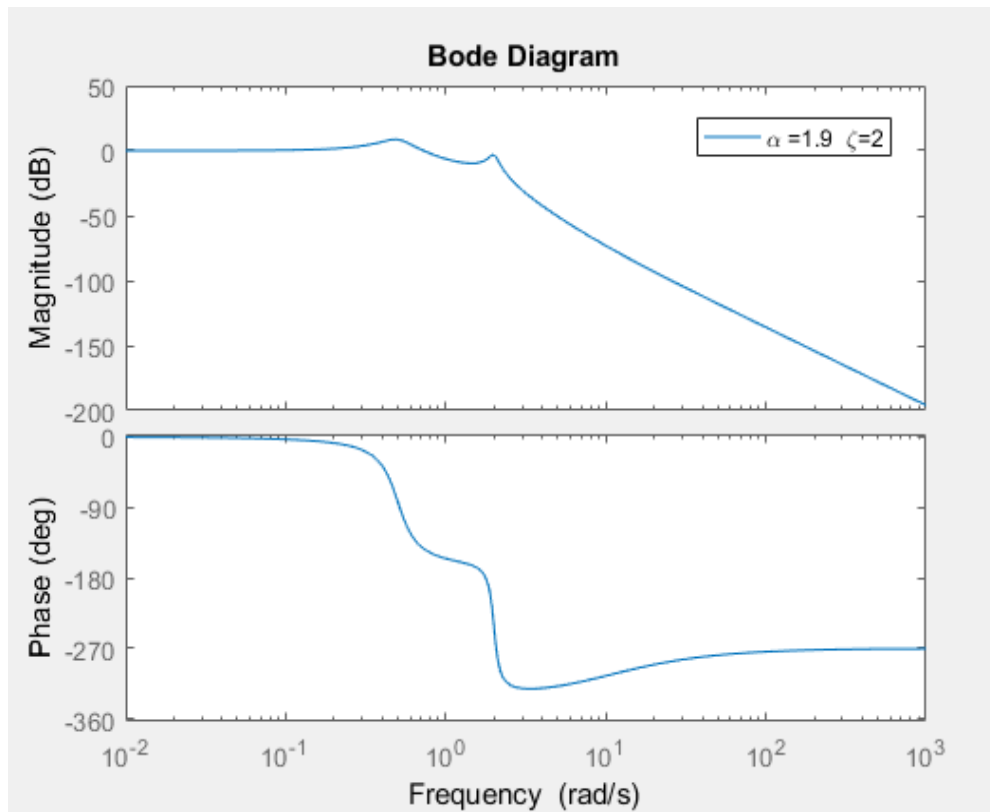
$$L(s) = \frac{1}{s^{3.8} + 4s^{1.9} + 1}$$

Bode Diagram

Figure 4.19: The frequency response of $\left(\dfrac{1}{s^{3.8} + 4s^{1.9} + 1} \right)$

Therefore, there are two positive real valued of $\left(\dfrac{\omega}{\omega_n} \right)$ correspond to maxima of

$\left| L\left(j\dfrac{\omega}{\omega_n} \right) \right|_{dB}$ in the following equation

$$\left(\frac{\omega}{\omega_n}\right)^{5.7} - 5.92613\left(\frac{\omega}{\omega_n}\right)^{3.8} + 4.95106\left(\frac{\omega}{\omega_n}\right)^{1.9} - 1.97538 = 0 \tag{4.139}$$

4.5 Oustaloup's Recursive Approximation

Oustaloup filter was introduced by the professor Alain Oustaloup in the mid-1990s. This filter is commonly used in fractional systems. It provides a simple method to approximate a fractional differentiator.

Figure 4.20: Professor Alain Oustaloup

This filer is given by the following expression

$$s^\alpha = K\prod_{k=-N}^{N}\frac{s+\omega_k^{'}}{s+\omega_k} \tag{4.140}$$

where the gain, zero, and the pole of the filer are calculated as

$$K = \omega_h^\alpha \tag{4.141}$$

$$\omega_k' = \omega_b \left(\frac{\omega_h}{\omega_b} \right)^{\frac{k+N+\frac{1}{2}(1-\alpha)}{2N+1}} \tag{4.142}$$

$$\omega_k = \omega_b \left(\frac{\omega_h}{\omega_b} \right)^{\frac{k+N+\frac{1}{2}(1+\alpha)}{2N+1}} \tag{4.143}$$

where (ω_b, ω_h) is the frequency range of the approximation. It can be seen that the approximation depends on the order of the filer (N) and the frequency range (ω_b, ω_h). The fractional integrator $\left(\dfrac{1}{s^{0.63}} \right)$ can be approximated using Matlab by selecting the order $(N = 4)$ and the frequency range $(10^{-3}, 10^3)$ as

$$
\begin{aligned}
\frac{1}{s^{0.63}} = & \frac{0.01288s^9 + 12.36s^8 + 2102s^7 + 7.419 \times 10^4 \, s^6 + 5.597 \times 10^5 \, s^5 + 9.077 \times 10^5 s^4 + \cdots}{s^9 + 364.8s^8 + 2.359 \times 10^4 \, s^7 + 3.165 \times 10^5 s^6 + 9.077 \times 10^5 s^5 + 5.597 \times 10^5 \, s^4 + \cdots} \\
& \frac{\cdots + 3.165 \times 10^5 \, s^3 + 2.359 \times 10^4 \, s^2 + 364.8s + 1}{\cdots + 7.419 \times 10^4 \, s^3 + 2102s^2 + +12.36s + 0.01288}
\end{aligned} \tag{4.144}
$$

Also, the frequency response of the approximated fractional integrator can be shown in Figure 4.21.
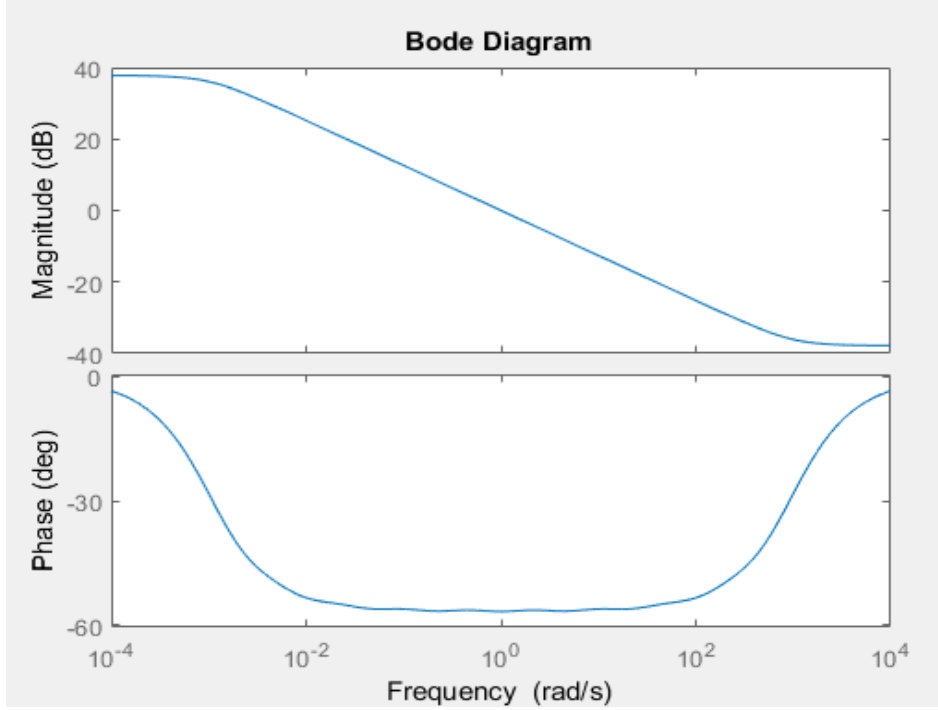
Figure 4.21: The frequency response of the fractional integrator $\left(\dfrac{1}{s^{0.63}}\right)$

The same figure shows that the approximation of the fractional integrator appears only in the frequency range (ω_b, ω_h). The approximation of the same fractional integrator may have another form. Selecting $(N = 3)$ and the frequency range $(10^{-2}, 10^2)$ provide the following approximation

$$\frac{1}{s^{0.63}} = \frac{0.05495s^7 + 5.887s^6 + 133.4s^5 + 766.2s^4 + 1160s^3 + 462.4s^2 + 46.76s + 1}{s^7 + 46.76s^6 + 462.4s^5 + 1160s^4 + 766.2s^3 + 133.4s^2 + 5.887s + 0.05495} \tag{4.145}$$

The fractional integrator shows that it can be expressed as a non fractional transfer function which contains zeros and poles. The frequency response of the two approximations can be combined together in Figure 4.22. It can be seen that the

78

frequency responses of the two filters are almost the same in the frequency range of the
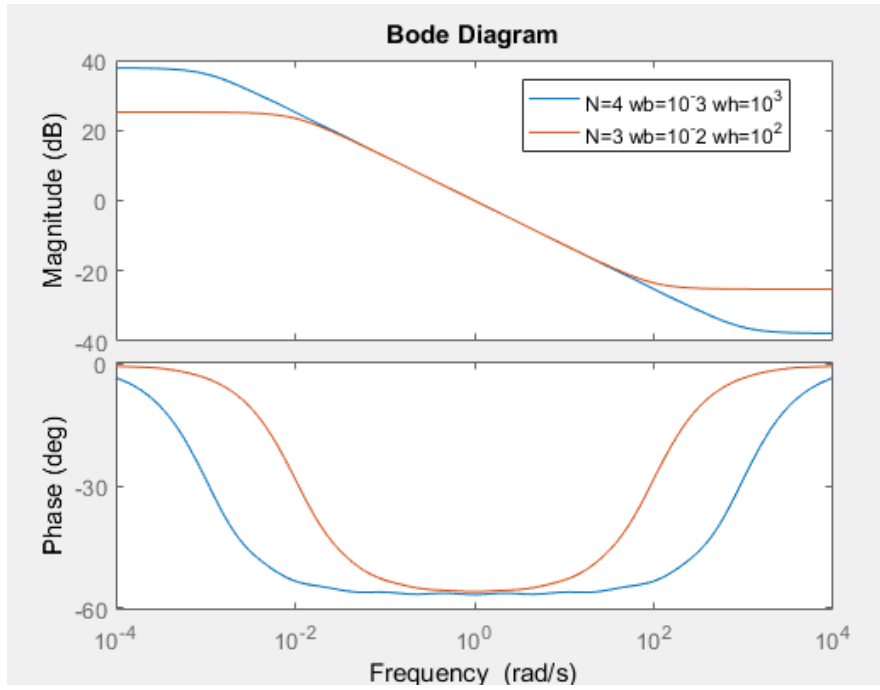
second approximation.

Figure 4.22: The frequency response of the fractional integrator $\left(\dfrac{1}{s^{0.63}}\right)$

CHAPTER 5

THE FRACTIONAL PID CONTROLLER

This chapter covers the properties of the fractional PID controller with the effect of the fractional orders on the system transient. The performance of the fractional PID is introduced.

5.1 PID Controller

The PID controller is a physical device which can be used in control systems to control the steady state error and enhance the transient response of a system. Figure 5.1 shows a simple closed loop feedback control system. The error signal $e(t)$ is the input of the controller and the output signal of the controller is $u(t)$. The classical PID controller can be presented as just a point in the fractional PID plane $(\lambda = 1 \text{ and } \mu = 1)$ as shown in Figure 5.2. There are infinite controllers in the fractional PID plane as shown in Figure 5.3. The fractional plane can be extended to have fractional controllers up to orders $(\lambda = 2 \text{ and } \mu = 2)$ as shown in Figure 5.4. The fractional PID controller was introduced in 1990s by Podlubny. This controller consists of five parameters $(K_p, K_i, K_d, \lambda, \mu)$, where (K_p, K_i, K_d) are the proportional gain, integral gain, derivative gain, respectively. The two parameters (λ, μ) represent the integral and derivative orders, respectively.
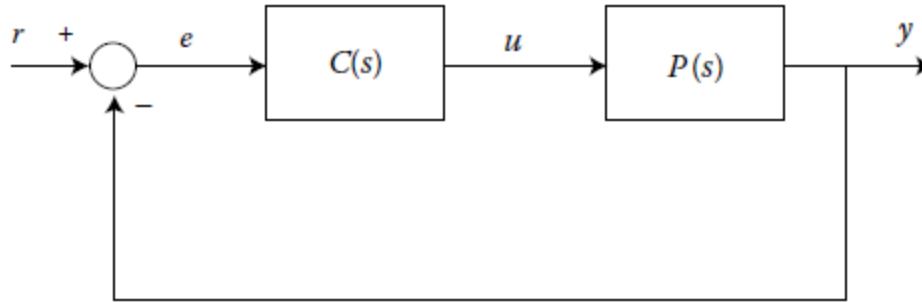
Figure 5.1: A feedback control system with controller $C(s)$ and plant $P(s)$
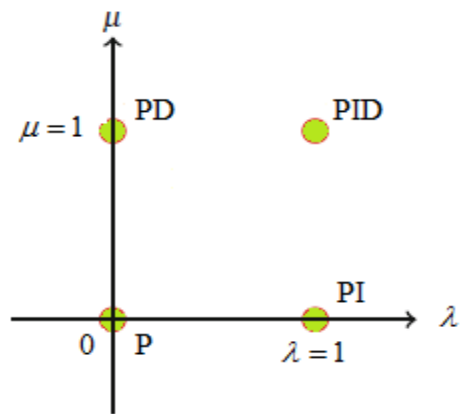

Figure 5.2: The representation of the classic PID controller in the fractional controller
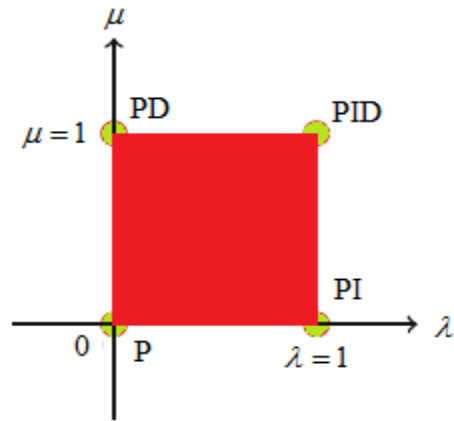
plane

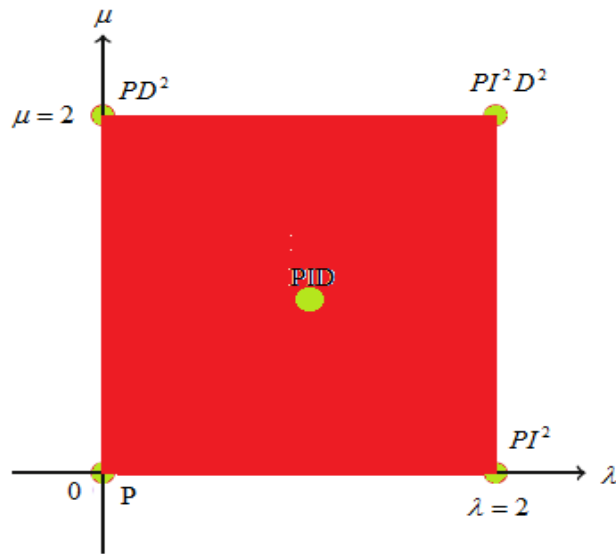Figure 5.3: The fractional controller $PI^\lambda D^\mu$ plane $(0 < \lambda < 1)$ and $(0 < \mu < 1)$

Figure 5.4: The extended fractional controller plane $(0 < \lambda < 2)$ and $(0 < \mu < 2)$

The classical controllers (PID, PI, PD) can be designed from $PI^\lambda D^\mu$ based on the values of λ and μ as shown in the following table.

Table 5.1: Values of λ and μ

The controller	λ	μ
PID	1	1
PI	1	0
PD	0	1

5.1.1   The Proportional Controller (P-Controller)

This controller can be presented as a gain (K_p). This gain is known as the proportional gain constant which describes the relation between the error signal and the controller output at present. This relation in time domain is given by

$$u(t) = K_p e(t) \tag{5.1}$$

Or, in Laplace domain as

$$U(s) = K_p E(s) \tag{5.2}$$

The P controller can be given as

$$C(s) = K_p \tag{5.3}$$

Figure 5.5: Representation of the proportional controller in the time and frequency domains

The relation between the input and output controller is linear. The increase in the proportional gain constant (K_p) improves the steady state but does not eliminate it as shown in Figure 5.6. Hence, offset error always is present. Large values of the proportional gain constant (K_p) may cause the system is unstable. The proportional controller has the following effects

- Rise time decreases as the proportional gain constant (K_p) increases.

- Steady state error decreases as the proportional gain constant (K_p) increases.

- Overshoot increases as the proportional gain constant (K_p) increases.
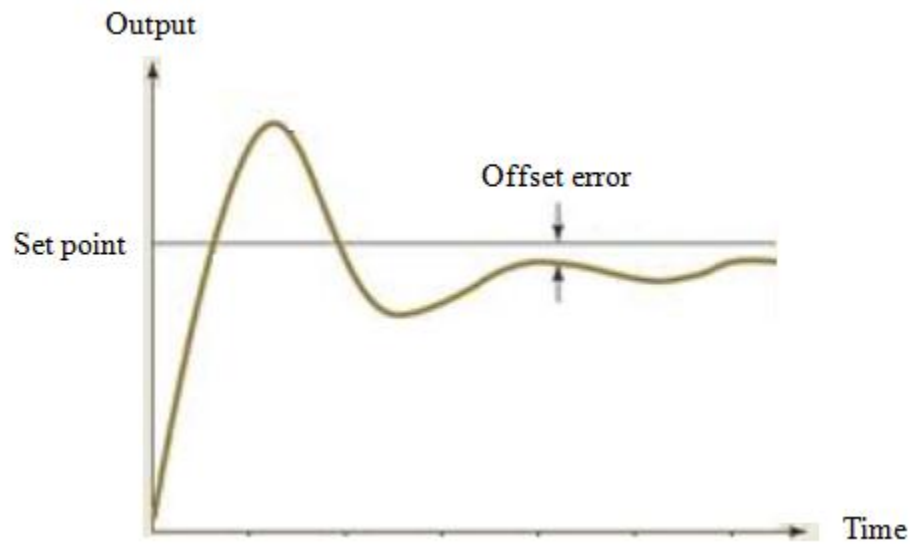

Figure 5.6: The offset error in proportional controller

5.1.2   Fractional Integrator

The fractional integrator produces the control signal $u(t)$ which is proportional to the fractional integral of the error signal $e(t)$. It can be described by the following relation in the time domain

$$u(t) = K_i D^{-\lambda} e(t) \tag{5.4}$$

Or, in Laplace domain as

$$U(s) = \frac{K_i}{s^\lambda} E(s) \tag{5.5}$$

The controller is given by
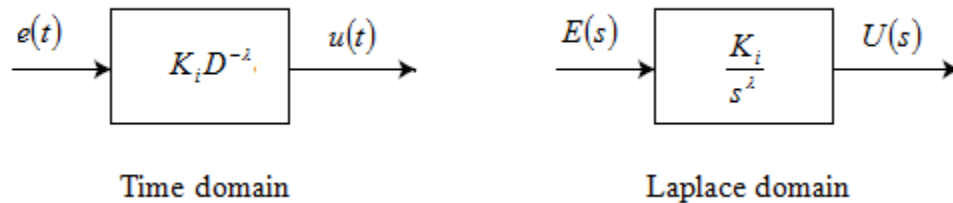
$$C(s) = \frac{K_i}{s^\lambda} \tag{5.6}$$

Figure 5.7: Representation of the fractional integrator controller in the time and frequency domains

The relation between the controller out and the error signal can be described by a fractional integral equation. Increasing the order (λ) reduces the steady state error. The

fractional integrator can eliminate the offset error completely when the order (λ) is equal or greater than one without making the integral constant (K_i) very large. It is possible to eliminate the offset error when the order (λ) is less than one by adding a pole and zero at the origin. Therefore, the fractional integrator in this case can be expressed as

$$\frac{1}{s^\lambda} = \frac{1}{s^\lambda}\frac{s}{s} = \frac{1}{s}s^{1-\lambda} \qquad 0 < \lambda < 1 \tag{5.7}$$

Equation (5.7) shows that fractional integrator can be expressed as the result of multiplying a pure integral by a fractional differentiator. Figure 5.8 shows the step response of fractional integrator $\left(\dfrac{1}{s^{0.6}}\right)$ before adding a pure integrator and differentiator at the origin and how the steady state error can be eliminated after adding them up.
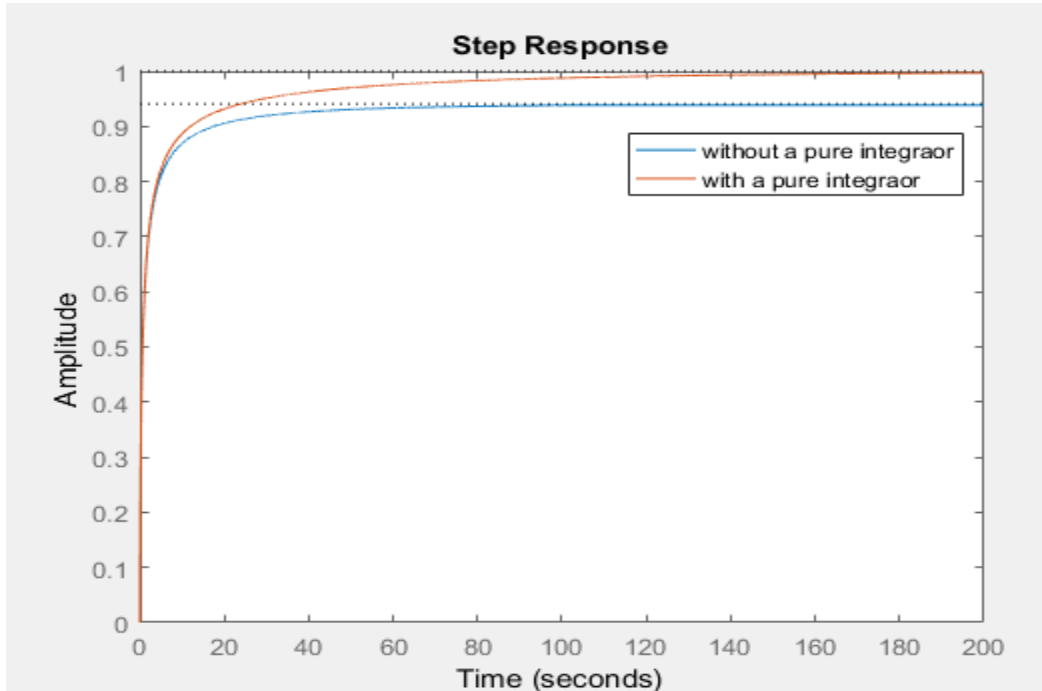

Figure 5.8: The step response of the fractional integrator $\dfrac{1}{s^{0.6}}$

86

5.1.3 Fractional Differentiator

The fractional differentiator produces the control signal $u(t)$ which is proportional to the fractional derivative of the error signal $e(t)$. The fractional differentiator action can be expressed in the time and Laplace domains as

$$u(t) = K_d D^\mu e(t) \tag{5.8}$$

$$U(s) = K_d s^\mu E(s) \tag{5.9}$$

The controller can be expressed as

$$C(s) = K_d s^\mu \tag{5.10}$$
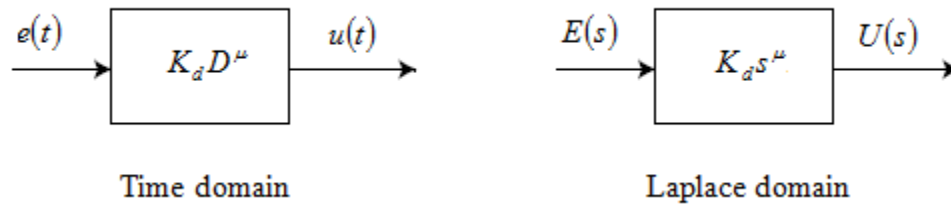

Time domain   Laplace domain

Figure 5.9: Representation of the fractional differentiator controller in the time and frequency domains

The relation between the controller output and the error signal can be described by a fractional differential equation. The fractional differentiator acts on the rate of change of the error based on the order (μ). The fractional differentiator can be used to anticipate the error. Therefore, it reduces the rate of change of error which improves the control performance. The fractional differentiator cannot be implemented alone. Hence,

87

proportional or integrator controllers should be added to the fractional differentiator in most cases. Fractional differentiators have some disadvantages such as amplifying noise signals especially when the order (μ) increases and have no effect on the steady state error. To illustrate that, Figure 5.10 shows that the noise signal appears in the feedback control system. The noise signal can be assumed as
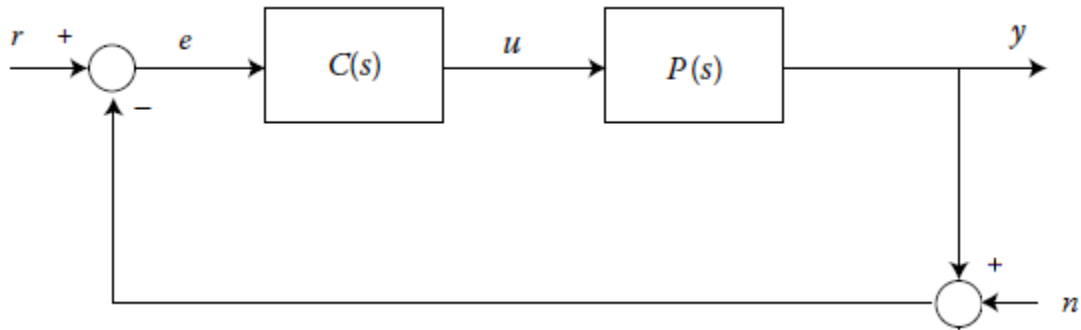
$$n(t) = A\sin(\omega t) \tag{5.11}$$

Figure 5.10: A feedback control system with noise

We have

$$e(t) = r(t) - y(t) - n(t) \tag{5.12}$$

So

The control signal is given by

$$u(t) = c(t)e(t) = c(t)[r(t) - y(t) - n(t)] \tag{5.13}$$

Therefore, the output signal of the controller contains the derivative part of the noise signal as

$$u_{Noise}(t) = -AK_d\omega^\mu \sin\left(\omega t + \frac{\pi\mu}{2}\right)$$ (5.14)

It can be seen that the amplitude of the controller output increases when the frequency is high and the differentiation order (μ) increases. Also, it can be noticed that the controller output due to the noise decreases when differentiation order (μ) decreases at high frequencies.

5.1.4 Fractional PI Controller (PI^λ)

This controller combines between the proportional action and the fractional integral action. It takes the following expression in the time domain

$$u(t) = K_p e(t) + K_i D^{-\lambda} e(t)$$ (5.15)

Or, in Laplace domain as

$$U(s) = K_p E(s) + \frac{K_i}{s^\lambda} E(s)$$ (5.16)

The controller can be expressed as

$$C(s) = K_p + \frac{K_i}{s^\lambda}$$ (5.17)

Figure 5.11 shows the frequency response of the following fractional PI

$$C(s) = 1 + \frac{1}{s^{0.7}}$$ (5.18)

It can be seen that at low frequencies, the integral action is present. The slope of the straight line is $(0.7 \times -20 = -14 \, \text{dB/dec})$ and the phase angle is $(0.7 \times -90 = -63°)$. At high frequencies, the proportional controller is dominant. The phase angle is almost zero.
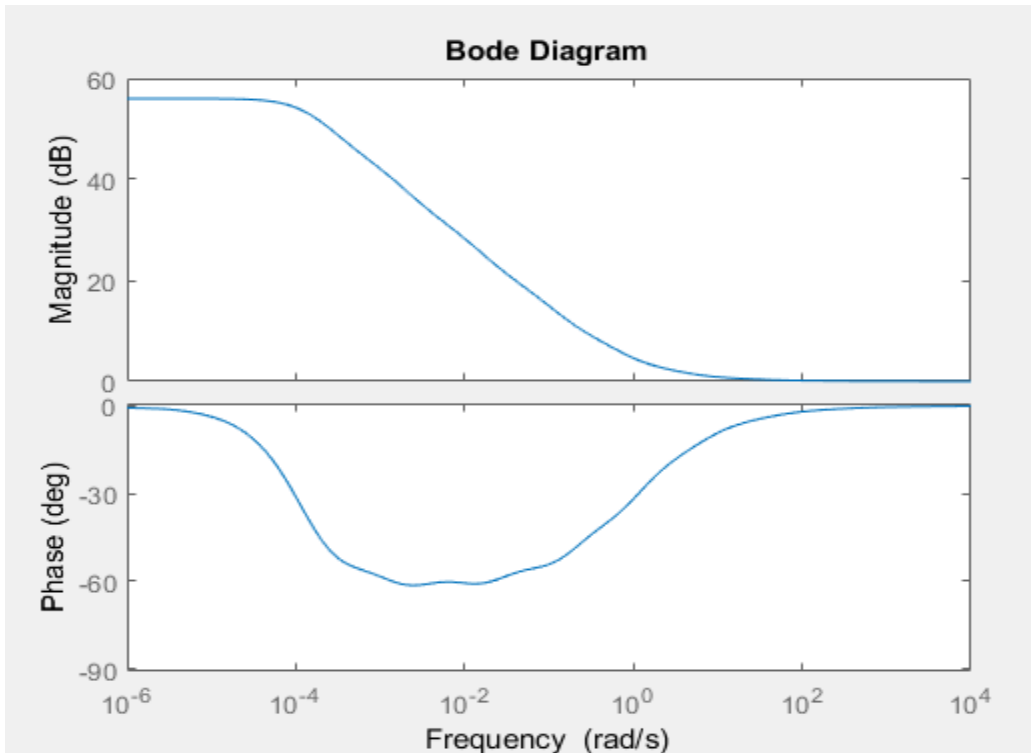

Figure 5.11: The frequency response of a PI controller

This controller has the following features

- It eliminates the steady state error as the order (λ) increases.

- It decreases the rise time as the order (λ) increases.

- It filters out the noise at high frequencies.

- It increases bandwidth of the system as the order (λ) increases.

- It increases order and type of the system.

90

5.1.5 Fractional PD Controller $\left(PD^{\mu}\right)$

The series combination of proportional controller and fractional derivative controller provides the fractional proportional derivative controller. The mathematical expression of this controller in time and Laplace domains can be expressed, respectively as

$$u(t) = K_p e(t) + K_d D^{\mu} e(t) \tag{5.19}$$

$$U(s) = K_p E(s) + K_d s^{\mu} E(s) \tag{5.20}$$

The controller can be give as

$$C(s) = K_p + K_d s^{\mu} \tag{5.21}$$

Figure 5.12 shows the frequency response of the following fractional PI

$$C(s) = 1 + s^{0.4} \tag{5.22}$$

It can be seen that at low frequencies, the proportional controller is dominant. The phase angle is almost zero. At high frequencies, the derivative action is present. The slope of the straight line is $\left(0.4 \times 20 = 5 \text{ dB/dec}\right)$ and the phase angle is $\left(0.4 \times 90 = 36°\right)$.
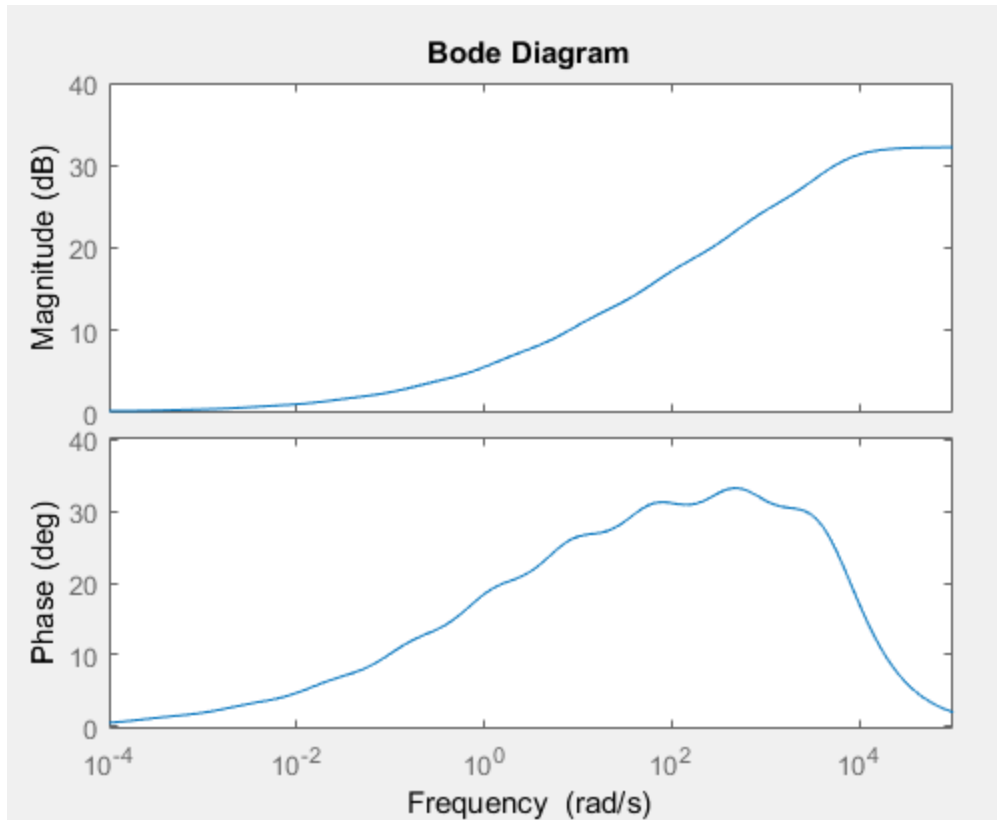
Figure 5.12: The frequency response of a PD controller

The fractional PD controller has the following properties

- It reduces the overshoot as the order (μ) increases.

- It improves transient.

- It reduces the settling time.

- It improves the bandwidth of the system.

- It may make noises at high frequencies as the order (μ) increases.

- It does not affect on steady state error.

5.1.6 Fractional PID $\left(PI^\lambda D^\mu\right)$

The combination of the three control actions (proportional, fractional integral and fractional derivative) gives the fractional PID. It can be given in the time domain as

$$u(t) = K_p e(t) + K_i D^{-\lambda} e(t) + K_d D^\mu e(t) \tag{5.23}$$

And, in Laplace domain as

$$U(s) = K_p E(s) + \frac{K_i}{s^\lambda} E(s) + K_d s^\mu E(s) \tag{5.24}$$

The noise at high frequencies is caused by the fractional differentiator. The noise can be reduced by adding a low pass filer whose time constant is (T). Therefore, the fractional PID may take this form

$$C(s) = K_p + \frac{K_i}{s^\lambda} + K_d \frac{1}{Ts+1} s^\mu \tag{5.25}$$

Figure 5.13 shows the effect of adding a low pass filer to a factional differentiator with $\left(K_d = 1 \quad T = 0.01 \quad \mu = 0.8\right)$.
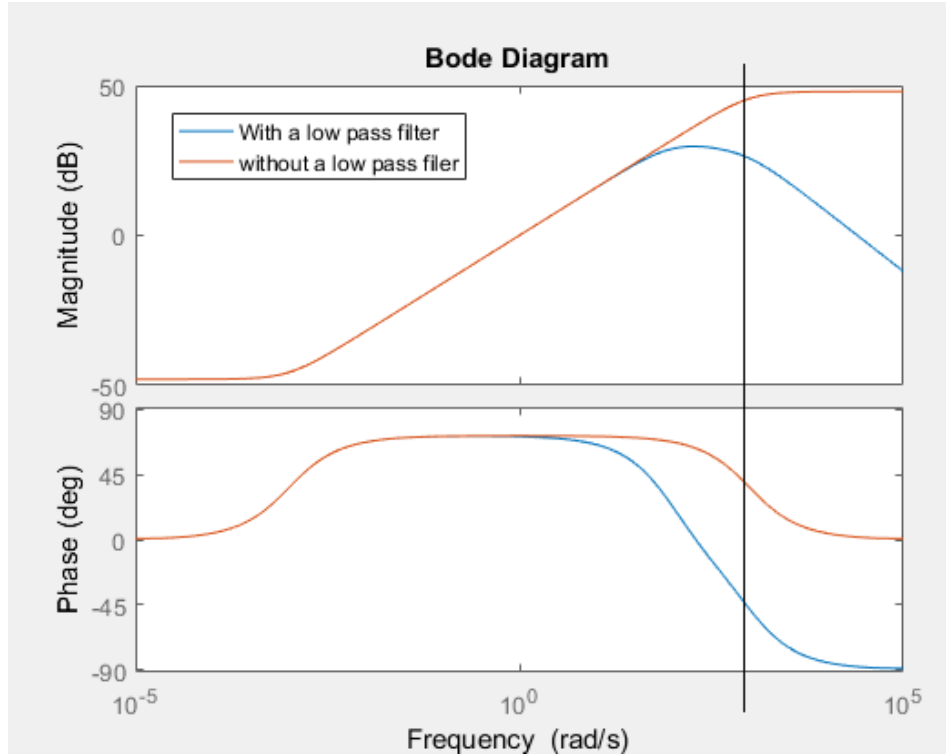
Figure 5.13: The effect of adding a low pass filter to a fractional differentiator

It can be seen that the low pass filter reduced the amplification from 42 dB to 28 dB at high frequencies. The range of approximation is $(10^{-3}, 10^{3})$ rad/s. The fractional PID controller improves the transient by reducing the settling time. Also, it eliminates the steady state error. The fractional PID controller should be tuned properly to achieve optimal performance. Figure 5.14 shows the frequency response of the following fractional controller with unity gains

$$C(s) = K_p + \frac{K_i}{s^{0.3}} + K_d s^{0.7} \qquad (5.26)$$

It can be seen that at low frequencies the controller behaves as a fractional integrator, at high frequencies behaves as a fractional differentiator in the range of approximation $(10^{-3}, 10^3)$ rad/sec.
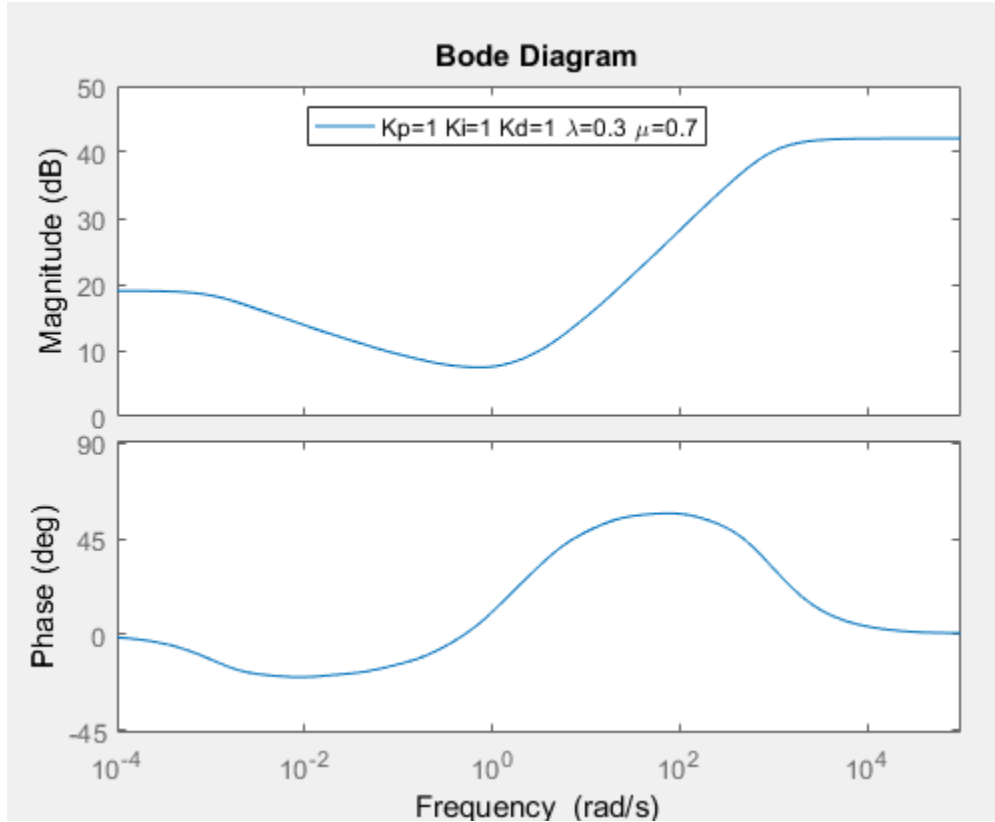

Figure 5.14: The frequency response of the fractional PID controller $C(s) = 1 + \dfrac{1}{s^{0.3}} + s^{0.7}$

The effect of the P-controller can be seen between the low and high frequencies as shown in Figure 5.15 where $K_p \gg K_i, K_d$.
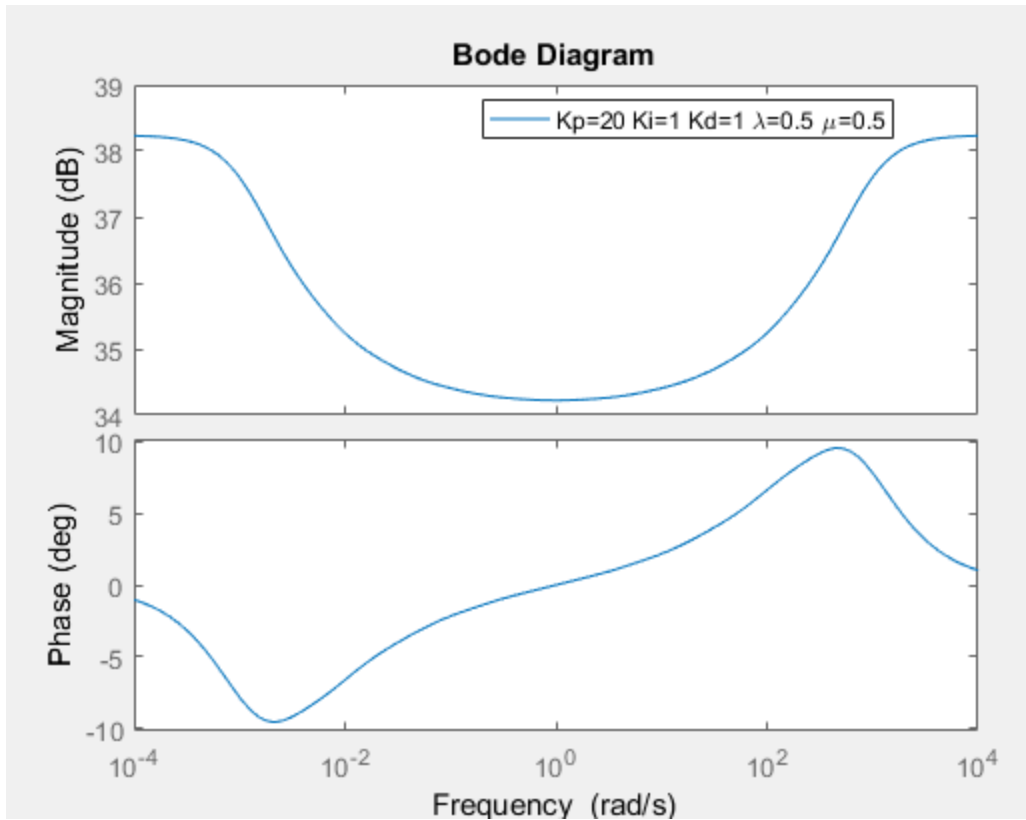
Figure 5.15: The frequency response of the fractional PID controller

$$C(s) = 20 + \frac{1}{s^{0.5}} + s^{0.5}$$

5.2 Robust Control system

The aim of the robust control is to deal with uncertainties caused by noise, disturbance, and modeling of the plant while designing a feedback controller. The controller is said to be robust if it is stable under different set of uncertainties. Figure 5.16 shows a closed loop system with uncertainties. Uncertainty can be found in the plant itself or due to the disturbance or the noise.
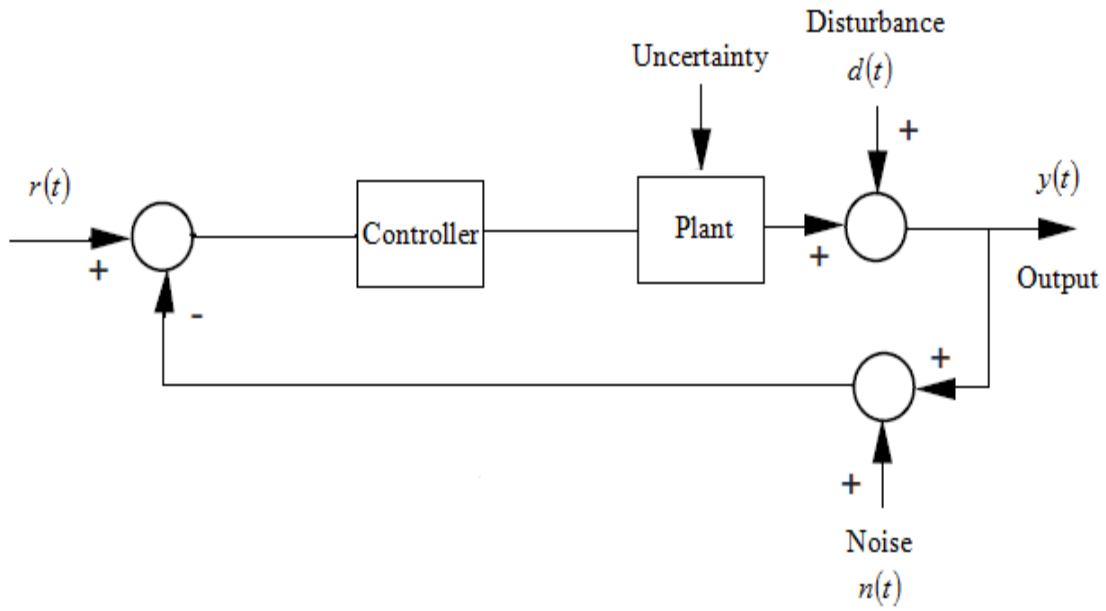
Figure 5.16: feedback control with uncertainties

The system in Figure 5.16 can be developed to the following robust control system as shown in Figure 5.17.
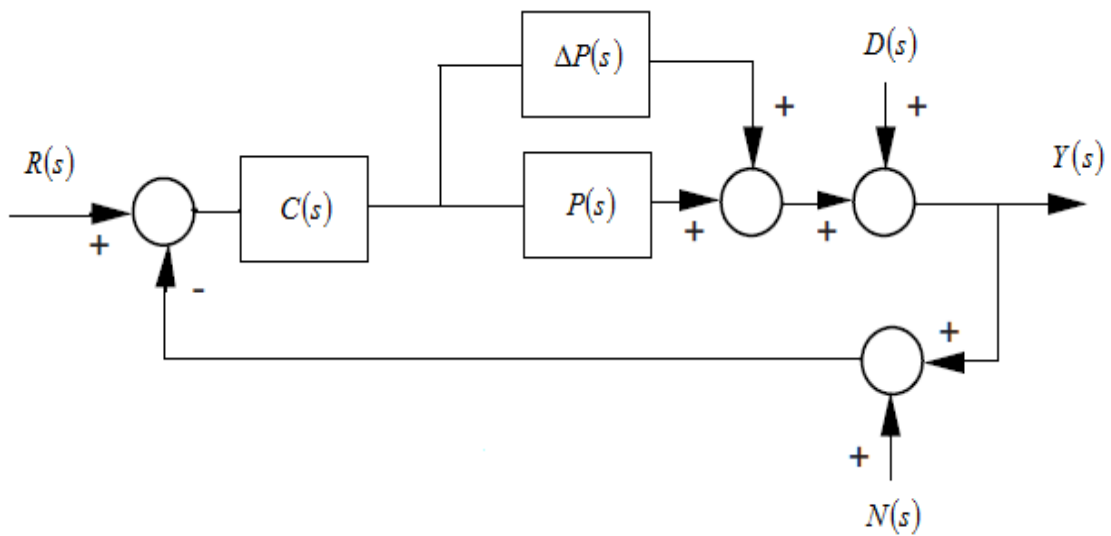

Figure 5.17: Robust control system

97

The transfer function $P(s)$ is the plant model without uncertainties which is considered to be nominal model where $\Delta P(s)$ represents the difference between the true and nominal values of the plant transfer function. In control theory, uncertainty can be represented by the following block diagram which shows additive uncertainty.
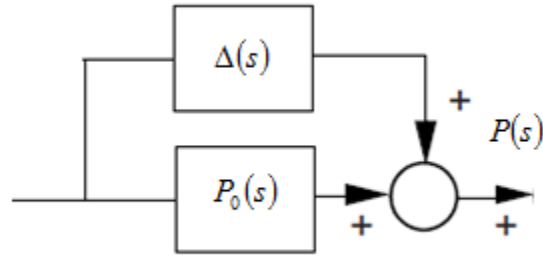

Figure 5.18: Additive uncertainty

The relationship between nominal plant $P_0(s)$ and the true plant or perturbed plant $P(s)$ is given by

$$P(s) = \Delta(s) + P_0(s) \tag{5.27}$$

The output of the system should be stable and work in the desired level of design when the nominal plant changes by an amount $\Delta(s)$. Disturbance and noise rejections measure the performance and robustness of the controller in the robust control system.

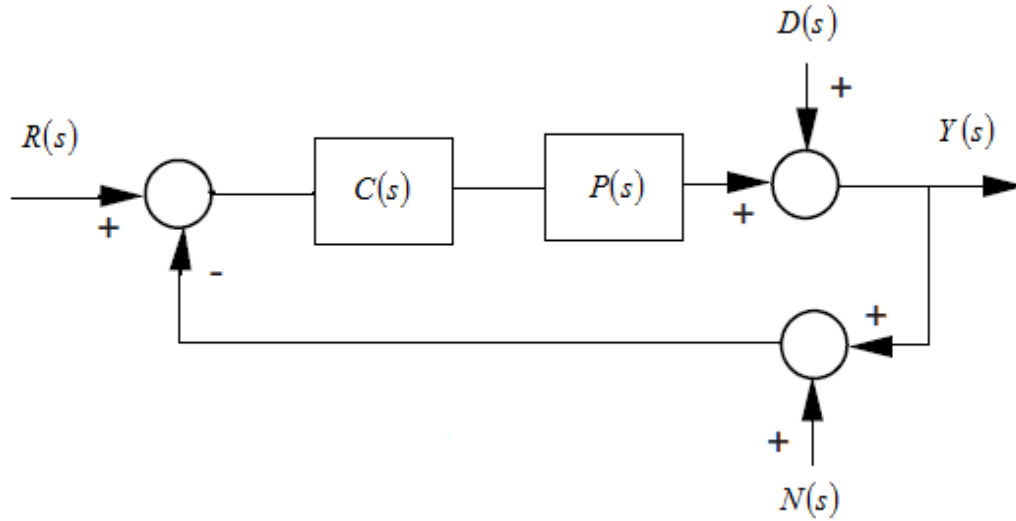### 5.2.1 The Sensitivity and Complementary Sensitivity Functions

Figure 5.19: A Simple feedback system

Figure 5.19 shows a simple feedback system in presence of disturbance and noise signals. The performance of the controller is measured by shaping the dynamic, rejecting the disturbance, and attenuating the noise. The output of the system can be expressed as

$$Y(s) = \frac{C(s)P(s)}{1+C(s)P(s)}R(s) + \frac{1}{1+C(s)P(s)}D(s) - \frac{C(s)P(s)}{1+C(s)P(s)}N(s) \qquad (5.28)$$

The definitions of sensitivity $S(s)$ and complementary sensitivity $T(s)$ are given by the following expressions

$$S(s) = \frac{1}{1+C(s)P(s)} \qquad (5.29)$$

$$T(s) = \frac{C(s)P(s)}{1+C(s)P(s)} \qquad (5.30)$$

Therefore, the error signal can be given by

$$E(s) = \frac{1}{1 + C(s)P(s)}R(s) - \frac{1}{1 + C(s)P(s)}D(s) - \frac{1}{1 + C(s)P(s)}N(s) \qquad (5.31)$$

Reducing the error signal can be done by making the sensitivity $S(s)$ and complementary sensitivity $T(s)$ small. The relationship between the sensitivity $S(s)$ and complementary sensitivity $T(s)$ is given by

$$S(s) + T(s) = 1 \qquad (5.32)$$

In applied applications, the sensitivity and complementary sensitivity should be small which is not applied mathematically at all frequencies. The solution to this problem is making both of them small at some frequencies. It is known that the disturbance signal is applied at low frequencies, while the noise signal is applied at high frequencies. Therefore, the sensitivity should be small at low frequencies to reduce the effect of the disturbance, while the complementary sensitivity should be small at low frequencies to reduce the effect of measurement noise. The magnitude of $1 + C(s)P(s)$ should be large enough to make $S(s)$ small. Therefore, the magnitude of the controller should be large if the magnitude of the plant is small at low frequencies. Similarly, the magnitude of the open loop $C(s)P(s)$ should be close to zero at high frequencies to make $T(s)$ small. The disturbance rejection of a fractional PID controller can be calculated by assuming that the fractional PID has the following form

$$C(s) = K_p + \frac{K_i}{s^\lambda} + K_d s^\mu$$

100

$$= \frac{K_p s^\lambda + K_i + K_d s^{\mu+\lambda}}{s^\lambda} \qquad (5.33)$$

Also, the plant is given by the following transfer function

$$P(s) = \frac{a(s)}{b(s)} \qquad (5.34)$$

Therefore, the open loop is

$$C(s)P(s) = \frac{a(s)\left(K_p s^\lambda + K_i + K_d s^{\mu+\lambda}\right)}{s^\lambda b(s)} \qquad (5.35)$$

The relationship between the output and the disturbance can be written as

$$\frac{Y(s)}{D(s)} = \frac{1}{1 + C(s)P(s)}$$

$$= \frac{1}{1 + \dfrac{a(s)\left(K_p s^\lambda + K_i + K_d s^{\mu+\lambda}\right)}{s^\lambda b(s)}}$$

$$= \frac{s^\lambda b(s)}{s^\lambda b(s) + a(s)\left(K_p s^\lambda + K_i + K_d s^{\mu+\lambda}\right)} \qquad (5.36)$$

From the final value theorem, we have

$$y(\infty) = \lim_{s \to 0} s\left[\frac{1}{1 + C(s)P(s)}\right]D(s) \qquad (5.37)$$

Assuming that $D(s) = \dfrac{A}{s^\alpha}$ \qquad (5.38)

Therefore

$$\lim_{s \to 0} s \frac{s^\lambda b(s)}{s^\lambda b(s) + a(s)\left(K_p s^\lambda + K_i + K_d s^{\mu+\lambda}\right)} \frac{A}{s^\alpha}$$

$$= \lim_{s \to 0} s \frac{Ab(0)}{a(0)K_i} s^{\lambda-\alpha}$$

Hence, the output can be evaluated as

$$y(\infty) = 0 \quad if \quad \lambda = \alpha \qquad\qquad (5.39)$$

The result above shows that the disturbance signal is attenuated at low frequencies when the order of the fractional integrator is equal to the order of the fractional disturbance signal.

CHAPTER 6

FRACTIONAL PID CONTROLLER TUNING BY FREQUENCY LOOP-SHAPING

This chapter includes the algorithms of the frequency loop shaping technique. It also contains some fractional order systems models from some references and the results are obtained by using a Matlab program.

6.1 The Frequency Loop-Shaping Technique

The frequency loop shaping technique is a method to tune the controller parameters. Minimizing the difference between the actual and a target transfer function is an objective to determine the fractional PID gains (K_p, K_i, K_d) and the fractional orders (λ, μ) to achieve a closed loop sensitivity bandwidth approximately to a desired bandwidth (Target bandwidth) with a small sensitivity peak value. The optimization problem using the frequency loop shaping can be illustrated by the following steps.
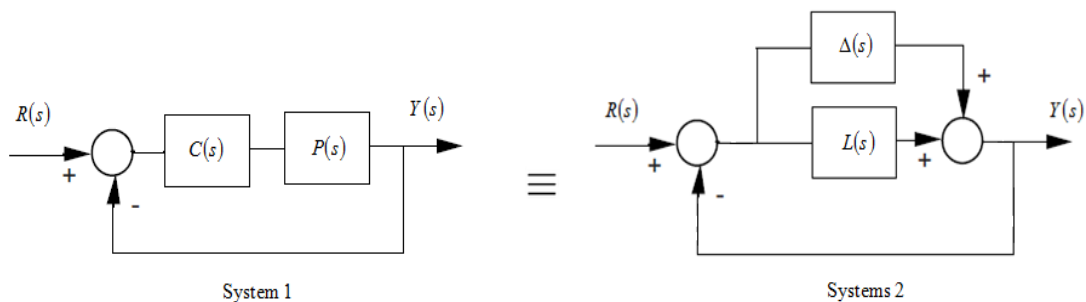
Figure 6.1: Two equivalent systems

Figure 6.1 shows system (1) which contains a controller $C(s)$ and plant $P(s)$ while system (2) contains a target representation with additive uncertainty. The two systems are

assumed to be equivalent. Therefore, the relationship between the two systems can be given as

$$\Delta(s) = C(s)P(s) - L(s) \tag{6.1}$$

The closed loop of system (2) is robustly stable according to the small gain theorem if

$$\|S(s)\|_\infty \|\Delta(s)\|_\infty < 1 \tag{6.2}$$

The expression above can be rewritten as

$$\|S(s)\|_\infty \|C(s)P(s) - L(s)\|_\infty < 1 \tag{6.3}$$

Therefore

$$\|S(s)C(s)P(s) - S(s)L(s)\|_\infty < 1 \tag{6.4}$$

Knowing that $S(s)L(s) = T(s)$, we have

$$\|S(s)C(s)P(s) - T(s)\|_\infty < 1 \tag{6.5}$$

The controller $C(s)$ can have this form

$$C(s) = K_p + \frac{K_i}{s^\lambda} + K_d s^\mu \tag{6.6}$$

Therefore

$$\left\| S(s)P(s)K_p + S(s)P(s)\frac{1}{s^\mu}K_i + S(s)P(s)s^\mu K_d - T(s) \right\|_\infty < 1 \tag{6.7}$$

The previous equation may take this form

$$\left\| f_1(j\omega)K_p + f_2(j\omega;\lambda)K_i + f_3(j\omega;\mu)K_d - T(s) \right\|_\infty < 1 \qquad (6.8)$$

A frequency weighting function W_1 can be introduced in equation 6.8 to adjust the overshoot and the sensitivity peak value over an interval of frequencies. The frequency range for the approximation is around the crossover frequency $(0.01 \times \text{Bw to } 100 \times \text{Bw})$. Therefore, the previous equation would become

$$\left\| W_1(j\omega)[f_1(j\omega)K_p + f_2(j\omega;\lambda)K_i + f_3(j\omega;\mu)K_d - T(s)] \right\|_\infty < 1 \qquad (6.9)$$

Assuming that

$$\begin{aligned} W_1(j\omega)f(j\omega;\lambda,\mu) &= F(j\omega;\lambda,\mu) \\ \theta &= [K_p, K_i, K_d]^T \\ W_1(j\omega)T(j\omega) &= Z(j\omega) \end{aligned} \qquad (6.10)$$

Equation 6.9 becomes

$$\left\| F(j\omega;\lambda,\mu)\theta - Z(j\omega) \right\|_\infty < 1 \qquad (6.11)$$

The fractional PID gains can be computed with a certain range for fractional orders (λ,μ) using the following optimization problem

$$\min_{\theta \in C} \left\| F(j\omega;\lambda,\mu)\theta - Z(j\omega) \right\| \qquad (6.12)$$

where C is the convex set of constraints for θ which provide positive gains for the fractional orders $(0 < \lambda < 2)$ and $(0 < \mu < 2)$. Also, the optimization problem can be solved by using the following expression

$$\min_{K_p, K_i, K_{d,}, \lambda, \mu} \|Ub\| \qquad (6.13)$$

where U_b is the fitting error. It can be given as

$$Ub = \left\| S(j\omega) \left[P(s)C(s; K_p, K_i, K_{d,}, \lambda, \mu) - L(s) \right] \right\|_{s=j\omega} \qquad (6.14)$$

The value of fitting error should be less than one to guarantee closed loop stability. The value around $(0.2 - 0.3)$ or less provides best results. Figure 6.2 shows the representation of the fitting error function (U_b) with the fractional orders (λ, μ) for computing the fraction PID gains.
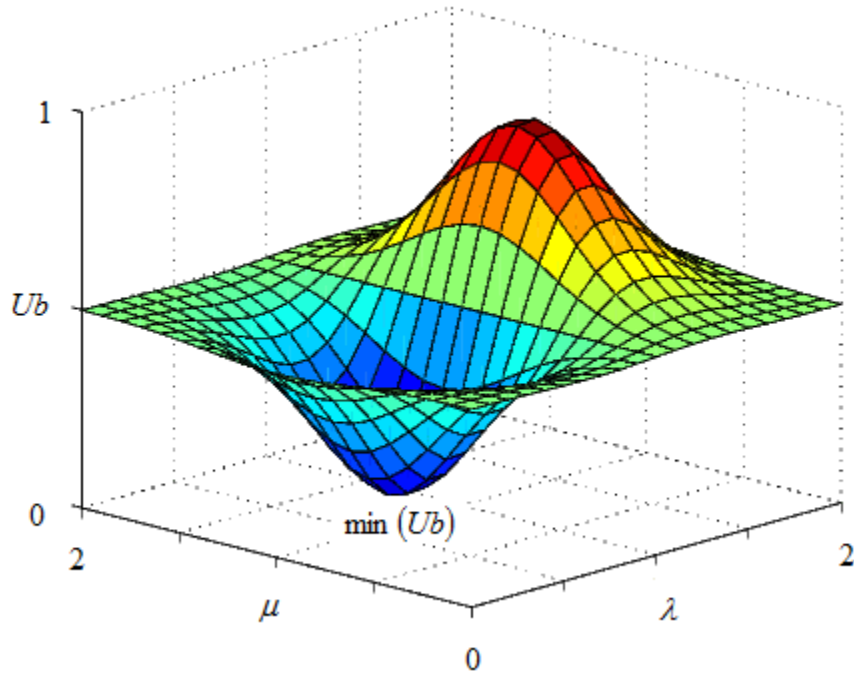
Figure 6.2: The fitting error (U_b) with fractional orders (λ, μ)

106

6.2 Choosing the Order of the Fractional Integrator as a Target

One of the most important questions is how the order of the fractional integrator can be chosen. The order of the fractional integrator can be chosen through of the following methods:

6.2.1 Knowing the Behavior of the Disturbance Signal

The resonant peak (M_r) is defined as the maximum value of the magnitude of the closed loop frequency response where the resonant frequency (ω_r) is the frequency at which the resonant peak occurs.

Figure 6.3 shows a closed loop system with the disturbance signal $d(t)$.

$$d(t) = \frac{At^{\alpha-1}}{\Gamma(\alpha)}$$

$$L(s) = \frac{A}{s^\alpha}$$
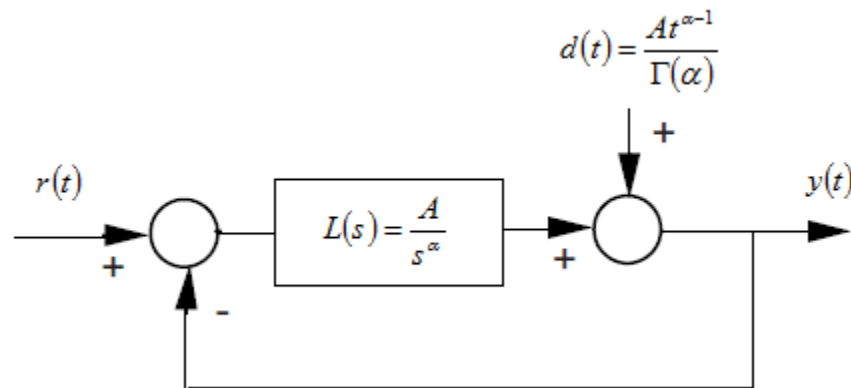
Figure 6.3: A closed loop with disturbance signal

It is possible to link between choosing the order of fractional integrator (α) and the resonant peak (M_r). In order to obtain the best rejection of the following disturbance

signal $\left(\dfrac{At^{\alpha-1}}{\Gamma(\alpha)}\right)$, the open loop of the system should contain a fractional integrator of order

(α). The output of the system in the presence of the disturbance signal can be expressed as

$$\frac{Y(s)}{D(s)} = \frac{1}{1 + L(s)} \qquad (6.15)$$

Hence

$$Y(s) = \frac{1}{1 + L(s)} D(s)$$

The target can be chosen as

$$L(s) = \frac{A}{s^{\alpha}} \qquad (6.16)$$

Therefore

$$Y(s) = \frac{s^{\alpha}}{A + s^{\alpha}} D(s) \qquad (6.17)$$

If the disturbance signal is $d(t) = \dfrac{At^{\alpha-1}}{\Gamma(\alpha)}$, the output will have this expression

$$Y(s) = \frac{A}{A + s^{\alpha}} \qquad (6.18)$$

The resonant peak can be obtained by finding the maximum frequency of the following expression

$$\frac{d}{d\omega}|Y(j\omega)| = 0 \tag{6.19}$$

We have

$$Y(j\omega) = \frac{A}{A + (j\omega)^{\alpha}} \tag{6.20}$$

Therefore

$$|Y(j\omega)| = \frac{A}{\sqrt{\left(A + \omega^{\alpha}\cos\left(\frac{\alpha\pi}{2}\right)\right)^2 + \left(\omega^{\alpha}\sin\left(\frac{\alpha\pi}{2}\right)\right)^2}}$$

$$= \frac{A}{\sqrt{A^2 + 2A\omega^{\alpha}\cos\left(\frac{\alpha\pi}{2}\right) + \omega^{2\alpha}}} \tag{6.21}$$

$$\frac{d}{d\omega}|Y(j\omega)| = 0$$

Therefore

$$\frac{-\alpha A\omega^{\alpha}\left(\omega^{\alpha} + \cos\left(\frac{\alpha\pi}{2}\right)A\right)}{\omega\left(\omega^{2\alpha} + 2\cos\left(\frac{\alpha\pi}{2}\right)A\omega^{\alpha} + A^2\right)^{\frac{3}{2}}} = 0 \tag{6.22}$$

Having the maximum at

$$-\alpha A\omega^{\alpha}\left(\omega^{\alpha} + \cos\left(\frac{\alpha\pi}{2}\right)A\right) = 0 \tag{6.23}$$

Therefore

109

$$\omega^{\alpha} = -A\cos\left(\frac{\alpha\pi}{2}\right) \tag{6.24}$$

The resonant peak is given by

$$\omega_r = \left[-A\cos\left(\frac{\alpha\pi}{2}\right)\right]^{\frac{1}{\alpha}}, \quad \alpha > 1 \tag{6.25}$$

The magnitude of resonant peak (M_r) at the resonant frequency (ω_r) can be calculated as

$$M_r = \max_{\omega}\left|Y(j\omega_r)\right| \tag{6.26}$$

$$= \frac{A}{\sqrt{A^2 + 2A\left(-A\cos\left(\frac{\alpha\pi}{2}\right)\right)\cos\left(\frac{\alpha\pi}{2}\right) + \left(-A\cos\left(\frac{\alpha\pi}{2}\right)\right)^2}}$$

$$= \frac{A}{\sqrt{A^2 - 2A^2\cos\left(\frac{\alpha\pi}{2}\right)\cos\left(\frac{\alpha\pi}{2}\right) + A^2\cos^2\left(\frac{\alpha\pi}{2}\right)}}$$

$$= \frac{A}{\sqrt{A^2\left(1 - 2\cos\left(\frac{\alpha\pi}{2}\right)\cos\left(\frac{\alpha\pi}{2}\right) + \cos^2\left(\frac{\alpha\pi}{2}\right)\right)}}$$

$$= \frac{A}{A\sqrt{1 - 2\cos^2\left(\frac{\alpha\pi}{2}\right) + \cos^2\left(\frac{\alpha\pi}{2}\right)}}$$

$$= \frac{1}{\sqrt{1 - \cos^2\left(\frac{\alpha\pi}{2}\right)}} = \frac{1}{\sqrt{\sin^2\left(\frac{\alpha\pi}{2}\right)}}$$

$$= \frac{1}{\sin\left(\frac{\alpha\pi}{2}\right)}$$

$$= \operatorname{cosec}\left(\frac{\alpha\pi}{2}\right) \tag{6.27}$$

It can be seen that the magnitude of resonant peak (M_r) depends only on the order of the

fractional integrator (α). Figure 6.4 shows the magnitude of resonant peak for different

values of the order of the fractional integrator. The slope of the straight line is

$(-20\alpha \text{ dB/dec})$.
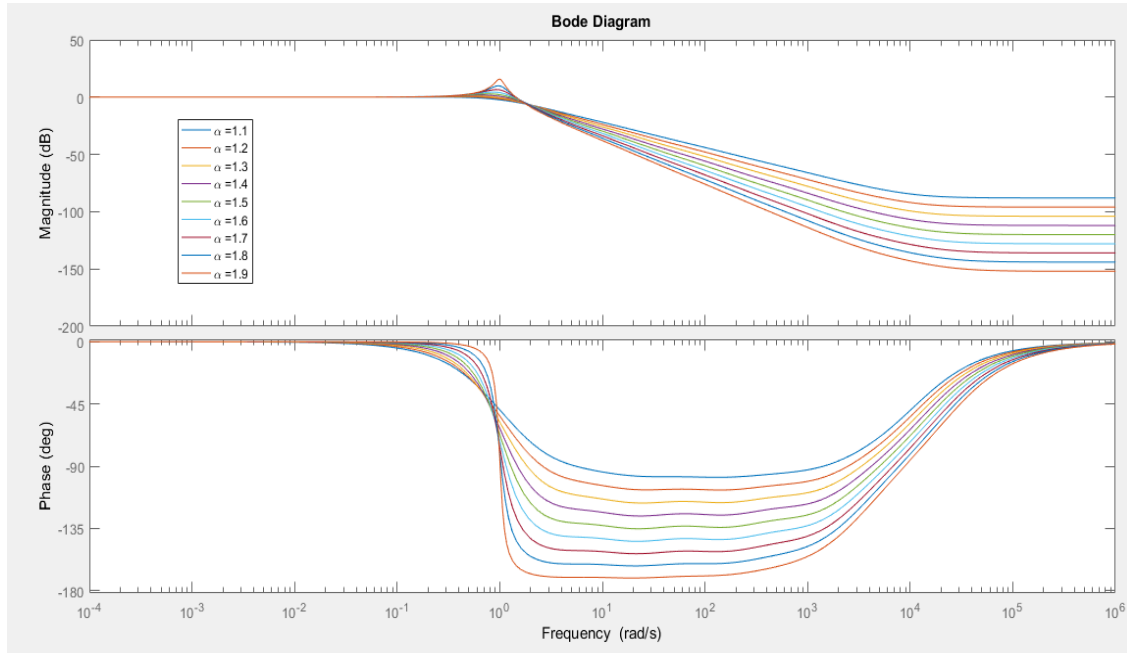
Figure 6.4: The frequency response of the system

It can be seen that the resonant peak value increases as the negative slop increases. Table

6.1 shows the resonant peak (M_r) and slope line for different values of the fractional

integrator order (α).

Table 6.1: The resonant peak and slope for different (α)

α	Resonant peak (M_r)	Slope
1	0 dB	0 dB/dec
1.1	0.107601 dB	-22 dB/dec
1.2	0.435873 dB	-24 dB/dec
1.3	1.00238 dB	-26 dB/dec
1.4	1.84085 dB	-28 dB/dec
1.5	3.0103 dB	-30 dB/dec
1.6	4.61563 dB	-32 dB/dec
1.7	6.85906 dB	-34 dB/dec
1.8	10.2004 dB	-36 dB/dec
1.9	16.1136 dB	-38 dB/dec

The resonant peak (M_r) provides a good way to measure the relative stability of a closed loop system. The overshoot in the transient response increases as the resonant peak increases. Many applied systems are designed with the resonant peak between 1.1 and 1.5. Similarly, the resonant frequency (ω_r) provides a good way to measure the speed response of the system. The system response is expected to be fast when the resonant frequency is high.

6.2.2 Bandwidth

The bandwidth is defined as the range of the frequencies for which the magnitude of the open loop system has dropped $(3\,\text{dB})$ from its DC gain. It is possible to link between the order of the fractional integrator (The target) and the bandwidth directly as the following

The target is assumed to be

$$L(s) = \frac{A}{s^{\alpha}}$$

(6.28)

The closed loop is

$$H(s) = \frac{A}{s^{\alpha} + A}$$

(6.29)

Therefore

$$H(j\omega) = \frac{A}{(j\omega)^{\alpha} + A}$$

$$= \frac{A}{j^{\alpha} \omega^{\alpha} + A}$$

(6.30)

It is known that

$$j^{\alpha} = \cos\left(\frac{\alpha\pi}{2}\right) + j\sin\left(\frac{\alpha\pi}{2}\right)$$

(6.31)

Therefore

$$H(j\omega) = \frac{A}{\left[\cos\left(\frac{\alpha\pi}{2}\right) + j\sin\left(\frac{\alpha\pi}{2}\right)\right]\omega^{\alpha} + A}$$

$$H(j\omega) = \frac{A}{\cos\left(\frac{\alpha\pi}{2}\right)\omega^{\alpha} + j\sin\left(\frac{\alpha\pi}{2}\right)\omega^{\alpha} + A}$$

$$H(j\omega) = \frac{A}{\left[A + \omega^{\alpha}\cos\left(\frac{\alpha\pi}{2}\right)\right] + j\left[\omega^{\alpha}\sin\left(\frac{\alpha\pi}{2}\right)\right]}$$

113

$$|H(j\omega)| = \frac{A}{\sqrt{\left(A + \omega^\alpha \cos\left(\frac{\alpha\pi}{2}\right)\right)^2 + \left(\omega^\alpha \sin\left(\frac{\alpha\pi}{2}\right)\right)^2}}$$

$$= \frac{A}{\sqrt{A^2 + \omega^{2\alpha} \cos^2\left(\frac{\alpha\pi}{2}\right) + 2A\omega^\alpha \cos\left(\frac{\alpha\pi}{2}\right) + \omega^{2\alpha} \sin^2\left(\frac{\alpha\pi}{2}\right)}}$$

$$= \frac{A}{\sqrt{\omega^{2\alpha}\left[\cos^2\left(\frac{\alpha\pi}{2}\right) + \sin^2\left(\frac{\alpha\pi}{2}\right)\right] + 2A\omega^\alpha \cos\left(\frac{\alpha\pi}{2}\right) + A^2}} \tag{6.32}$$

Since

$$\cos^2\left(\frac{\alpha\pi}{2}\right) + \sin^2\left(\frac{\alpha\pi}{2}\right) = 1 \tag{6.33}$$

Thus

$$|H(j\omega)| = \frac{A}{\sqrt{\omega^{2\alpha} + 2A\omega^\alpha \cos\left(\frac{\alpha\pi}{2}\right) + A^2}} \tag{6.34}$$

The bandwidth is found by equating the magnitude of $H(j\omega)$ to $\frac{1}{\sqrt{2}}$.

Hence

$$\left|H(j\omega_{3db})\right|^2 = \frac{1}{2} \tag{6.35}$$

Therefore

114

$$\frac{A^2}{\omega_{3dB}^{2\alpha} + 2A\omega_{3dB}^{\alpha} \cos\left(\frac{\alpha\pi}{2}\right) + A^2} = \frac{1}{2}$$

$$\omega_{3dB}^{2\alpha} + 2A\omega_{3dB}^{\alpha} \cos\left(\frac{\alpha\pi}{2}\right) + A^2 = 2A^2 \qquad (6.36)$$

Solving the quadratic equation for ω_{3dB}^{α}, yields

$$\omega_{3dB}^{\alpha} = -A\cos\left(\frac{\alpha\pi}{2}\right) \pm A\sqrt{\cos^2\left(\frac{\alpha\pi}{2}\right) + 1}$$

$$\omega_{3dB}^{\alpha} = A\left[-\cos\left(\frac{\alpha\pi}{2}\right) \pm \sqrt{\cos^2\left(\frac{\alpha\pi}{2}\right) + 1}\right] \qquad (6.37)$$

Since ω_{3dB}^{α} is always positive, Therefore

$$\omega_{3dB}^{\alpha} = A\left[\sqrt{\cos^2\left(\frac{\alpha\pi}{2}\right) + 1} - \cos\left(\frac{\alpha\pi}{2}\right)\right] \qquad (6.38)$$

Thus

$$\omega_{3dB} = A^{\frac{1}{\alpha}}\left[\sqrt{\cos^2\left(\frac{\alpha\pi}{2}\right) + 1} - \cos\left(\frac{\alpha\pi}{2}\right)\right]^{\frac{1}{\alpha}} \qquad (6.39)$$

It can be seen that the bandwidth of the system depends directly on the values of fractional integrator order (α) and the constant (A) which depends on the raise time of the system. Therefore, it is expected to have a faster rise time when the bandwidth is high.

6.2.3 Phase Margin

The phase margin is the difference between the phase of the open loop system at the gain crossover frequency and $(-180°)$. It is possible to link between the order of the fractional integrator (The target) and phase margin as the following

The target is assumed to be

$$L(s) = \frac{A}{s^{\alpha}} \tag{6.40}$$

The phase margin can be calculated from

$$\text{Phase Margin} = \arg\left|L(j\omega_c)\right| + \pi \tag{6.41}$$

where $\arg\left|L(j\omega_c)\right| = -\dfrac{\alpha\pi}{2}$ (6.42)

Therefore

$$-\frac{\alpha\pi}{2} = \pi + \text{Phase Margin} \tag{6.43}$$

So

$$\alpha = 2 - \frac{2}{\pi}\text{Phase Margin}$$

$$= 2 - \frac{\text{Phase Margin}}{90°} \tag{6.44}$$

Table 6.2 shows the phase margin for different values of the order of the fractional integrator (α).

Table 6.2: The phase margin for different (α)

α	Phase Margin
0	$180°$
0.1	$171°$
0.2	$162°$
0.3	$153°$
0.4	$144°$
0.6	$126°$
0.7	$117°$
1	$90°$
1.1	$81°$
1.2	$72°$
1.3	$63°$
1.5	$45°$
1.7	$27°$
1.9	$9°$
2	$0°$

6.3   Fractional Order Systems and Results

This section contains three fractional examples with their mathematical modeling. The first example is the motion of an immersed plate in a viscous Newtonian fluid. The second example is the Buck converter circuit. The third example is furnace temperature control. All mathematical equations with their fractional transfer functions are found in the listed references. All results and plots were made using Matlab.

6.3.1 Heating Furnace

Furnaces are used for extracting metals from their ores. They are mainly used for the production of iron and steel as used for other metals. Figure 6.5 shows a blast furnace in a factory.

Figure 6.5: Blast furnace in Luxembourg

Fuel is supplied in the form of coal and iron ore continuously from the top of the furnace. The air which is powered by extra oxygen is blown into the bottom of the furnace, so that the chemical reactions occur inside the furnace as shown in Figure 6.6.
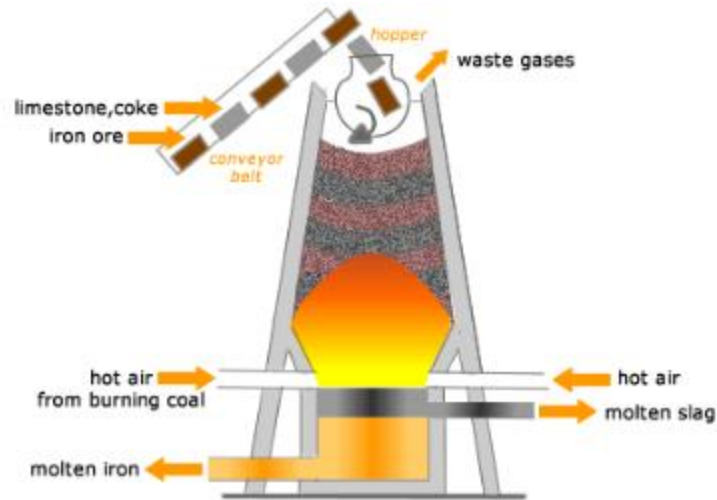
Figure 6.6: Mechanism of heating furnace system

When the materials are heated inside the furnace, the gas is formed inside the chambers, which may cause an explosion due to the high pressure on the furnace wall, causing a threat to the facility and its employees. One solution is to reduce the heat inside the furnace to ensure that there is no explosion occurs but this solution is useless because the end result will have steady state error and the settling time is too high.

Therefore, the material flow rate and gas pressure must be adjusted inside the furnace. The end result will eliminate the steady state error and reduce the settling time when the maximum heat is used. The dynamical modeling of the system contains the mass, energy, and all heat transfer inside the system

The heating furnace can be expressed mathematically as the following differential equation

$$F = m\ddot{x} + b\dot{x} + kx \tag{6.45}$$

The equation above shows that the total force is the sum of individual forces caused by mass (m), damping (b) and spring (k) element. Reference [16] shows that the differential equation of the heating furnace system is giving by

$$F = 73043\ddot{x} + 4893\dot{x} + 1.93x \qquad (6.46)$$

It can be expressed in the Laplace domain as the following transfer function

$$G(s) = \frac{1}{73043s^2 + 4893s + 1.93} \qquad (6.47)$$

The fractional order model of heating furnace system can be evaluated using Grunwald-Letnikov definition as

$$G_{FOM}(s) = \frac{1}{14494s^{1.31} + 6009.5s^{0.97} + 1.69} \qquad (6.48)$$

Where $G_{FOM}(s)$ represent the transfer function of the plant in the fractional order system. In the same reference, the fractional order controller was obtained using Nelder-Mead optimization technique as

$$C(s) = 99.998 + \frac{99.852}{s^{0.35073}} + 99.94s^{0.068221} \qquad (4.49)$$

120

6.3.1.1 Results
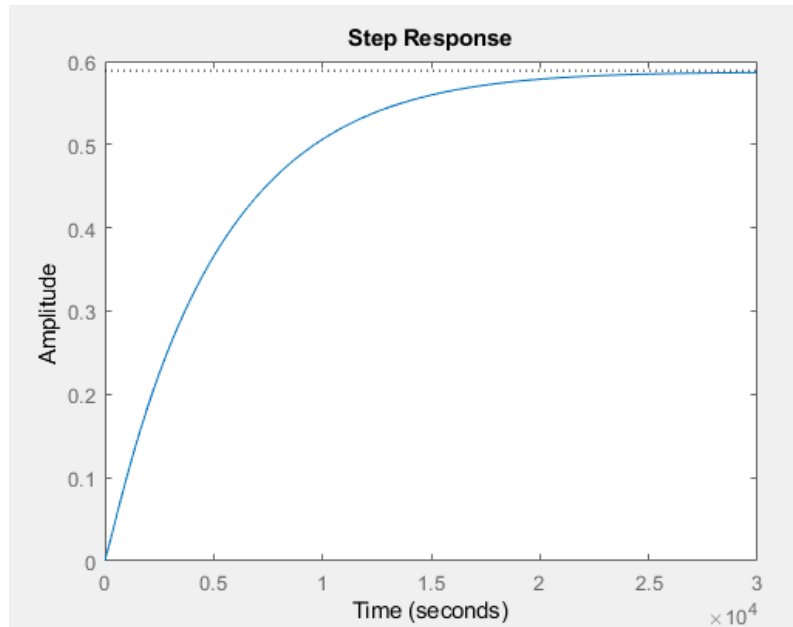
Figure 6.7: The step response of the uncompensated system

Figure 6.7 shows the step response of the uncompensated system. It can be seen that the uncompensated system is stable and has a steady state response of (0.4) in response. The bandwidth of the desired system is around (0.048928) rad/sec.

A fractional PID controller can be designed to eliminate the steady state error and improve the system transient. The target can be chosen to have the desired bandwidth as

$$L(s) = \frac{0.00987}{s^{1.35}}$$

(6.50)

The obtained results would be as follows

The distribution of the fitting error all over the range of the fractional orders is shown in

121
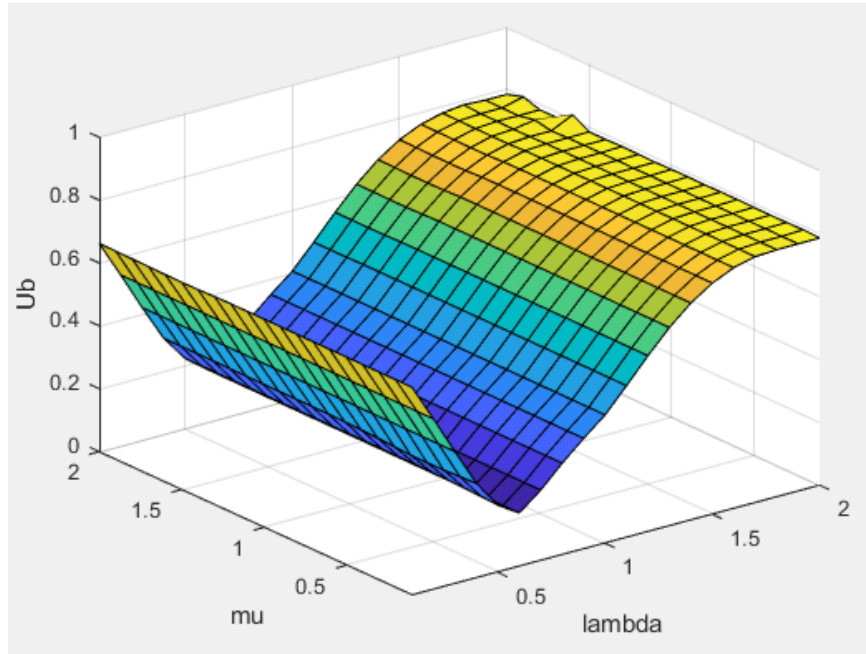
Figure 6.8.

Figure 6.8: The fitting error (U_b) with fractional orders (λ, μ)
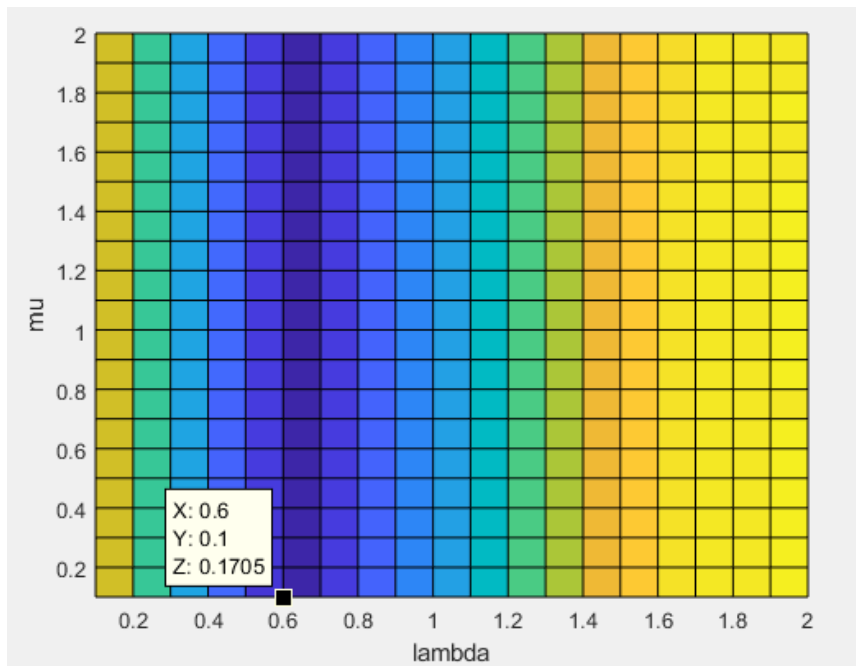
Figure 6.9: The fitting error at $(\lambda = 0.6$ and $\mu = 0.1)$

From Figure 6.9, the best choice for the orders of the fractional PID controller would be $(\lambda = 0.6$ and $\mu = 0.1)$. It satisfies the relationship $\min\limits_{K_p, K_i, K_{d,}, \lambda, \mu} \|Ub\|$.

The values of the fractional PID parameters are:

$K_p = 2.8186 \times 10^2$
$K_i = 13.272$
$K_d = 9.6543 \times 10^{-6}$
$\lambda = 0.6$
$\mu = 0.1$
$U_b \approx 0.17$

The information above shows that the fractional PID behaves as a fractional PI controller.
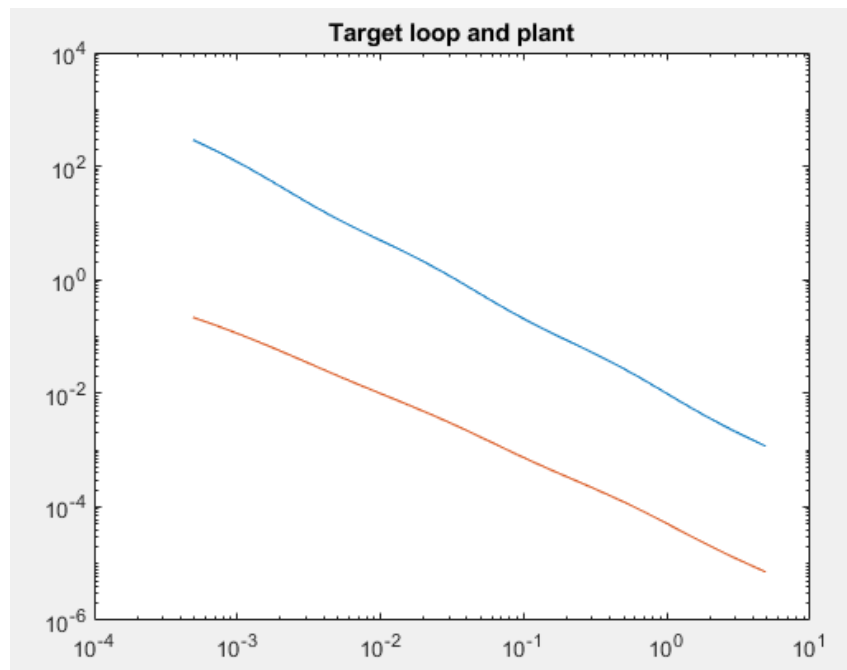
Figure 6.10: The target loop and plant
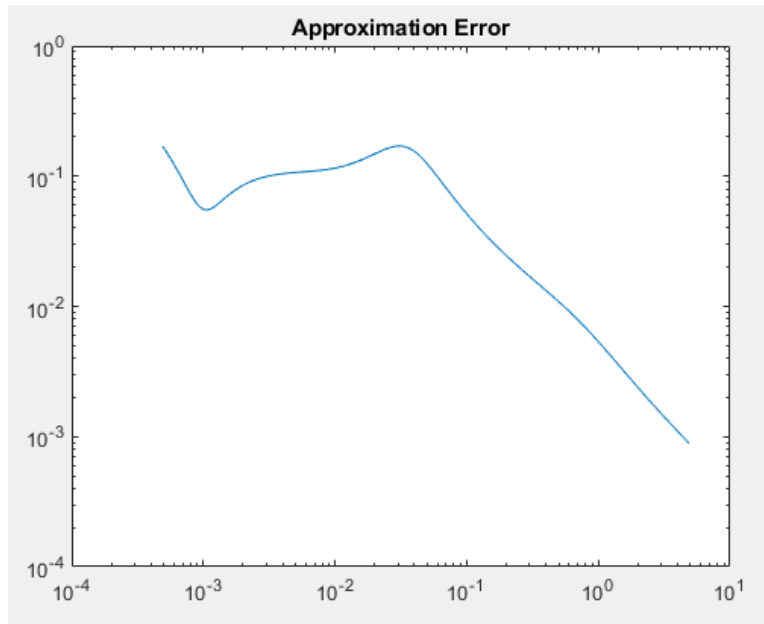
Figure 6.11: The approximation error (fitting error)

The obtained approximation error is (≈ 0.1705) at the bandwidth frequency which is less than (0.3). Figure 6.11 shows that the approximation error decreases at high frequencies.
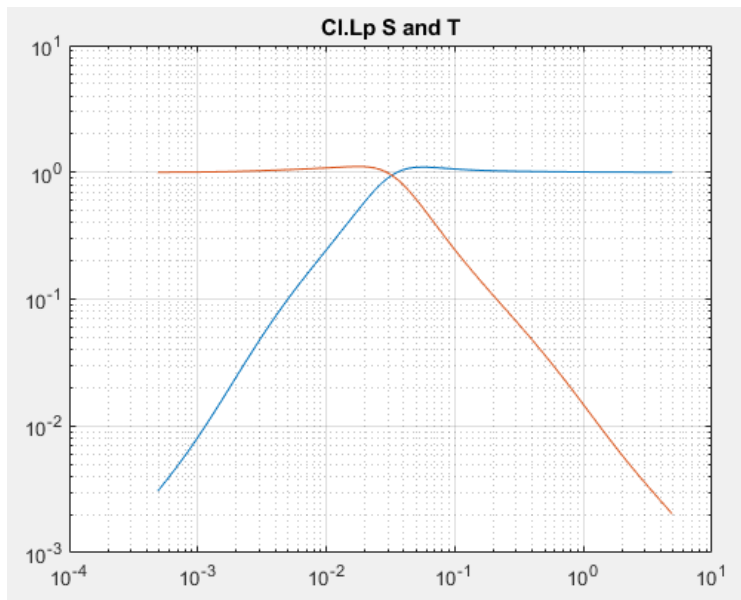
Figure 6.12: The sensitivity and complementary sensitivity functions

Figure 6.12 shows that the closed loop transfer function has good noise rejection at high frequencies and the disturbance at low frequencies will not affect the output. Also, it can be seen that the bandwidth of the closed loop sensitivity is approximately around the desired bandwidth (0.048928) rad/sec.
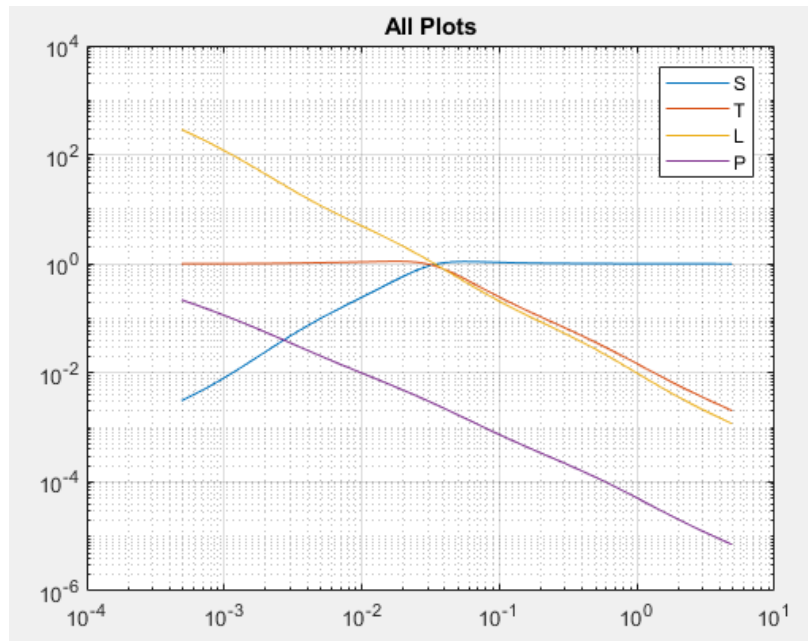
Figure 6.13: The frequency responses of the system

The frequency responses and the step response of the system are shown in Figure 6.13 and Figure 6.14, respectively.
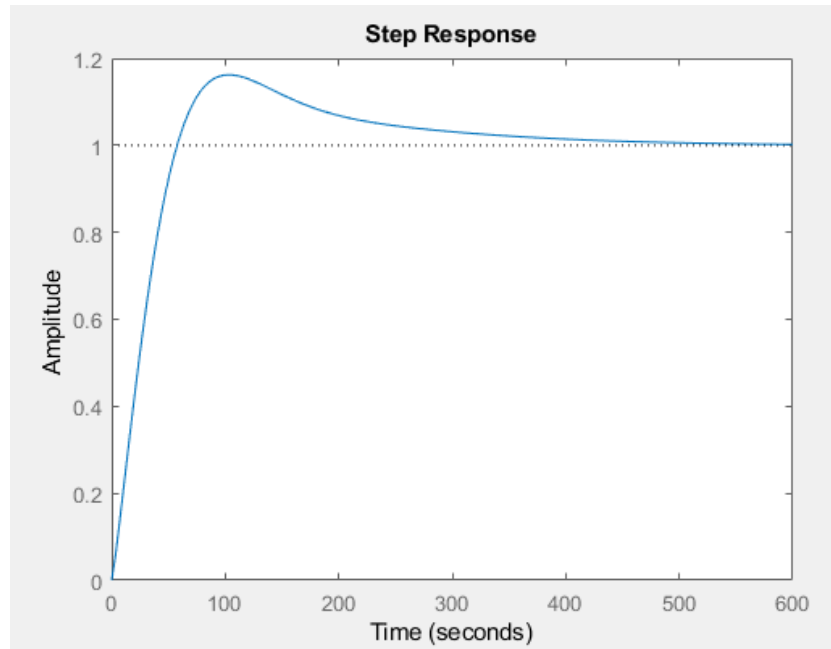
Figure 6.14: The step response of the system

The fractional integrator $\left(\dfrac{1}{s^{0.6}}\right)$ needs adding a pure integrator and differentiator at the

origin to eliminate the steady state error as shown in Figure 6.14. Figure 6.15 shows that

disturbance at the plant input has been eliminated for the same reason.
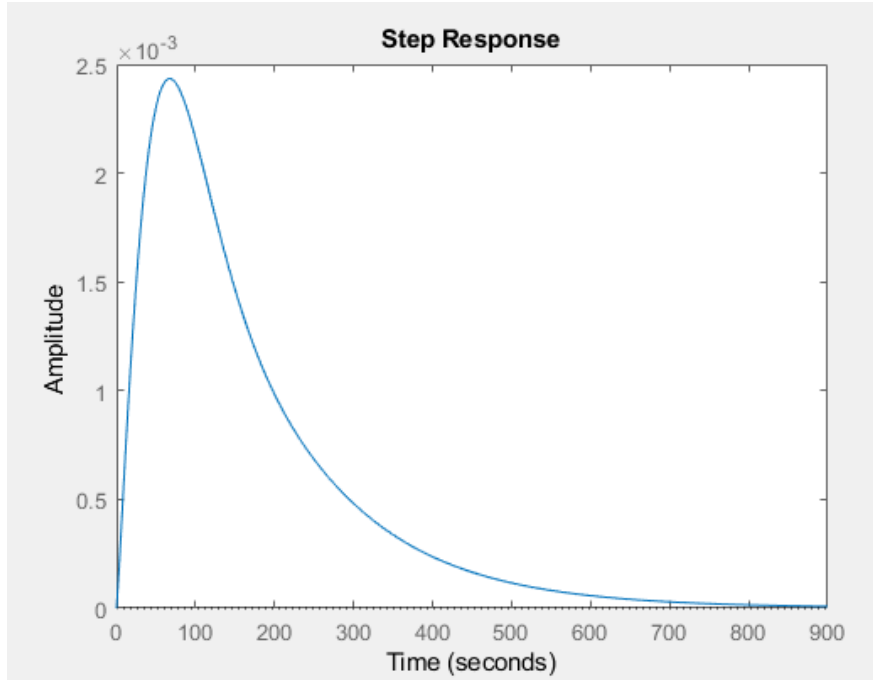
Figure 6.15: The disturbance rejection response

Therefore, the final form of the fractional PID is

$$C(s) = 2.8186 \times 10^2 + \frac{13.272}{s^{0.6}} + 9.6543 \times 10^{-6} \left(\frac{1}{0.01s + 1} \right) s^{0.1} \qquad (6.51)$$

Or, equivalently

$$C(s) = 2.8186 \times 10^2 + \frac{13.272}{s} s^{0.4} + 9.6543 \times 10^{-6} \left(\frac{1}{0.01s + 1} \right) s^{0.1} \qquad (6.52)$$

Choosing $(\lambda = 1$ and $\mu = 1)$ with the same target gives a classical PID controller with the following results

$$K_p = 3.8905 \times 10^2$$
$$K_i = 0.59278$$
$$K_d = 3.0682 \times 10^{-4}$$
$$U_b \approx 0.4088$$

The information above shows that classical PID controller behaves as a PI controller. The fitting error is slightly higher than the typical value $(0.2 - 0.3)$. The following Figure shows a comparison between the fractional PID controller and the classical PID controller.
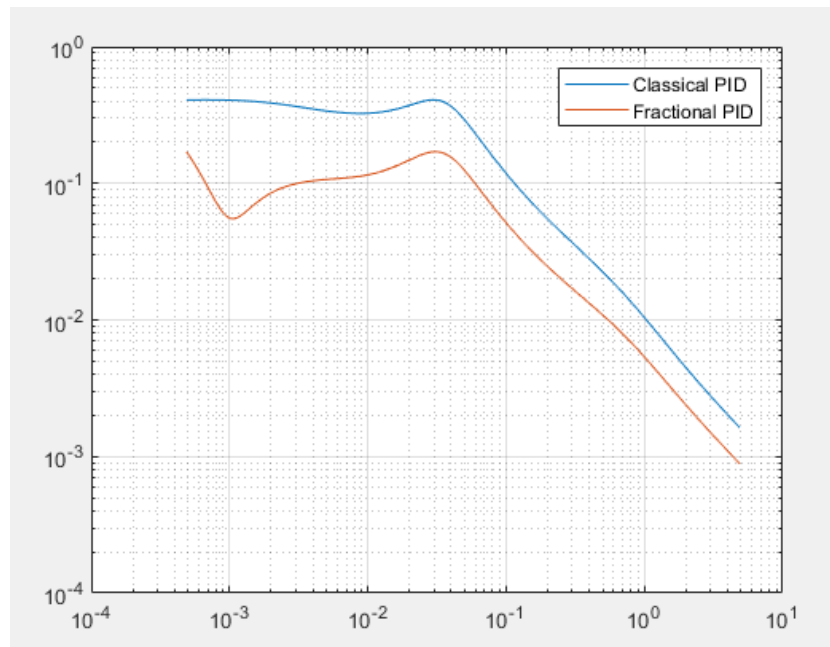
Figure 6.16: The approximation error (fitting error)
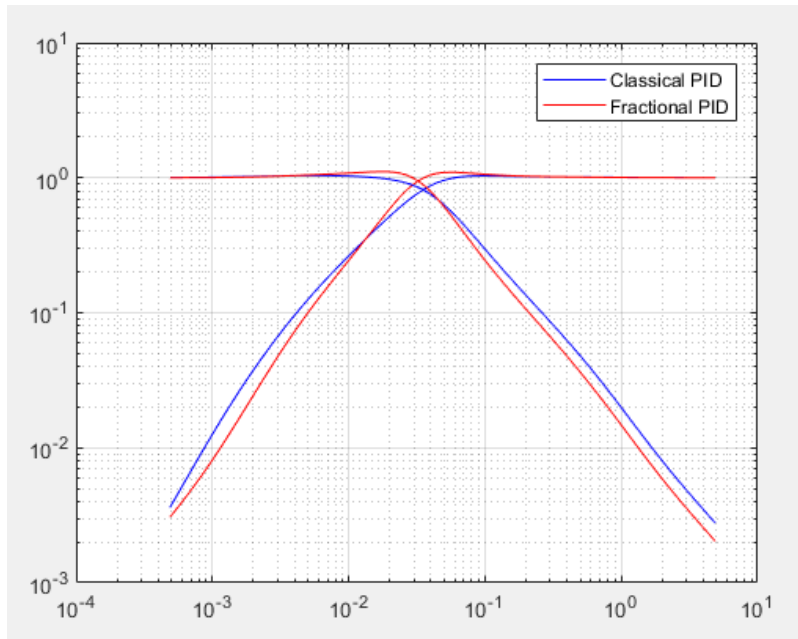
Figure 6.17: The sensitivity and complementary sensitivity functions

Figure 6.17 shows that the fractional PID and the classical PID achieved the closed loop sensitivity bandwidth approximately equal to the desired value.
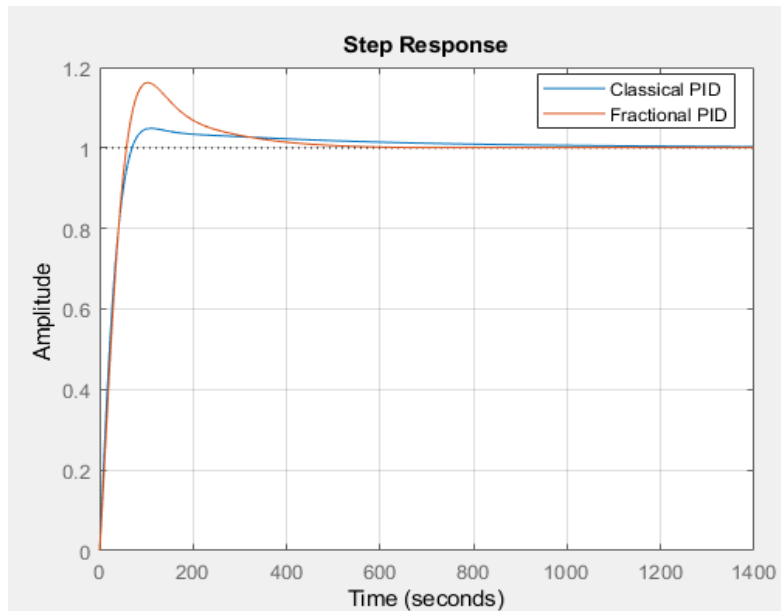
Figure 6.18: The step responses

Figure 6.18 shows that the fractional PID controller has eliminated the steady state error faster than the classical PID controller despite the obtained overshoot is higher than the overshoot caused by the classical PID. Figure 6.19 shows that disturbance rejection due to the fractional PID controller is faster than the used classical PID.
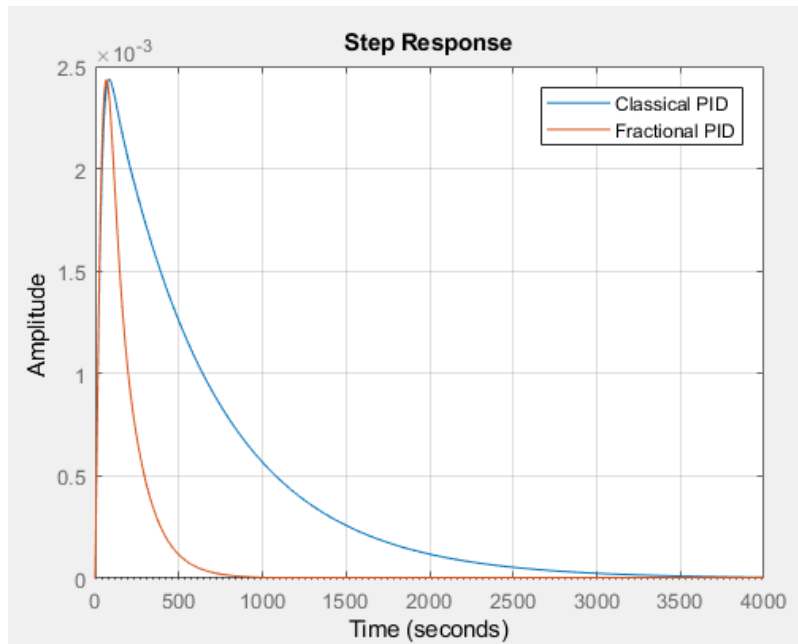
Figure 6.19: The disturbance rejection responses

The fractional controller in Reference [16] has the following form

$$C(s) = 100 + \frac{100}{s^{0.2972}} + 0.66945s^{0.3486} \tag{6.53}$$

The compared results between the fractional controller obtained by the frequency loop shaping and the fractional controller in Reference [16] are shown in the following figures
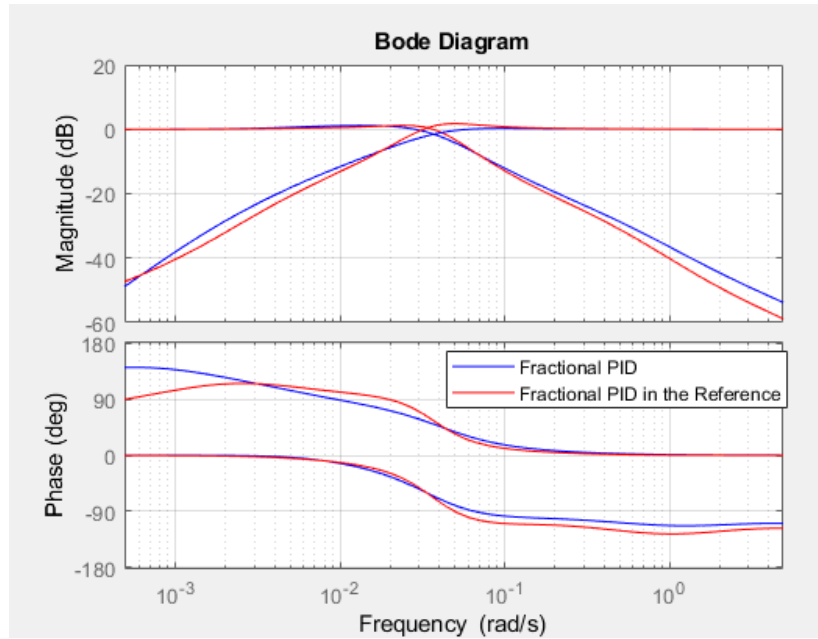
Figure 6.20: The sensitivity and complementary sensitivity functions

Figure 6.20 shows that the fractional PID and the fractional PID in Reference [16] achieved the closed loop sensitivity bandwidth approximately equal to the desired value.
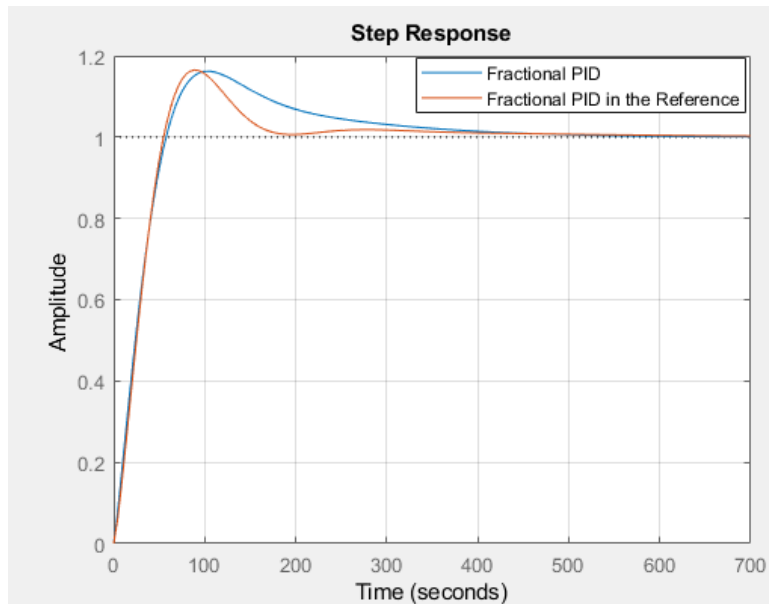
Figure 6.21: The step responses

Figure 6.21 shows both of step responses of the two systems have no steady state error. Figure 6.22 shows that disturbance rejection due to the fractional PID using the frequency loop shaping is faster than the used fractional PID in Reference [16]. The fractional controller should contain a pure integrator to reject the disturbance at the input plant.
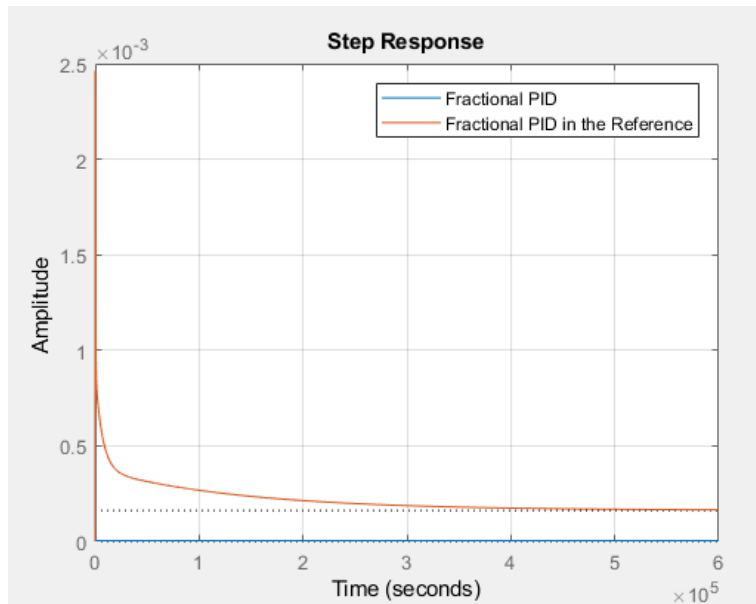
Figure 6.22: The disturbance rejection responses

Therefore, an integrator and differentiator are added at the origin to the fractional controller in Reference [16] to eliminate the disturbance as shown in Figure 6.23.
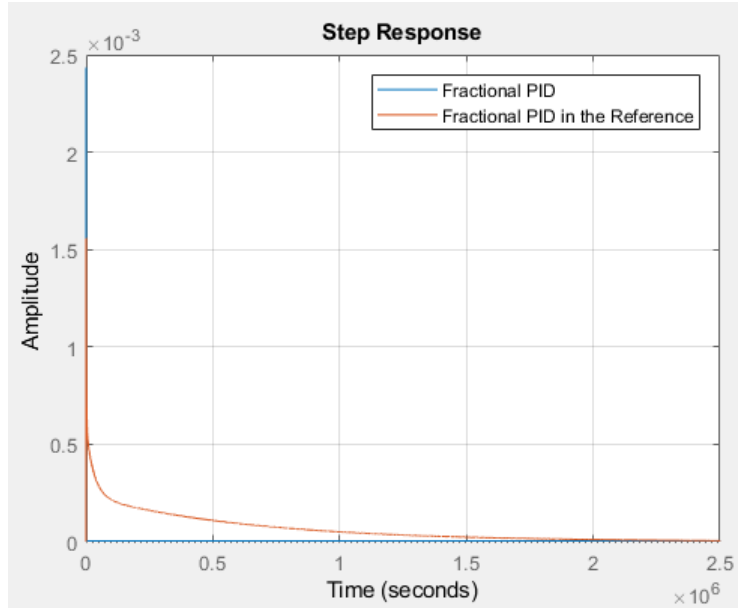
Figure 6.23: The disturbance rejection responses

It can be seen that the fractional PID using the frequency loop shaping has rejected the disturbance faster than one used in Reference [16].

Similarly, the following target can be chosen to achieve the desired design

$$L(s) = 0.01586 \frac{(s+a)^{0.9}}{s^{2.1}} \qquad (6.54)$$

where $\left(a = \frac{1}{4} BW \right)$

The obtained results would be as follows

The distribution of the fitting error all over the range of the fractional orders is shown in Figure 6.24.
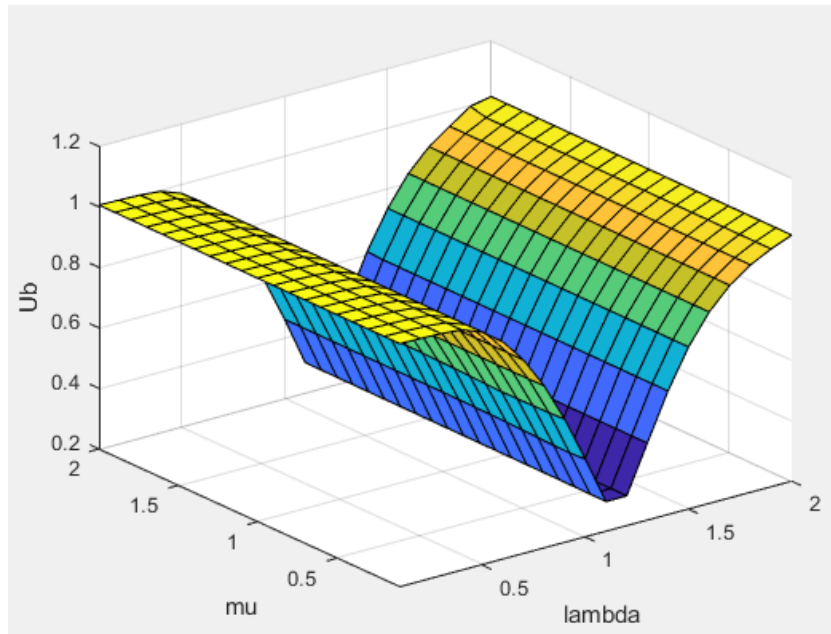
Figure 6.24: The fitting error (U_b) with fractional orders (λ, μ)
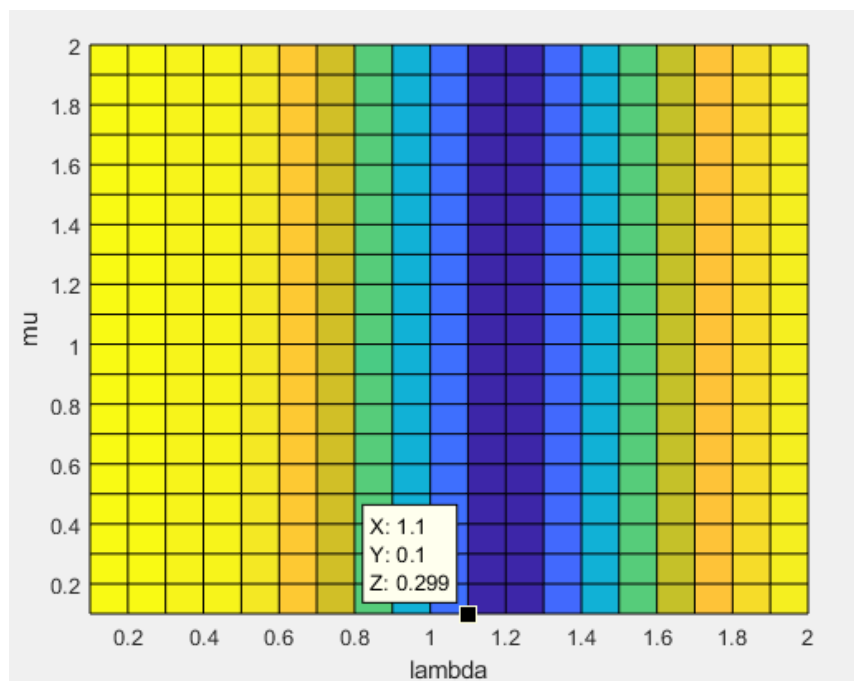
Figure 6.25: The fitting error at $(\lambda = 1.1$ and $\mu = 0.1)$

From Figure 6.25, the best choice for the orders of the fractional PID controller would be $(\lambda = 1.1 \quad \mu = 0.1)$. It satisfies the relationship $\min\limits_{K_p,K_i,K_{d,},\lambda,\mu} \|Ub\|$.

The values of the fractional PID parameters are:

$K_p = 1.8725 \times 10^2$
$K_i = 2.7737$
$K_d = 2.1412 \times 10^2$
$\lambda = 1.1$
$\mu = 0.1$
$U_b \approx 0.299$

The information above shows that the fractional PID behaves as a fractional PD controller.
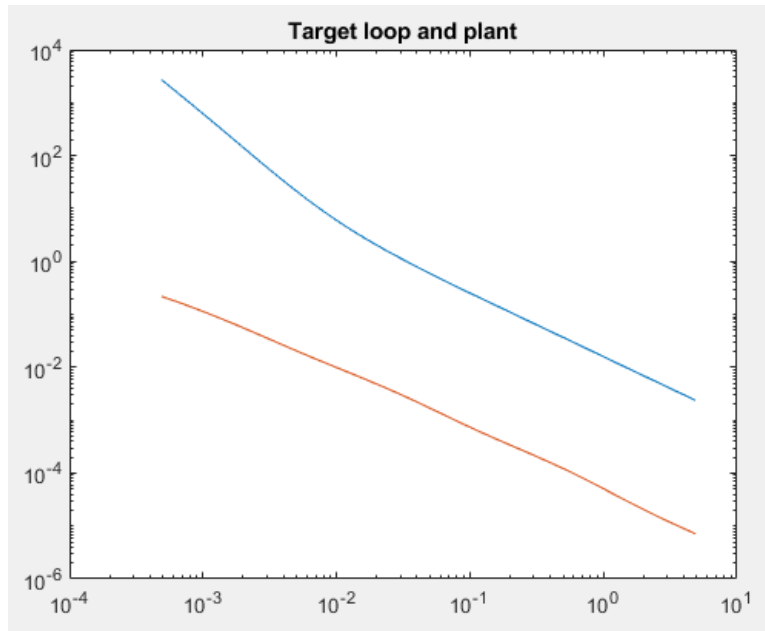
Figure 6.26: The target loop and plant
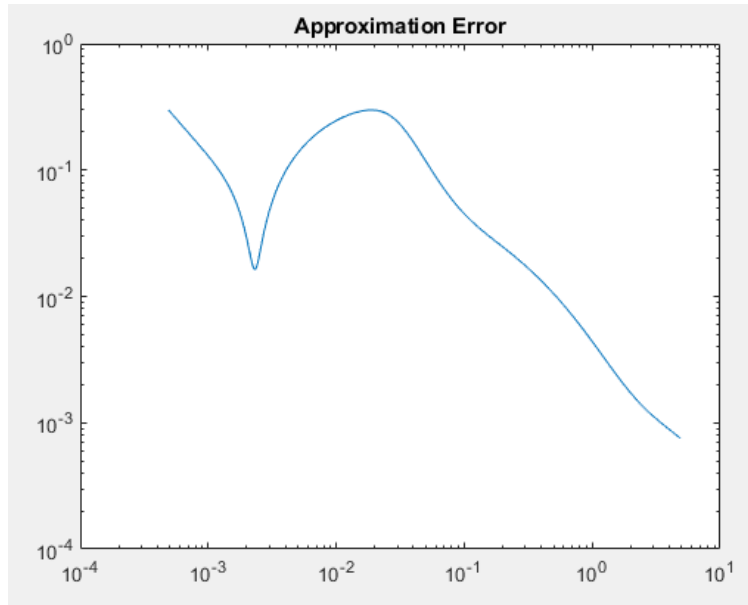
Figure 6.27: The approximation error (fitting error)

The obtained approximation error is (≈ 0.299) at the bandwidth frequency which is in between $(0.2 - 0.3)$. Figure 6.27 shows that the approximation error decreases at high frequencies.
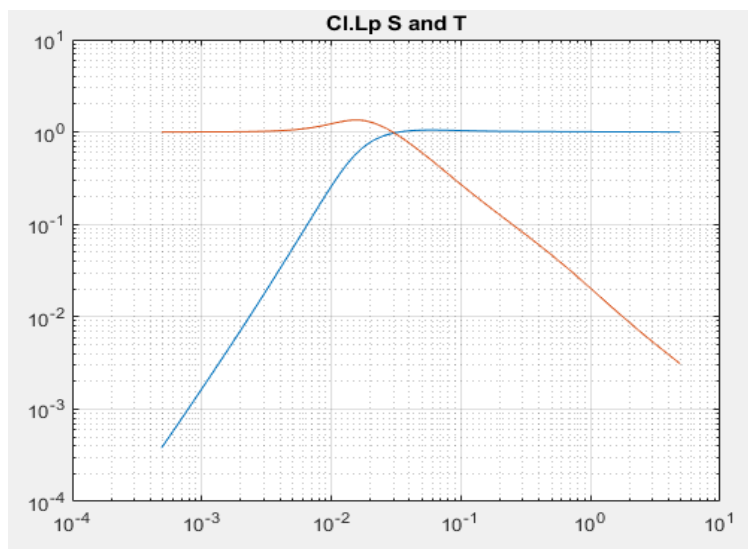
Figure 6.28: The sensitivity and complementary sensitivity functions

Figure 6.28 shows that the closed loop transfer function has good noise rejection at high frequencies and the disturbance at low frequencies will not affect the output. Also, it can be seen that the bandwidth of the closed loop sensitivity is approximately around the desired bandwidth (0.048928) rad/sec.
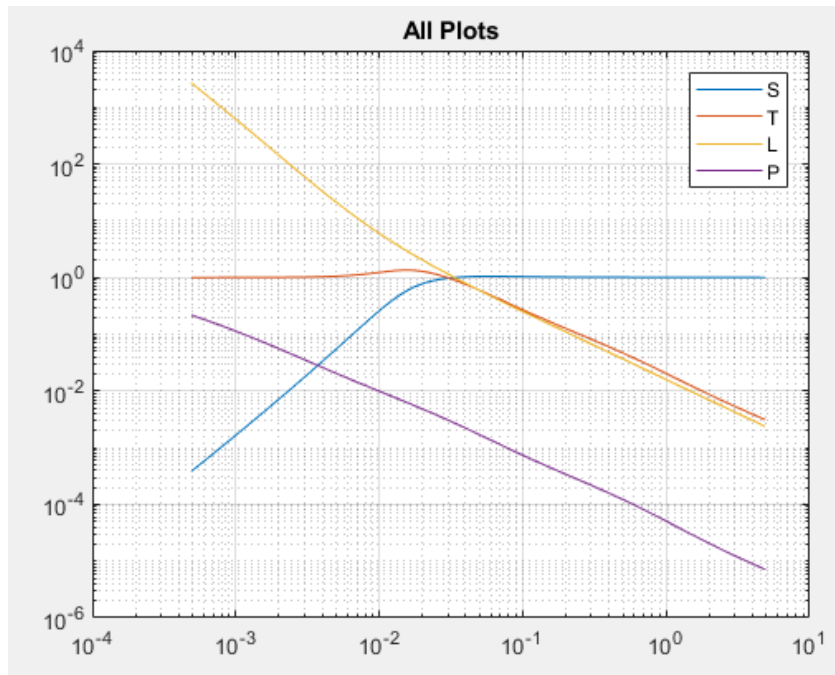
Figure 6.29: The frequency responses of the system

The frequency responses and the step response of the system are shown in Figure 6.29 and Figure 6.30, respectively.
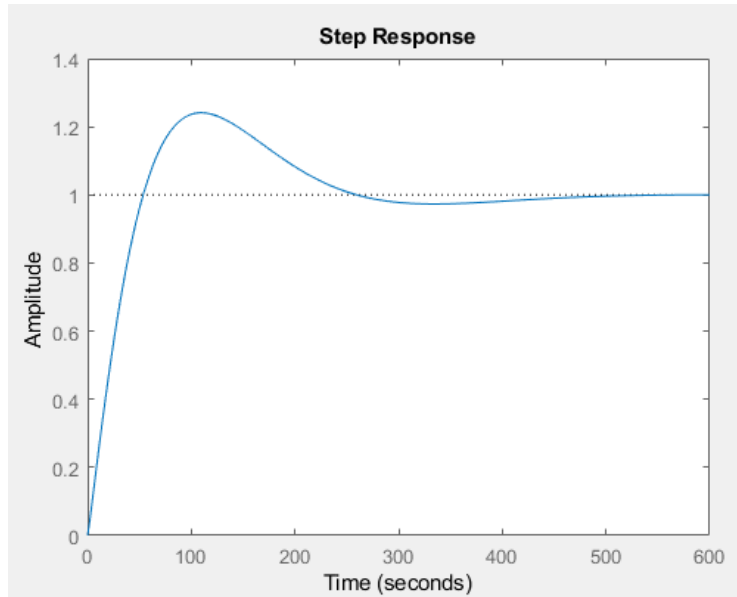
Figure 6.30: The step response of the system

It can be seen that the fractional integrator $\left(\dfrac{1}{s^{1.1}}\right)$ which contains a pure integrator $\left(\dfrac{1}{s}\right)$ eliminates the steady state error. Figure 6.31 shows that disturbance at the plant input has been eliminated for the same reason.
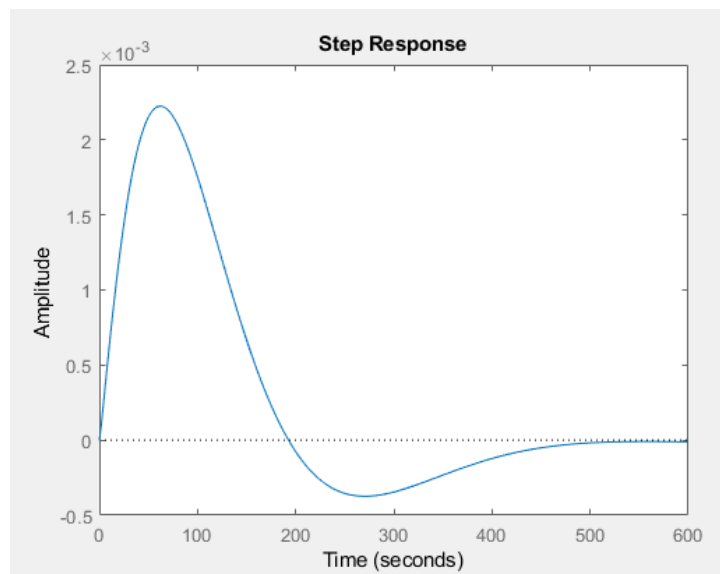
Figure 6.31: The disturbance rejection response

138

Therefore, the final form of the fractional PID is

$$C(s) = 1.8725 \times 10^2 + \frac{2.7737}{s^{1.1}} + 2.1412 \times 10^2 \left(\frac{1}{0.01s + 1} \right) s^{0.1} \tag{6.55}$$

Choosing $(\lambda = 1$ and $\mu = 1)$ with the same target gives a classical PID controller with the following results

$$K_p = 1.9752 \times 10^2$$
$$K_i = 5.4420$$
$$K_d = 3.6102 \times 10^2$$
$$U_b \approx 0.46$$

The fitting error is greater than the typical value $(0.2 - 0.3)$. The following figure shows a comparison between the fractional PID controller and the classical PID controller.
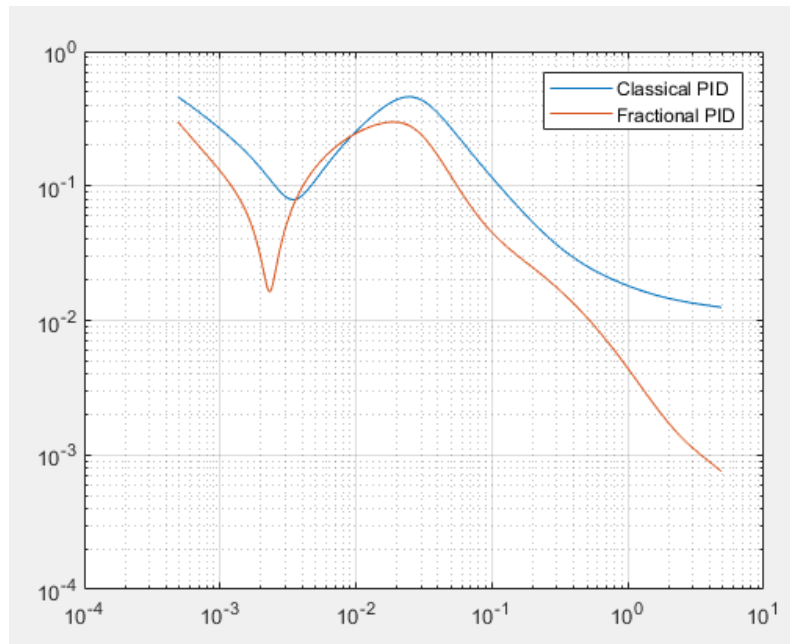
Figure 6.32: The approximation error (fitting error)
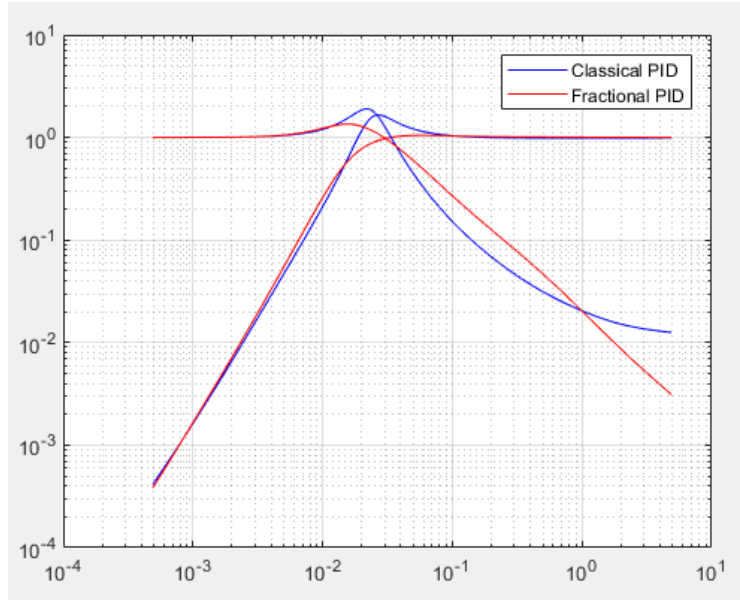
Figure 6.33: The sensitivity and complementary sensitivity functions

Figure 6.33 shows that resonant peak due to the classical PID controller is higher than the resonant peak due to the classical PID.
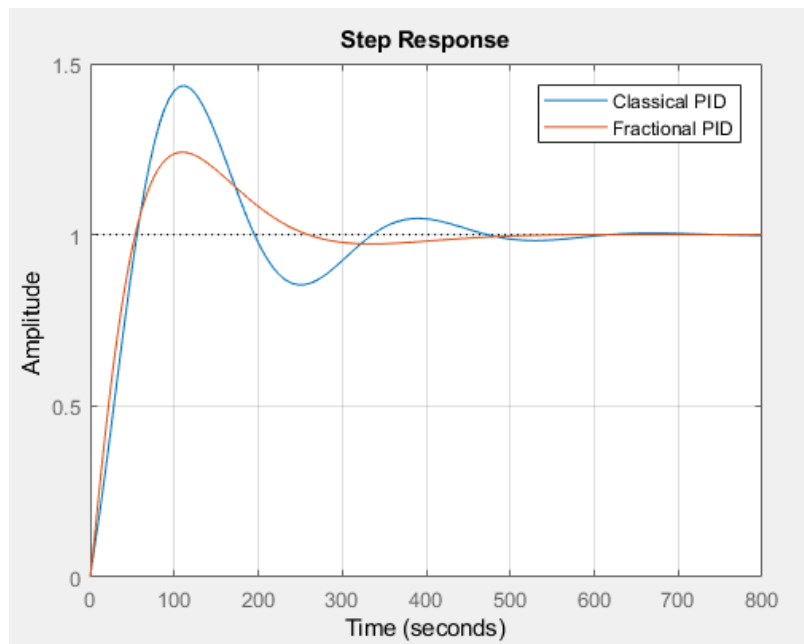
Figure 6.34: The step responses

Figure 6.34 shows that the fractional PID controller has improved the transient of the system with a reduction of overshoot and oscillation are obtained. Figure 6.35 shows that disturbance rejection responses are eliminated as time goes to infinity.
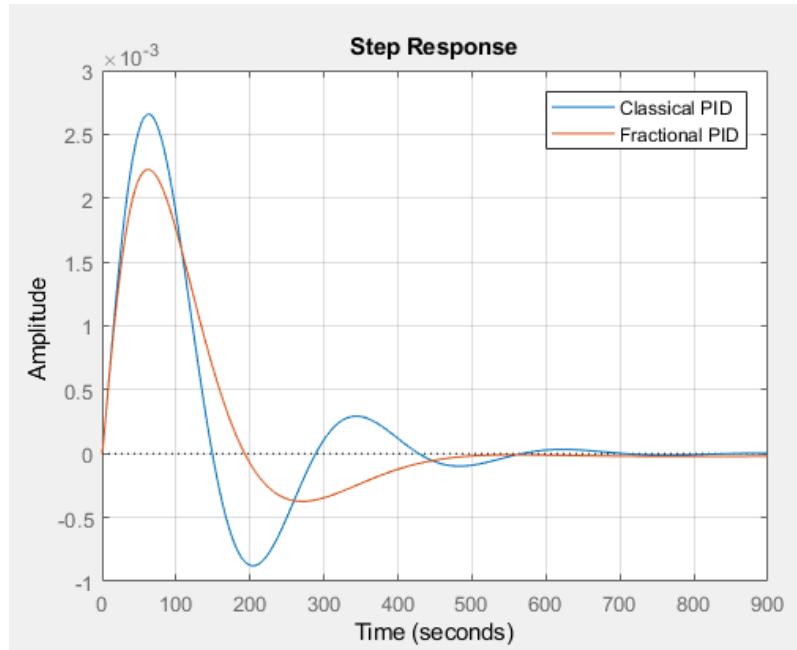

Figure 6.35: The disturbance rejection responses

The compared results between the fractional controller obtained by the frequency loop shaping and the fractional controller in Reference [16] are shown in the following figures
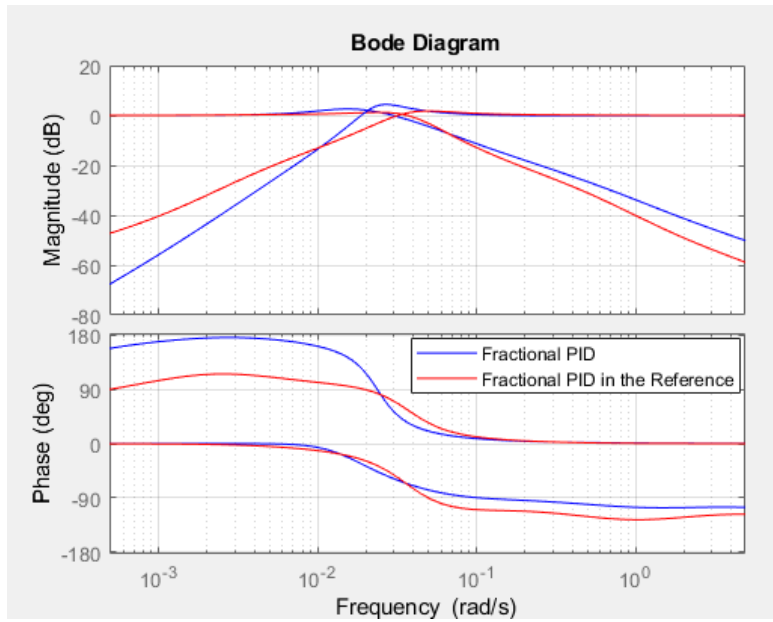
Figure 6.36: The sensitivity and complementary sensitivity functions

It is expected that fractional PID using the frequency loop shaping has a high resonant peak due to the value of the fitting error which is around (0.3). Therefore, an overshoot should appear in the step response as shown in Figure 6.37.
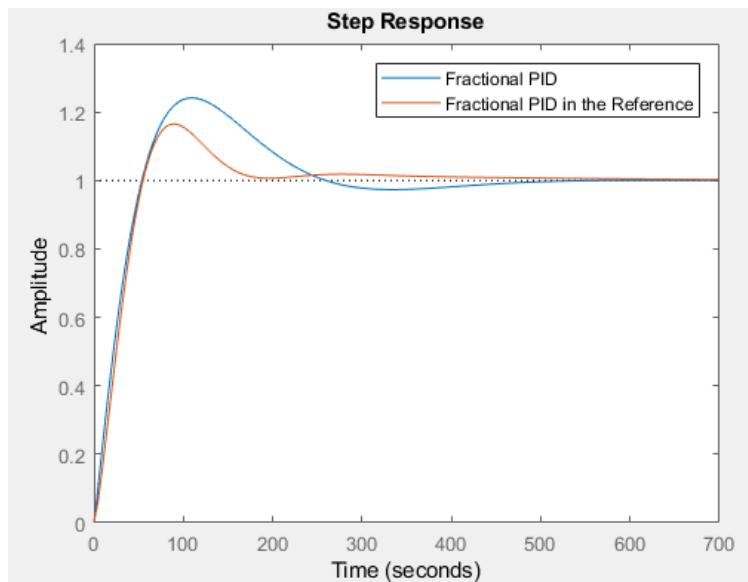
Figure 6.37: The step responses

142

Figure 6.37 shows both of the step responses of the two systems have no steady state error. Figure 6.38 shows that disturbance rejection due to the fractional PID using the frequency loop shaping is faster than the used fractional PID in Reference [16]. The fractional controller should contain a pure integrator to reject the disturbance at the input plant. The same figure shows the effect of adding a pure integrator and differentiator at the origin to the fractional controller used in Reference [16].
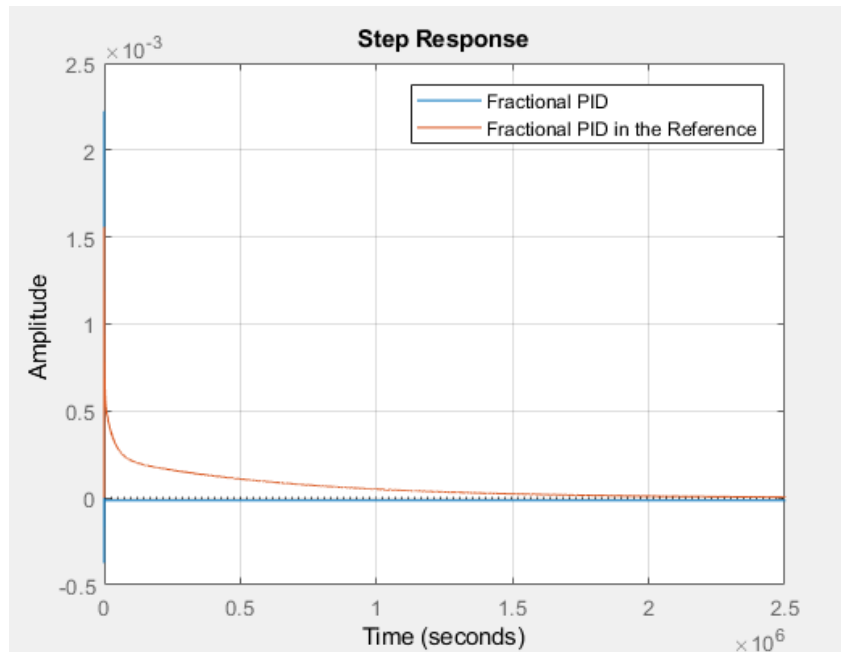
Figure 6.38: The disturbance rejection responses

6.3.2 Motion of an Immersed Plate

The motion of a rigid plate immersed in a viscous Newtonian fluid can be described by a fractional differential equation. The system consists of a thin rigid plate of

mass (M) in a Newtonian fluid with density (ρ) and viscoelastic constant (μ) connected by a spring of stiffness constant (K) as shown in Figure 6.39.
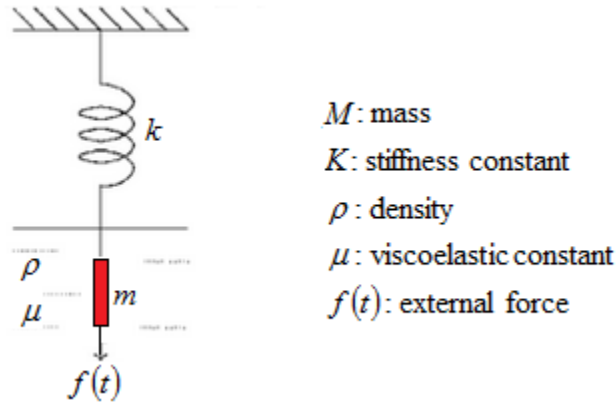

Figure 6.39: A rigid plate immersed in a viscous Newtonian fluid

R.L. Bagley and P.J.Torvik showed that the displacement $x(t)$ of the plate due to an external force $f(t)$ in a Newtonian fluid system can be described by the following fractional differential equation

$$M \ddot{x}(t) = f(t) - Kx(t) - 2\sqrt{\mu\rho} \; _0D_t^{\frac{3}{2}} x(t) \tag{6.56}$$

By taking the Laplace transform of equation 6.56, we have

$$Ms^2 X(s) = F(s) - KX(s) - 2\sqrt{\mu\rho} \, s^{\frac{3}{2}} X(s) \tag{6.57}$$

Therefore, the transfer function of the system is given by

$$G(s) = \frac{1}{Ms^2 + 2\sqrt{\mu\rho} \, s^{\frac{3}{2}} + K} \tag{6.58}$$

144

Comparing between equation 6.58 and the transfer function given in References [29] and [24] with unity stiffness constant

$$G(s) = \cfrac{1}{\left(\cfrac{s}{\omega_n}\right)^2 + 2\zeta\left(\cfrac{s}{\omega_n}\right)^m + 1} \tag{6.59}$$

It can be deduced that

$$\omega_n = \frac{1}{\sqrt{M}} \tag{6.60}$$

$$\zeta = \sqrt{\omega_n \mu \rho} \quad \text{for} \quad m = \frac{3}{2} \tag{6.61}$$

The analytical solution $x(t)$ for the inhomogeneous Bagley-Torvik equation in (6.56) can be calculated as

$$x(t) = \int_0^t h(t-\tau)f(\tau)d\tau \tag{6.62}$$

where

$$h(t) = \frac{1}{M}\sum_{n=0}^{\infty}\frac{(-1)^n}{n!}\left(\frac{k}{M}\right)^n t^{2n+1} E_{\frac{1}{2},2+\frac{3n}{2}}^{(n)}\left(-\frac{2\sqrt{\mu\rho}}{M}\sqrt{t}\right) \tag{6.63}$$

and

$$E_{\frac{1}{2},2+\frac{3n}{2}}^{(n)}\left(-\frac{2\sqrt{\mu\rho}}{m}\sqrt{t}\right) = \sum_{r=0}^{\infty}\frac{(r+n)!\left(-\dfrac{2\sqrt{\mu\rho}}{m}\sqrt{t}\right)^r}{r!\,\Gamma\left(\dfrac{1}{2}r+2+2n\right)}, \qquad n = 0,1,2,\cdots \tag{6.64}$$

145

6.3.2.1 Results

The transfer function of the system with the parameters values used in Reference [29] is

$$G(s) = \frac{1}{0.25s^2 + 0.28284s^{1.5} + 1} \qquad (6.65)$$

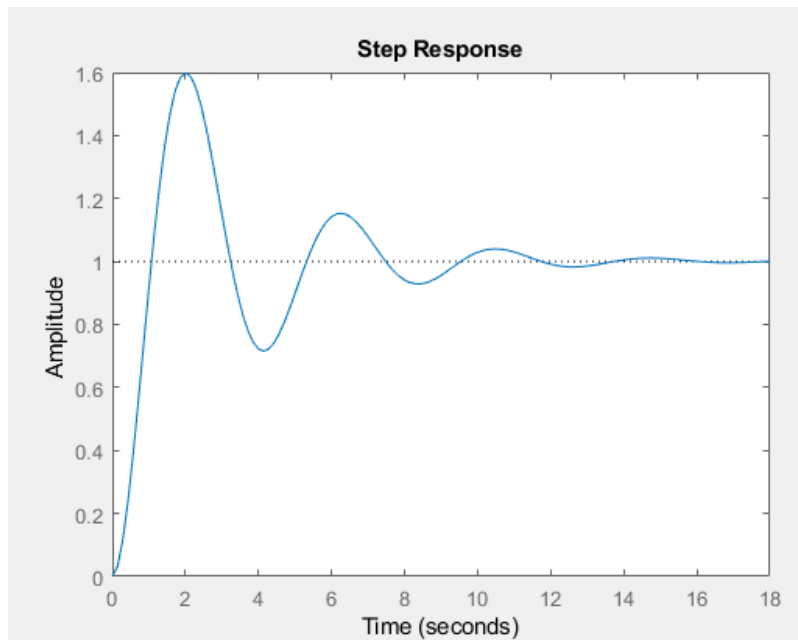Figure 6.40 shows the step response of the uncompensated system.

Figure 6.40: The step response of the uncompensated system

It can be seen that the uncompensated system oscillatory. The bandwidth of the system is around (3.5523) rad/sec. The fractional PID controller for the design is expected to reduce the overshoot and reach the stability faster than the uncompensated system.

The target can be chosen to have the desired bandwidth as

$$L(s) = \frac{3.37}{s^{1.4}}$$

(6.66)

The obtained results would be as follows

The distribution of the fitting error all over the range of the fractional orders is shown in

Figure 6.41.
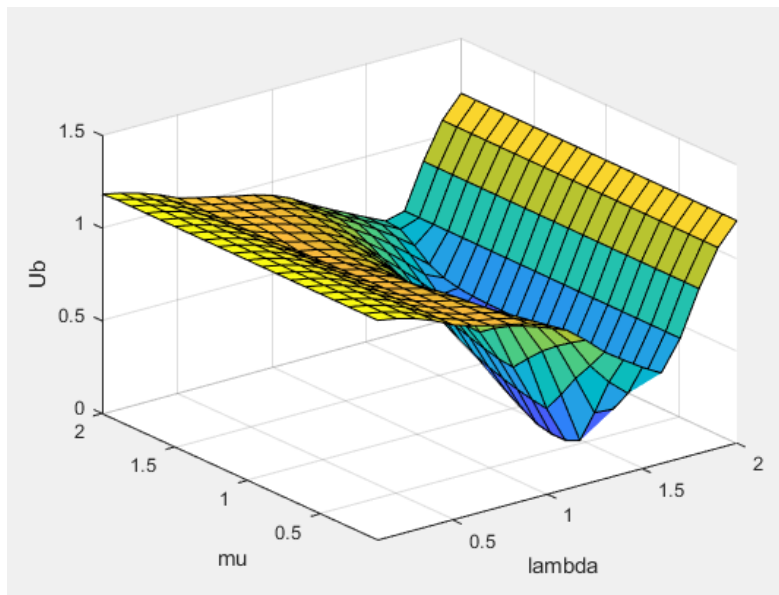
Figure 6.41: The fitting error (U_b) with fractional orders (λ, μ)
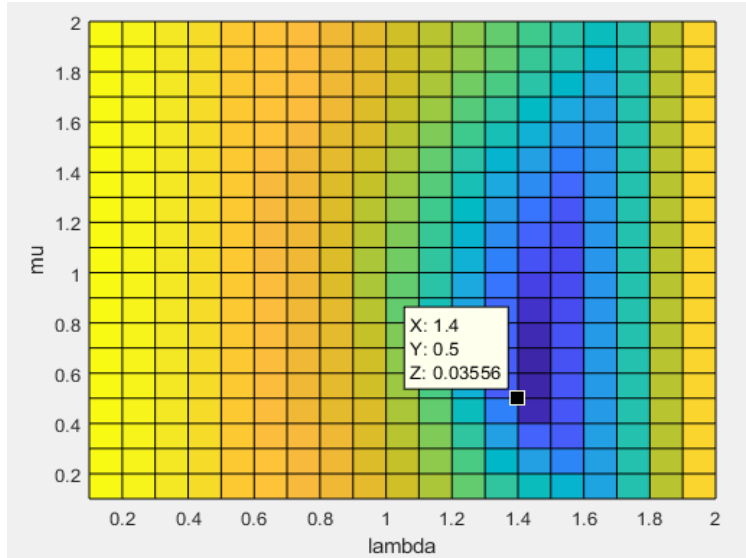
Figure 6.42: The fitting error at $(\lambda = 1.4 \quad \mu = 0.5)$

From Figure 6.42, the best choice for the orders of the fractional PID controller would be

$(\lambda = 1.4 \quad \mu = 0.5)$. It satisfies the relationship $\min\limits_{K_p, K_i, K_{d,}, \lambda, \mu} \|Ub\|$.

The values of the fractional PID controller

$K_p = 0.51383$

$K_i = 3.388$

$K_d = 1.2387$

$\lambda = 1.4$
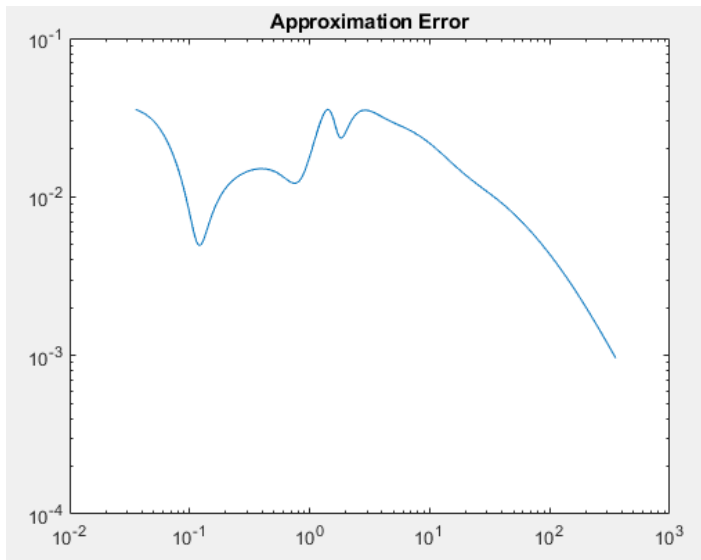
$\mu = 0.5$
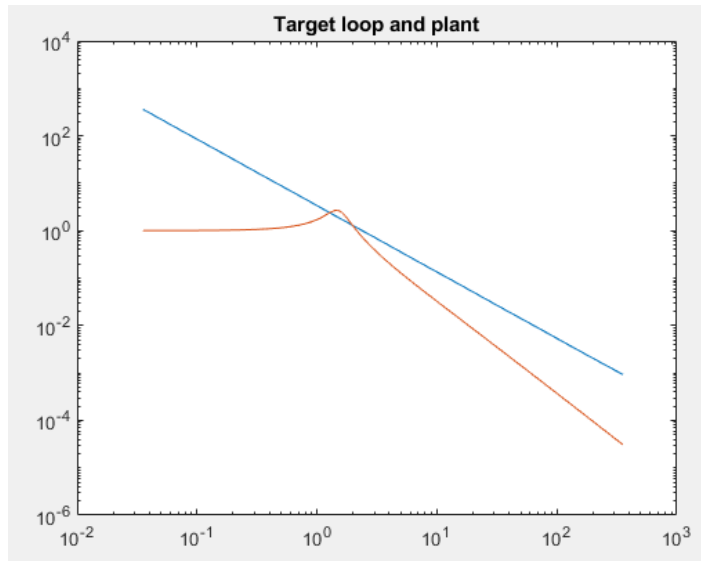
Figure 6.43: The target loop and plant

Figure 6.44: The approximation error (fitting error)

149

The obtained approximation error is (≈ 0.035) at the bandwidth frequency which is less than $(0.2 - 0.3)$. Figure 6.44 shows that the approximation error decreases at high frequencies.
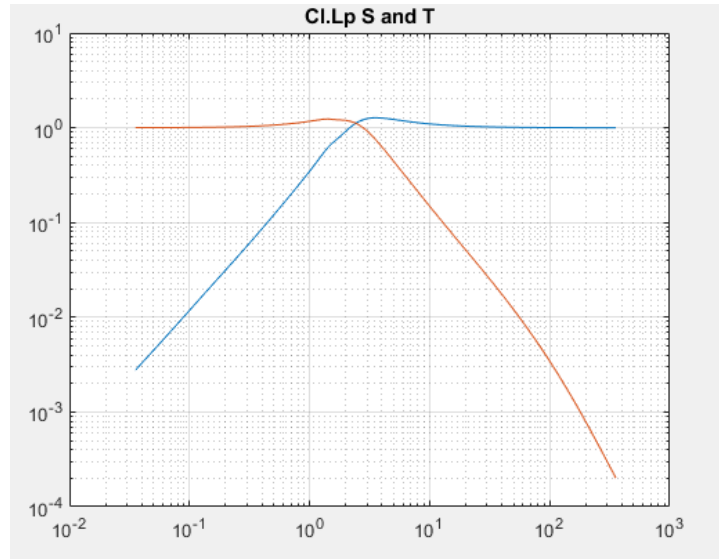

Figure 6.45: The sensitivity and complementary sensitivity functions

Figure 6.45 shows that the closed loop transfer function has good noise rejection at high frequencies and the disturbance at low frequencies will not affect the output. Also, it can be seen that the bandwidth of the closed loop sensitivity is approximately around the desired bandwidth (2.7144×10^4) rad/sec.
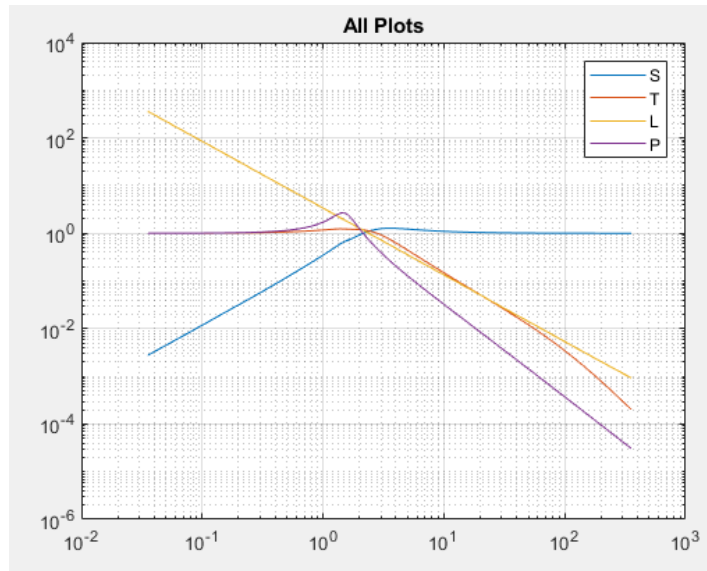
Figure 6.46: The frequency responses of the system

The frequency responses of and the step response of the system are shown in Figure 6.46 and Figure 6.47, respectively.
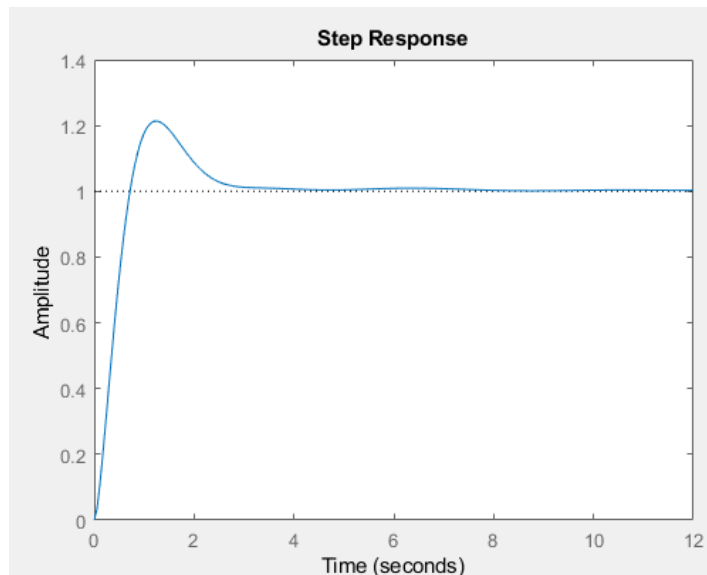

Figure 6.47: The step response of the system

It can be seen that the fractional integrator $\left(\dfrac{1}{s^{1.4}}\right)$ which contains a pure integrator $\left(\dfrac{1}{s}\right)$ eliminates the steady state error. Figure 6.48 shows that disturbance at the plant input has been eliminated for the same reason.
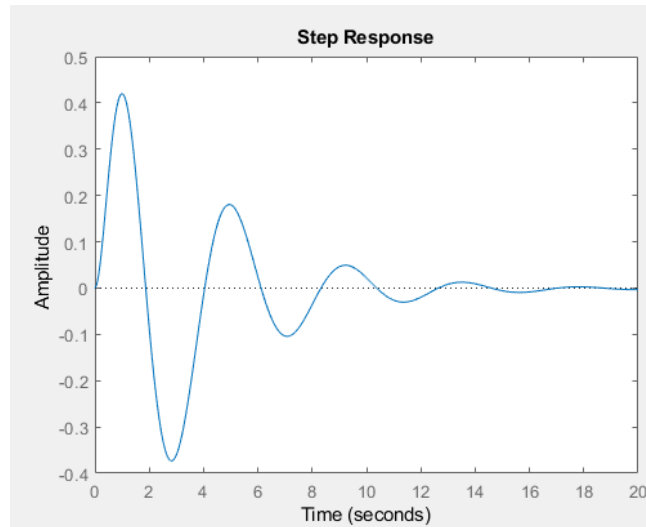

Figure 6.48: The disturbance rejection response

Therefore, the final form of the fractional PID is

$$C(s) = 0.51383 + \frac{3.388}{s^{1.4}} + 1.2387\left(\frac{1}{0.01s+1}\right)s^{0.5} \tag{6.67}$$

Choosing $(\lambda = 1$ and $\mu = 1)$ with the same target gives a classical PID controller with the following results

$K_p = 0.39769$
$K_i = 3.7821$
$K_d = 1.0939$
$U_b \approx 0.78$

The information above shows that classical PID controller behaves as a pure integrator. The fitting error is greater than the typical value $(0.2 - 0.3)$. The following figures show a comparison between the fractional PID controller and the classical PID controller.
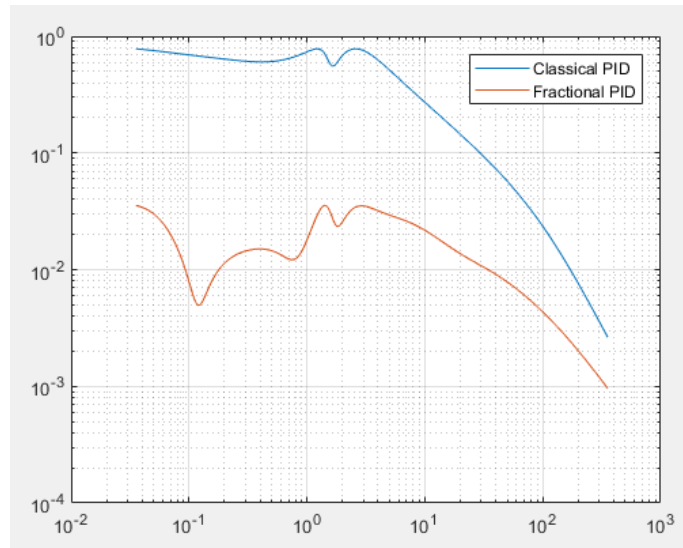

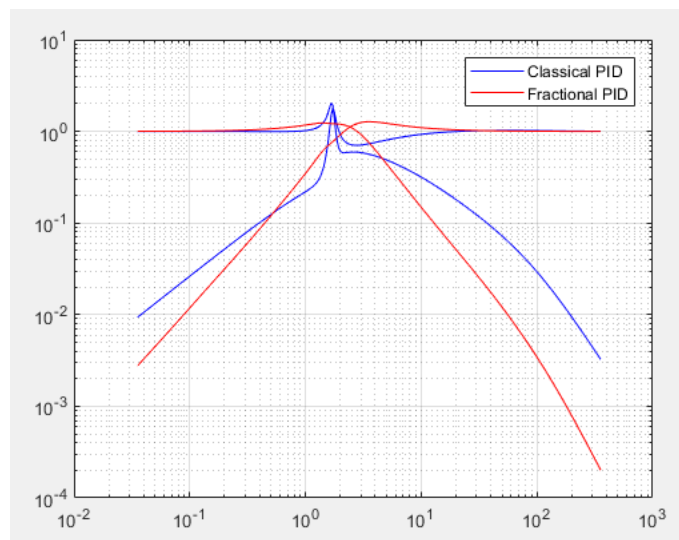Figure 6.49: The approximation error (fitting error)

Figure 6.50: The sensitivity and complementary sensitivity functions

153

Figure 5.50 shows that resonant peak due to the classical PID controller is higher than the resonant peak due to the fractional PID. Definitely, the fractional PID meets the desired design.
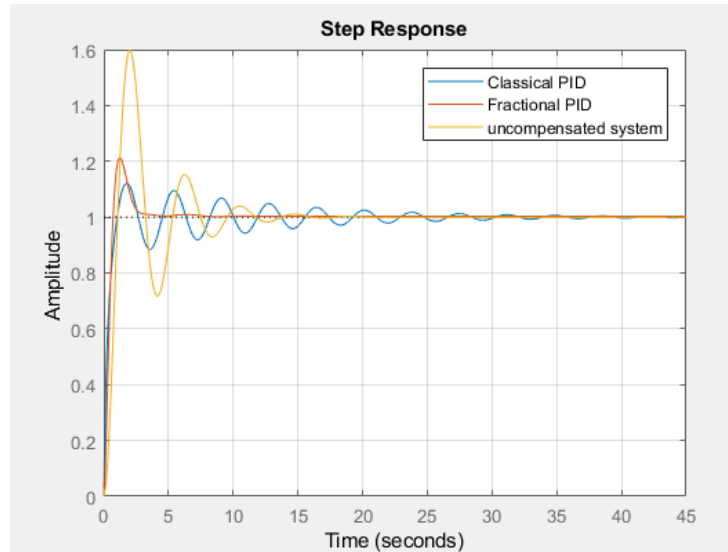

Figure 6.51: The step responses

Figure 6.51 shows that the fractional PID controller has improved the transient of the system with a reduction of overshoot and oscillation are obtained. Figure 6.52 shows that disturbance rejection due to the fractional PID controller is faster than the used classical PID.
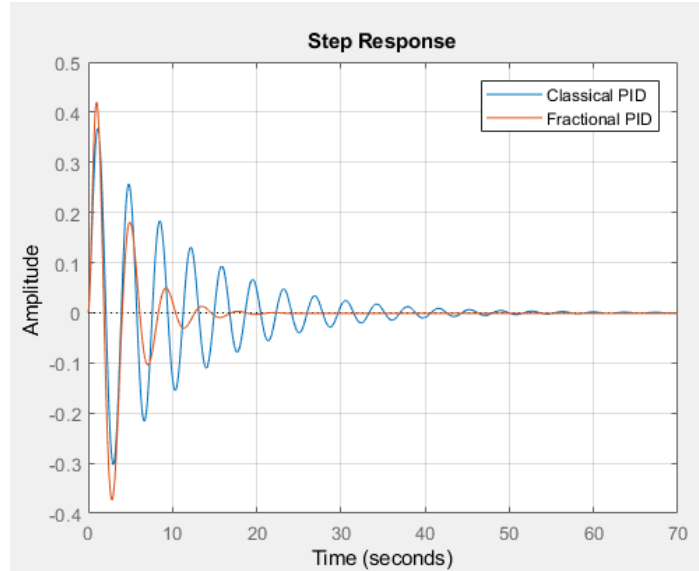
Figure 6.52: The disturbance rejection responses

6.3.3 The Buck Converter

The Buck circuit is a DC to DC converter. It is used to step down the input voltage to a lower output voltage. The buck network contains a voltage source (v_{in}), switch (S), fractional inductor (L_α), fractional capacitor (C_β), Diode (D), and the load (R) which has the output voltage (v_o) as shown in Figure 6.53.
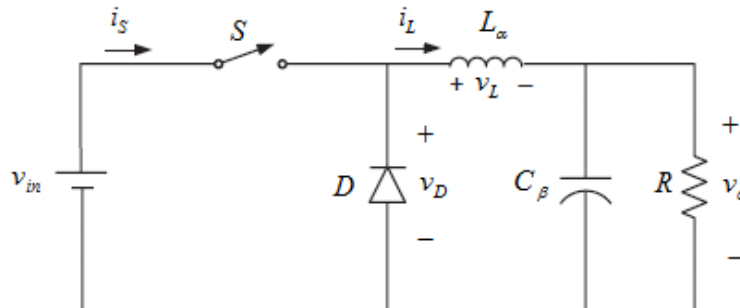

Figure 6.53: Buck converter circuit

155

The fractional order inductor contains a chain of resistors and a chain of capacitors in parallel combinations at each node connected with a series resistor as shown in Figure 6.54.
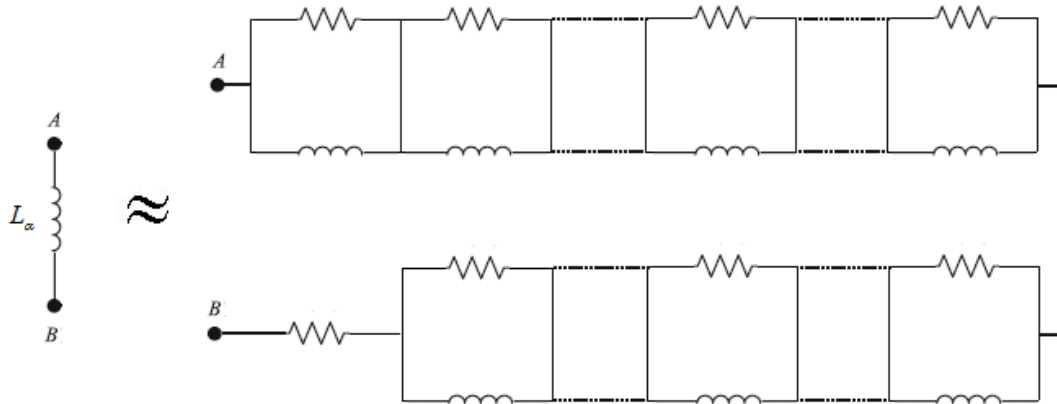

Figure 6.54: Fractional order inductor

The voltage and current in the fractional order inductor (L_α) are related as

$$v_L(t) = L_\alpha \frac{di_L{}^\alpha(t)}{dt^\alpha}$$ (6.68)

Taking Laplace transform,

$$v_L(s) = L_\alpha s^\alpha i_L(s)$$ (6.69)

Similarly, the fractional order capacitor can be represented by a chain of resistors and a chain of capacitors in parallel combinations at each node as shown in Figure 6.55.
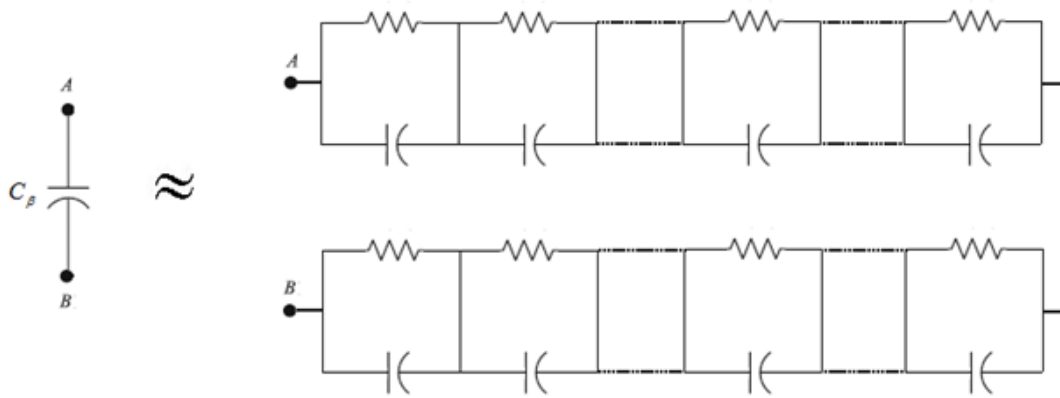
Figure 6.55: Fractional order capacitor

The current across a fractional order capacitor (C_β) is given by

$$i_c(t) = C_\beta \frac{dv_o^{\beta}(t)}{dt^\beta} \tag{6.70}$$

Taking Laplace transform,

$$i_c(t) = C_\beta v_o^{\beta}(s) \tag{6.71}$$

The transfer function from the input voltage to the output voltage $\left(\dfrac{v_o}{v_{in}}\right)$ of the circuit can

be obtained by replacing the switch and the diode by a current-dependent current source

and voltage-dependent current source as shown in Figure 6.56 which represents the

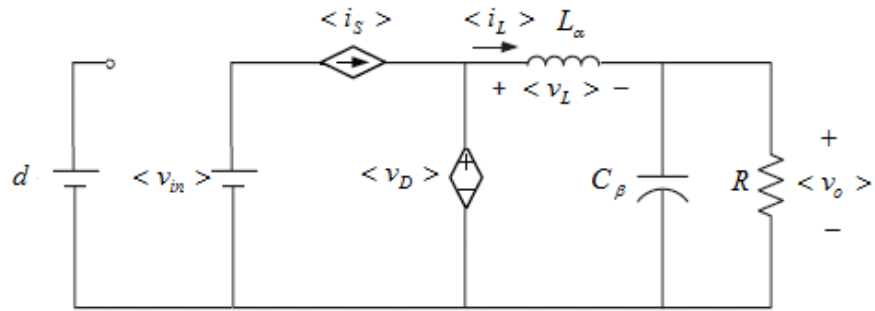circuit averaged model of the Buck circuit.

157

Figure 6.56: Circuit averaged model of the Buck converter

Therefore

$$< i_S >= d < i_L >$$ (6.72)

$$< v_D >= d < v_{in} >$$ (6.73)

where (d) is the duty cycle with a value between 0 and 1. The DC equivalent circuit of Figure can be obtained by replacing the inductor with a short circuit and replacing the capacitor with an open circuit as shown in Figure 6.57.
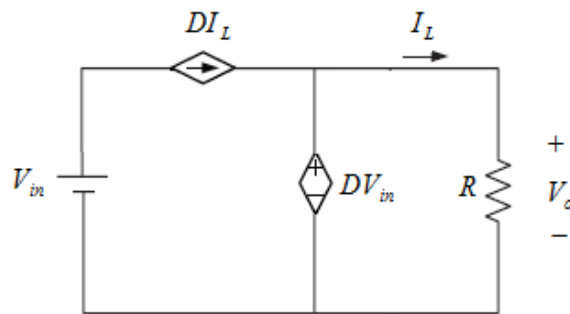

Figure 6.57: The DC equivalent circuit

Therefore

158

$$V_o = DV_{in} \tag{6.74}$$

$$I_L = \frac{D}{R}V_{in} \tag{6.75}$$

Also, the small-signal (AC-signal) equivalent circuit model can be obtained from the following relationships as

$$<i_L> = I_L + \hat{i}_L \tag{6.76}$$

$$<v_o> = V_o + \hat{v}_o \tag{6.77}$$

$$<v_{in}> = V_{in} + \hat{v}_{in} \tag{6.78}$$

$$d = D + \hat{d} \tag{6.79}$$

Substituting equations (6.76), (6.77), (6.78) and (6.79) into (6.74) and (6.75), yields

$$<i_S> = DI_L + \hat{d}I_L + D\hat{i}_L \tag{6.80}$$

$$<v_S> = DI_L + \hat{d}V_L + D\hat{v}_L \tag{6.81}$$

Equations (6.80) and (6.81) represent the summation of the DC and AC signals. Therefore, the small-signal equivalent circuit model can be designed as shown in Figure 6.58.
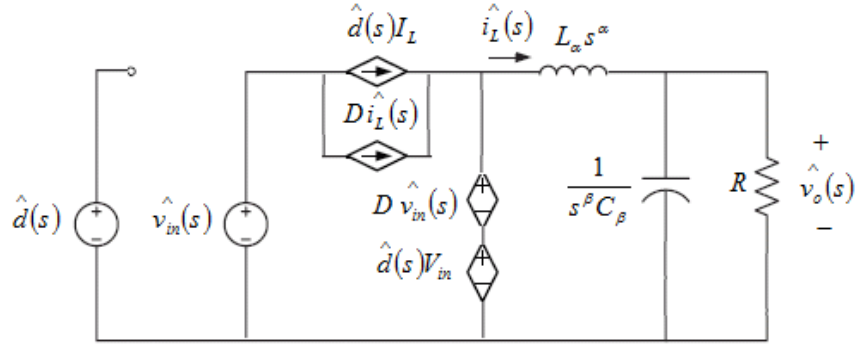
Figure 6.58: The small-signal equivalent circuit

The circuit in Figure 6.58 can be reduced to the following circuit
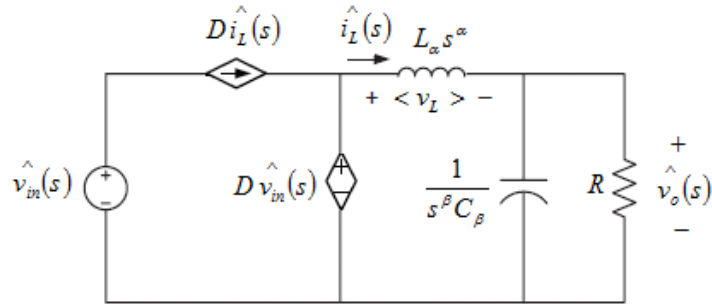

Figure 6.59: The small-signal equivalent circuit model of the Buck converter circuit

The relationship between the input voltage and the output voltage can be determined using Kirchhoff's current and voltage laws as

$$L_\alpha s^\alpha \, \hat{i}_L(s) = D \hat{v}_{in}(s) - \hat{v}_o(s) \tag{6.82}$$

$$C_\beta s^\beta \, \hat{v}_o(s) = \hat{i}_L(s) - \frac{\hat{v}_o(s)}{R} \tag{6.83}$$

The transfer function $\left(\dfrac{\hat{v}_o(s)}{\hat{v}_{in}(s)} \right)$ can be easily obtained by solving the previous two fractional order equations. Therefore,

$$\frac{\hat{v}_o(s)}{\hat{v}_{in}(s)} = \frac{D}{L_\alpha C_\beta s^{\alpha+\beta} + \dfrac{L_\alpha}{R} s^\alpha + 1} \tag{6.84}$$

which represents the transfer function of the open loop Buck converter.

The following parameters are used as in Reference [27].

$C_\beta = 100\,\mu\text{F}$
$L_\alpha = 3\,m\text{H}$
$R = 20\Omega$
$D = 0.6$

6.3.3.1 Results

Since (D) is a constant, the fractional transfer function of the system can be written as

$$\frac{\hat{v}_o(s)}{\hat{v}(s)} = \frac{1}{L_\alpha C_\beta s^{\alpha+\beta} + \dfrac{L_\alpha}{R} s^\alpha + 1} \tag{6.85}$$

where

$$\hat{v}(s) = \hat{v}_{in}(s)D \tag{6.86}$$

161

Therefore, fractional the transfer function of the system with the parameters values used in Reference [27] would be

$$\frac{\hat{v}_o(s)}{\hat{v}(s)} = \frac{1}{3\times10^{-7}\,s^{1.6} + 1.5\times10^{-4}\,s^{0.8} + 1} \qquad (6.87)$$
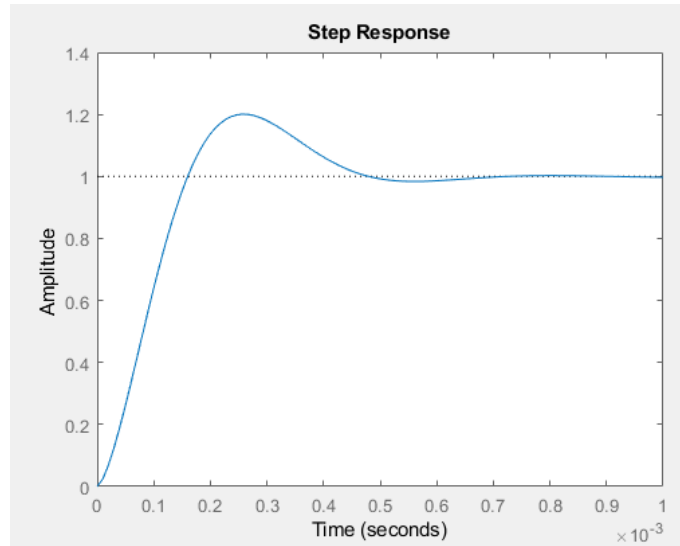

Figure 6.60: The step response of the uncompensated system

Figure 6.60 shows the step response of the uncompensated system. It can be seen that the uncompensated system is stable and has overshoot. The bandwidth of the system is around (2.7144×10^4) rad/sec.

A fractional PID controller can be designed to reduce the overshoot and improve the system transient. The target can be chosen to have the desired bandwidth as

$$L(s) = \frac{6.435\times10^4}{s^{1.1}} \qquad (6.88)$$

The obtained results would be as follows

The distribution of the fitting error all over the range of the fractional orders is shown in
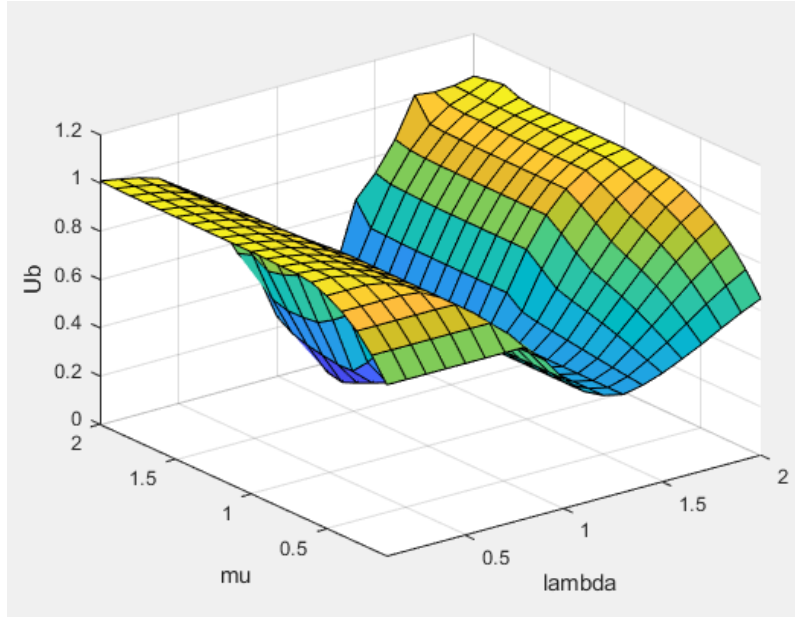
Figure 6.61.

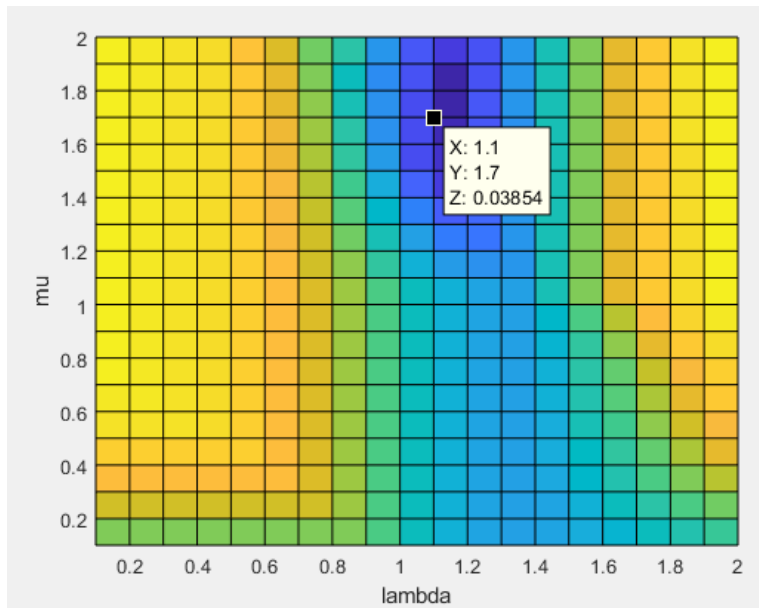Figure 6.61: The fitting error (U_b) with fractional orders (λ, μ)

Figure 6.62: The fitting error at $(\lambda = 1.1 \quad \mu = 1.7)$

From Figure 6.62, the best choice for the orders of the fractional PID controller would be $(\lambda = 1.1 \quad \mu = 1.7)$. It satisfies the relationship $\min\limits_{K_p, K_i, K_{d,}, \lambda, \mu} \|Ub\|$.

The values of the fractional PID parameters are:

$K_p = 1.3171$

$K_i = 6.5182 \times 10^4$

$K_d = 1.8718 \times 10^{-5}$

$\lambda = 1.1$

$\mu = 1.7$

$U_b \approx 0.038$

The information above shows that the fractional PID behaves as a fractional PI controller.
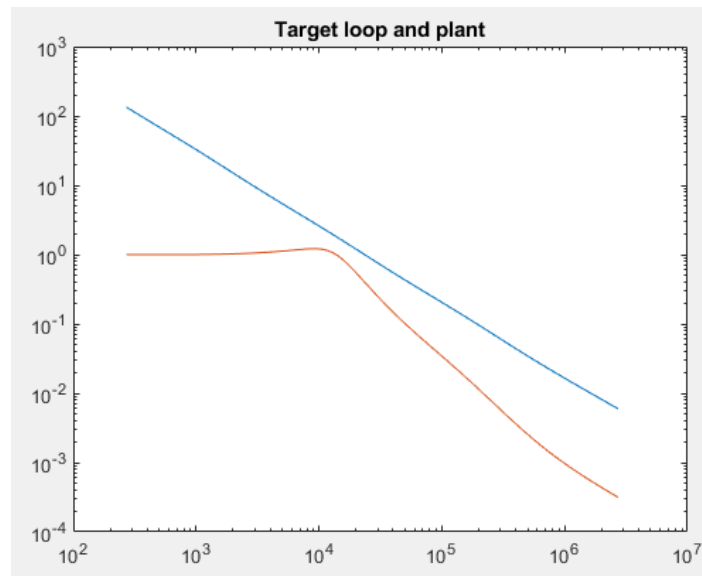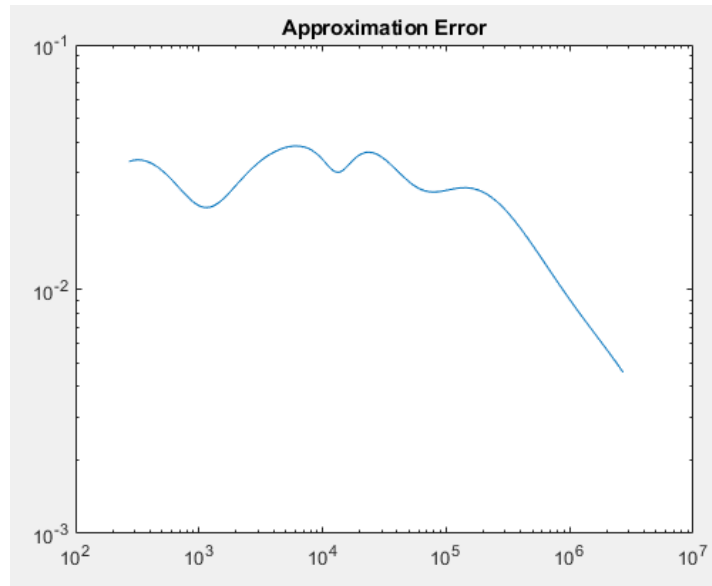

Figure 6.63: The target loop and plant

Figure 6.64: The approximation error (fitting error)

The obtained approximation error is (≈ 0.038) at the bandwidth frequency which is less than $(0.2 - 0.3)$. Figure 6.64 shows that the approximation error decreases at high frequencies.
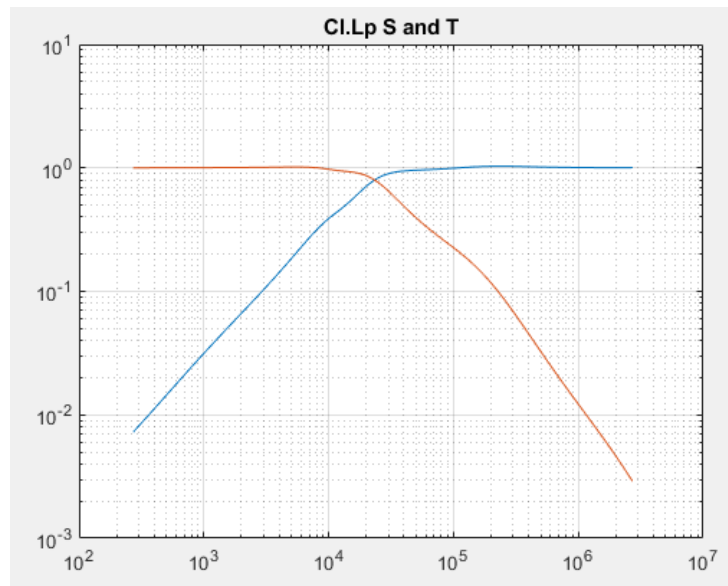
Figure 6.65: The sensitivity and complementary sensitivity functions

Figure 6.65 shows that the closed loop transfer function has good noise rejection at high frequencies and the disturbance at low frequencies will not affect the output. Also, it can be seen that the bandwidth of the closed loop sensitivity is approximately around the desired bandwidth (2.7144×10^4) rad/sec.
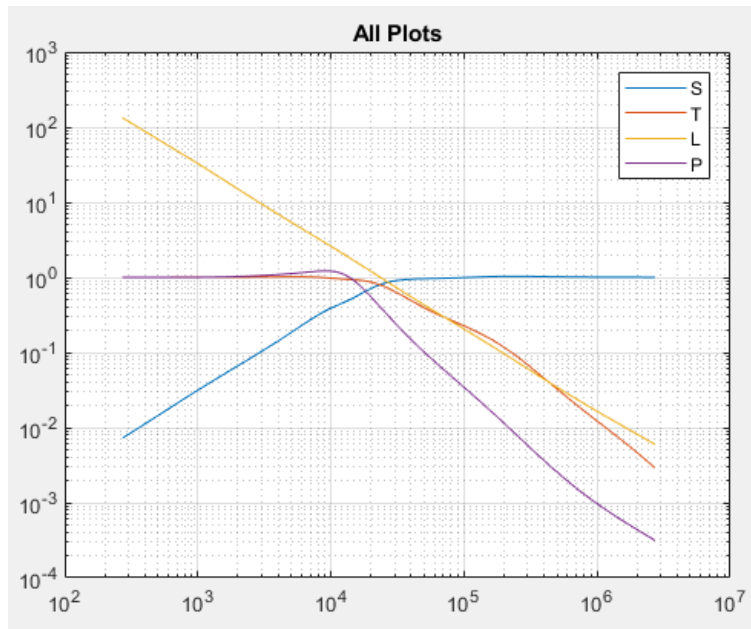
Figure 6.66: The frequency responses of the system

The frequency responses and the step response of the system are shown in Figure 6.66 and Figure 6.67, respectively.
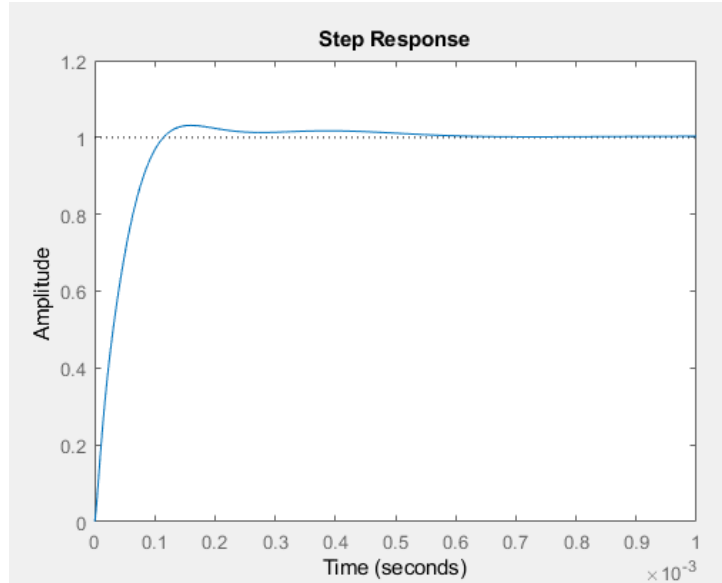
Figure 6.67: The step response of the system

It can be seen that the fractional integrator $\left(\dfrac{1}{s^{1.1}}\right)$ which contains a pure integrator $\left(\dfrac{1}{s}\right)$

eliminates the steady state error. Figure 6.68 shows that disturbance at the plant input has

been eliminated for the same reason.
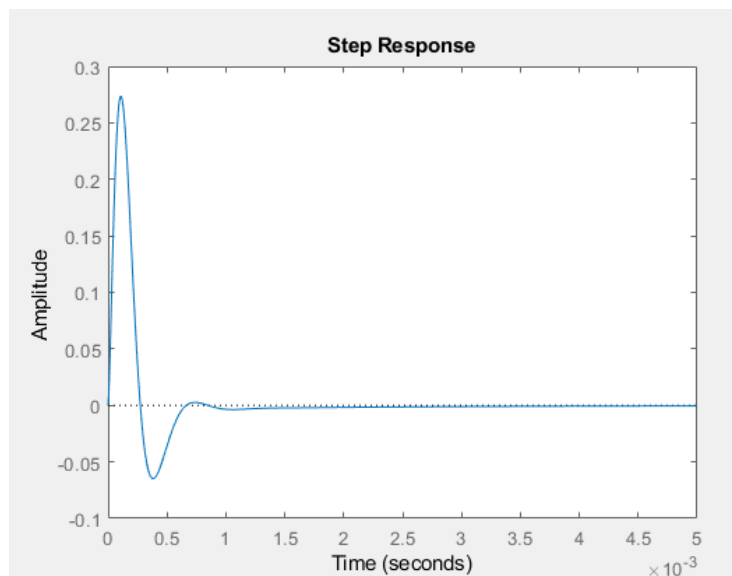
Figure 6.68: The disturbance rejection response

167

Therefore, the final form of the fractional PID is

$$C(s) = 1.3171 + \frac{6.5182 \times 10^4}{s^{1.1}} + 1.8718 \times 10^{-5} \left(\frac{1}{0.01s + 1} \right) s^{1.7} \qquad (6.89)$$

Choosing $(\lambda = 1$ and $\mu = 1)$ with the same target gives a classical PID controller with the following results

$$K_p = 3.8617 \times 10^{-6}$$
$$K_i = 1.7542 \times 10^4$$
$$K_d = 2.1007 \times 10^{-2}$$
$$U_b \approx 0.53$$

The information above shows that classical PID controller behaves as a pure integrator. The fitting error is greater than the typical value $(0.2 - 0.3)$. The following figure shows a comparison between the fractional PID controller and the classical PID controller.
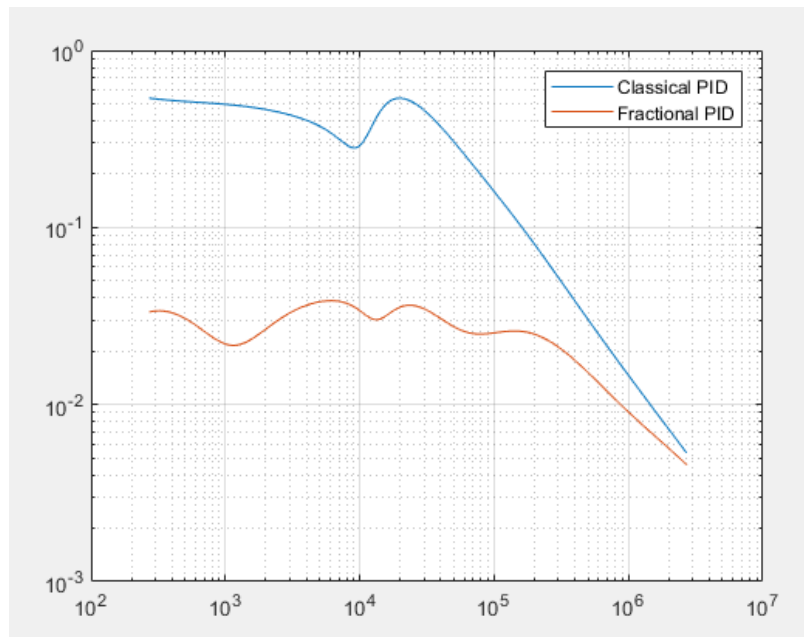
Figure 6.69: The approximation error (fitting error)
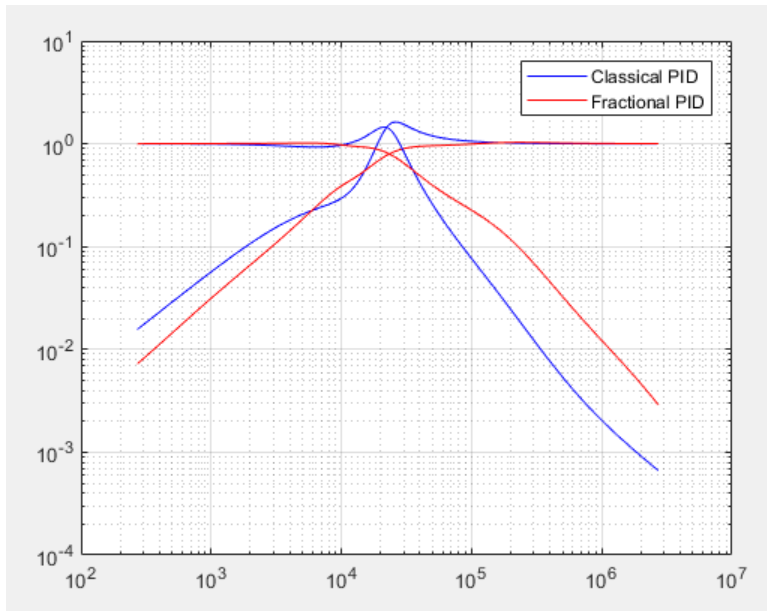
Figure 6.70: The sensitivity and complementary sensitivity functions

Figure 6.70 shows that resonant peak due to the classical PID controller is higher than the resonant peak due to the classical PID.
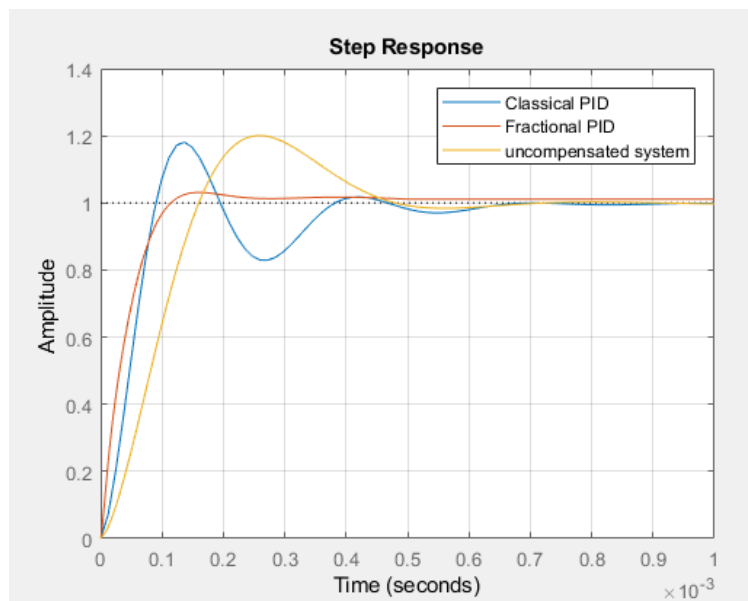
Figure 6.71: The step responses

Figure 7.71 shows that the fractional PID controller has improved the transient of the system with a reduction of overshoot and oscillation are obtained. Figure 7.72 shows that disturbance rejection responses are eliminated as time goes to infinity.
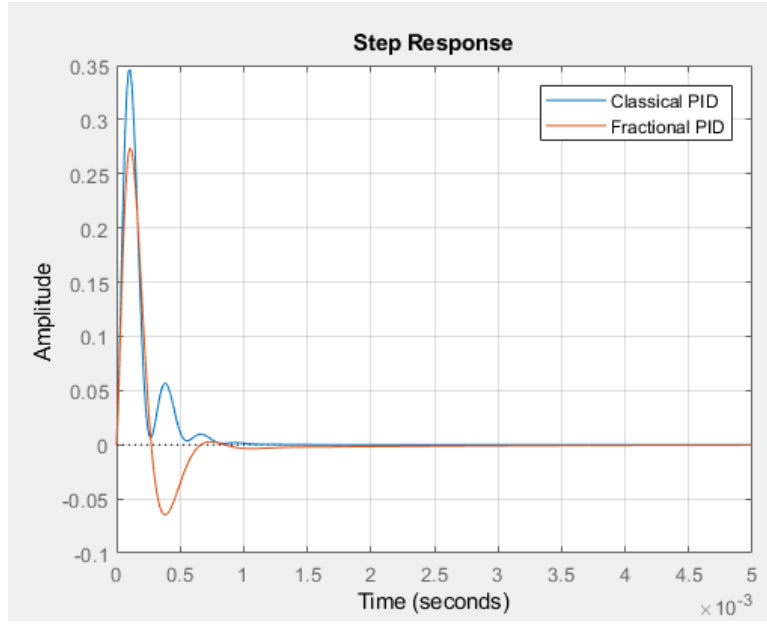
Figure 6.72: The disturbance rejection responses

The step response of the system when the duty cycle is (0.6) can be obtained as shown in

Figure 6.73. It has the following fractional transfer as shown in Reference [27].

$$\frac{\hat{v}_o(s)}{\hat{v}_{in}(s)} = \frac{0.6}{3\times10^{-7}\,s^{1.6} + 1.5\times10^{-4}\,s^{0.8} + 1} \tag{6.90}$$
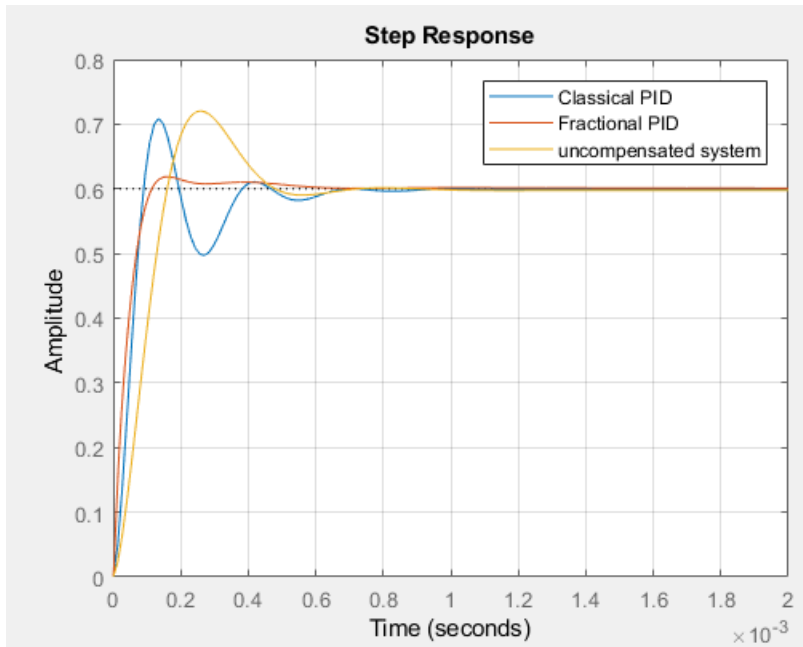
Figure 6.73: The step responses

CHAPTER 7

CONCLUSIONS

Fractional order calculus provides a good way to study the behavior of functions in the past and future. The fractional orders tell how far the behavior of a function is from present. Also, fractional order calculus can be used to approximate functions without using a sub of functions for the same purpose. The Oustaloup filter can be used to approximate fractional order systems although the shape around the boundary frequencies is not ideal due the expression of approximation. Instead of having slopes in multiple of $(\pm 20\,\text{dB/dec})$ or zero in the frequency response of a certain system, slopes in multiple of $(\pm 20\alpha\,\text{dB/dec})$ or zero can be used in the frequency response to describe fractional order systems. Fractional PID controller has some advantages over classical PID controller like increasing stability as shown in Riemann surface plan, improving the performance of fractional systems and more freedom to tune. Riemann surface plan shows that the response of a fractional order integrator whose order is less than one is slow. This problem can be solved by adding a pure integrator and differentiator at origin. The effect of the fractional orders on the shape of fractional transfer functions is presented. A target can be used for the tuning to achieve a robust performance. Choosing a fractional integrator as a target in the frequency loop shaping technique has some advantages such as rejecting disturbances or satisfying frequency domain constraints (e.g., arising from an associated uncertainty description). The fractional orders play an important role on sensitivity shaping, and they have been shown to provide a significant advantage in cases where the plant itself or the target loop shape are fractional. The

Sensitivity and Complementary Sensitivity transfer functions describe both the effect of the standard perturbation signals on the loop, as well as provide metrics to characterize the loop robustness to dynamic uncertainty. The results obtained in this dissertation show significant improvement in the transient response and satisfactory results through the achievement of a closed loop sensitivity bandwidth approximately to a desired value of bandwidth. Future work will be focusing on the following points:

- Generating the target loop shape using LQR techniques. Such techniques have been known to yield general controllers with excellent properties, so it is reasonable to use the resulting loop shapes as targets for approximation with a fractional PID.

- Development of the corresponding fractional system identification and uncertainty estimation framework to complement the controller design from input-output data. It is anticipated that such an approach may have an advantage over the classical, general, high-order identification and controller design approach in the case of fractional order systems because it would require less degrees of freedom (tunable parameters) and, hence, impose weaker excitation conditions on the test signals.

REFERENCES

[1] Zhang, X., & Chen, Y.Q., *Remarks on fractional order control systems*, In: American Control Conference (ACC), IEEE, pp. 5169–5173, 2012.

[2] Caponetto, R., Dongola , G., Fortuna , L., and Petras, I., *Fractional order systems: Modeling and Control Applications*, Series A -Vol.72, World Scientific Publishing Co. Pte. Ltd., 2010.

[3] Podlubny, I., *Fractional Differential Equations*, Academic Press, San Diego, 1999.

[4] Grassi, E., & Tsakalis, K., *PID Contoller Tuning by Frequency Loop-Shaping: Application to Diffusion Furnace Temperature Control*, IEEE Transactions on Control Systems Technology, Vol. 8, NO.5, September 2000.

[5] Jesus, I.S., & Tenreiro Machado, J.A., *Fractional control of heat diffusion systems,* Nonlinear Dynamics (2008) 54: 263. https://doi.org/10.1007/s11071-007-9322-2

[6] Malti, R., Moreau, X., Khemane, F., Oustaloup, A., *Stability and resonance conditions of elementary fractional transfer functions*, Automatica, Volume 47, Issue 11, pp. 2462-2467, 2011.

[7] Malti, R., Aoun, M., Levron, F., & Oustaloup, A., *Analytical computation of the $\mathcal{H}$2-norm of fractional commensurate transfer functions*, Automatica, Volume 47, Issue 11, pp. 2425-2432, November 2011.

[8] Monje, C.A., Chen, Y,Q., Vinagre , B,M., Xue, D., and Feliu, V., *Fractional-order Systems and Controls: Fundamentals and Applications,* Springer-Verlag London Limited., 2010.

[9] Povstenko,Y., *Linear Fractional Diffusion-Wave Equation for Scientists and Engineers*, Springer-Verlag, Switzerland, 2015.

[10] Petras, I., *Fractional-Order Nonlinear Systems: Modeling, Analysis and Simulation*, Higher Education Press, Beijing and Springer-Verlag Berlin Heidelberg, 2011.

[11] Xue, D., Chen , Y,Q., and Atherton, D,P., *Linear Feedback Control: Analysis and Design with MATLAB*, Society for Industrial and Applied Mathematics., Philadelphia., 2007.

[12] Matusu, R., *Application of Fractional Order Calculus to Control Theory* , International Journal of Mathematics Models and Methods in Applied Science, Vol. 5, no, 7, pp. 1162-1169, 2011.

[13] Maiti, D., Konar, A., *Approximation of a Fractional Order System by an integer Order Model Using Particle Swarm Optimization Technique*, IEEE CICCRA, pp149-152., 2008.

[14] Ma. C., and Hori, Y,. *Fractional-Order Control: Theory and Applications in Motion Control*, IEEE Industrial Electronics Magazine, 2007.

[15] Chen, Y,Q., Petras, I., & Xue, D., *Fractional Order Control –A Tutorial* , American Control Conference, Hyatt Regency Riverfront, St. Louis, MO, USA, pp. 1397-1411, June 10-12, 2009.

[16] Basu, A., Mohanty, S., & Sharma, R., *Dynamic Modeling of Heating Furnace & Enhancing the Performance with $PI^{\lambda}D^{\mu}$ Controller for Fractional Order Model using Optimization Techniques*, International Journal of Electronics Engineering Research 9 (1), 69-85, 2016.

[17] Assi, A.H., *Engineering Education and Research Using MATLAB,* Chapter 10, InTech., 2011.

[18] Yeroglu, C., Onat, C., & Tan, N., *A new tuning method for $PI^{\lambda}D^{\mu}$ controller*, Electrical and Electronics Engineering, ELECO 2009, pp. II-312-II-316, 2009.

[19] Farges, C., Fadiga, L., & Sabatier, J., *H∞ analysis and control of commensurate fractional order systems*, Mechatronics, Volume 23, Issue 7, pp. 772-780, 2013

[20] Sierociuk, D., *Fractional Order Discrete State-Space System Simulink Toolkit User Guide V.1.7*, 2005. http://www.ee.pw.edu.pl/.

[21] Klafter, J., Lim, S.C., & Metzler, R., *Fractional Dynamics: Recent Advances,* World Scientific Publishing Co. Pte. Ltd, 2012.

[22] Sierociuk, D., *Simulation and Experimental Tools for Fractional Order Control Education*, In Proceedings of 17th World Congress The International Federation of Automatic Control, Seoul, Korea, July 6-11, pp. 11654-11659, 2008.

[23] Zhou, Y., *Basic Theory of Fractional Differential Equations*, World Scientific Publishing Co. Pte. Ltd, 2014.

[24] Saha Ray, S. & Bera, R.K., *Analytical Solution of the Bagley Torvik Equation by Adomian Decomposition Method*, Applied Mathematics and Computation, 168, pp. 398-410, 2005.

[25] Petras, I., *Fractional-Order Feedback Control of a DC Motor*, Journal of Electrical Engineering, Vol. 60, no, 3, pp. 117-128, 2009.

[26] Al-Asmari, A.K., *Useful Formulas and Algorithms for Engineering and Science*, King Fahd National Library, Riyadh, Saudi Arabia, 2003.

[27] Qiang, W.F., & Kui, M.X., *Transfer function modeling and analysis of the open-loop Buck converter using the fractional calculus*, Chin. Phys. B, 2013, 22(3):030506.

[28] Ortigueira, M.D., *Fractional Calculus for Scientists and Engineers*. Lecture Notes in Electrical Engineering, 84, Springer Science, 2011.

[29] Gherfi, K., Charef, A., & Abbassi, H.A., *Bagley-Torvik Fractional Order System Performance Characteristics Analysis*, IEEE 8th International Conference on Modeling, Identification and Control (ICMIC), November 2016.

[30] Luo, Y., & Chen, Y., *Fractional Order Motion Controls*. Wiley, NewYork, 2012.

[31] Valerio, D., & Costa,J., *An introduction to fractional control*, IET, 2013.

[32] Wang, Y., Hartley, T.T., Lorenzo, C.F., Adams, J.L., Carletta, J.E., & Veillette, R.J., *Modeling Ultracapacitors as Fractional-Order Systems*, In: Baleanu, D., Guvenc, Z., Machado, J., (eds) *New Trends in Nanotechnology and Fractional Calculus Applications*, Springer, Dordrecht, 2010.

[33] Kaczorek, T., & Rogowski, K., *Fractional Linear Systems and Electrical Circuits*, Springer International Publishing, 2015.

[34] Tepljakov, A., Petlenkov, E., & Belikov, J., *FOMCON: Fractional-order modeling and control toolbox for MATLAB*, IEEE 18th International Conference "Mixed Design of Integrated Circuits and Systems", June 16-18, 2011, Gliwice, Poland.

[35] Das, S., & P, I., *Fractional Order Signal Processing: Introductory Concepts and Applications*, Springer-Verlag Berlin Heidelberg, 2012.

[36] Li, C., & Zeng, F., *Numerical Methods for Fractional Calculus*, Chapman & Hall/CRC Numerical Analysis and Scientific Computing Series, 2015.

[37] Bakshi, U.A., & Bakshi, M.V., *Modern Control Theory*, Technical Publications, Pune, India, 2015.

[38]   https://en.wikipedia.org/wiki/Blast_furnace

[39]   https://en.wikipedia.org/wiki/Buck_converter

[40]   http://www.mathworks.com